A compartmentalized signaling network mediates crossover control in meiosis

Liangyu Zhang[1,2,3,4], Simone Köhler[1,2,3,4], Regina Rillo-Bohn[1,2,3,4], and Abby F. Dernburg[1,2,3,4,*]

[1]Department of Molecular and Cell Biology, University of California, Berkeley, Berkeley, CA 94720, USA

[2]Howard Hughes Medical Institute, 4000 Jones Bridge Road, Chevy Chase, MD 20815, USA

[3]Biological Systems and Engineering Division, Lawrence Berkeley National Laboratory, Berkeley, CA 94720, USA

[4]California Institute for Quantitative Biosciences, Berkeley, CA 94720, USA

* For correspondence: afdernburg@berkeley.edu (AFD)

Abstract

During meiosis, each pair of homologous chromosomes typically undergoes at least one crossover (crossover assurance), but these exchanges are strictly limited in number and widely spaced along chromosomes (crossover interference). The molecular basis for this chromosome-wide regulation remains mysterious. A family of meiotic RING finger proteins has been implicated in crossover regulation across eukaryotes. *Caenorhabditis elegans* expresses four such proteins, of which one (ZHP-3) is known to be required for crossovers. Here we investigate the functions of ZHP-1, ZHP-2, and ZHP-4. We find that all four ZHP proteins, like their homologs in other species, localize to the synaptonemal complex, an unusual, liquid crystalline compartment that assembles between paired homologs. Together they promote accumulation of pro-crossover factors, including ZHP-3 and ZHP-4, at a single recombination intermediate, thereby patterning exchanges along each chromosome. These proteins also act at the top of a hierarchical, symmetry-breaking process that enables crossovers to direct accurate chromosome segregation.

KEYWORDS: meiosis, E3 ligase, recombination, crossover, cohesion, chromosome segregation, phase separation, auxin-inducible degradation

Introduction

Meiosis gives rise to haploid gametes through two sequential rounds of nuclear division. To ensure faithful meiotic chromosome segregation in most organisms, every pair of homologous chromosomes must attain at least one crossover (CO) recombination product, which creates a stable interhomolog connection known as a chiasma (Page and Hawley, 2003). However, the total number of COs per cell is typically far too low to assure CO formation on each chromosome by a Poisson process; indeed, in many species each homolog pair undergoes only a single CO (Mercier et al., 2015). In cases where multiple COs occur per chromosome pair, they are nonrandomly far apart, a phenomenon known as “crossover interference” (Muller, 1916; Sturtevant, 1915). Despite our longstanding awareness of crossover patterning, the mechanisms that ensure this highly nonrandom process remain poorly understood and controversial.

Meiotic recombination is initiated by programmed DNA double-strand breaks (DSBs) catalyzed by the conserved topoisomerase-like enzyme Spo11 (SPO-11 in *C. elegans*) (Dernburg et al., 1998; Keeney, 2008; Keeney et al., 1997). A subset of DSBs are processed to become COs, while the rest are repaired through alternate pathways. In several model organisms, two CO pathways have been elucidated: The “class I” pathway, which is subject to CO assurance and interference, requires two meiosis-specific homologs of the MutS bacterial mismatch repair protein, Msh4 and Msh5, which form a complex known as MutSγ. Components of the synaptonemal complex (SC), an ordered, periodic proteinaceous structure that assembles between homologous chromosomes during meiotic prophase, are also required for class I COs. An alternate

58 enzymatic pathway can give rise to both noncrossovers and “class II” COs, which do not
59 show interference.

60 In the nematode *C. elegans*, only class I COs normally occur, and only a single
61 CO occurs per chromosome pair (Martinez-Perez and Colaiacovo, 2009). No COs occur
62 in the absence of SC assembly (MacQueen et al., 2002). Additional factors required for
63 meiotic COs, but not for homolog pairing, synapsis, or other homologous recombination,
64 include MSH-4 and MSH-5 (Kelly et al., 2000; Zalevsky et al., 1999), the cyclin-related
65 protein COSA-1 (Yokoo et al., 2012), and ZHP-3, a RING finger protein (Jantsch et al.,
66 2004).

67 COs act together with sister chromatid cohesion to orchestrate two successive
68 rounds of chromosome segregation. In mammals and most other model organisms,
69 cohesion between sister chromatids is maintained near centromeres during the first
70 division (MI), but arm cohesion must be released to allow homologs to separate (Duro
71 and Marston, 2015). In *C. elegans*, which lacks defined centromeres, cohesion is
72 spatially regulated downstream of CO designation. Late in meiotic prophase, the
73 chromosome region on one side of the designated CO site becomes enriched for
74 several proteins, including HTP-1/2, LAB-1, and REC-8, which act together to maintain
75 cohesion through the first division. Conversely, the reciprocal chromosome region
76 becomes depleted of these proteins but retains a stretch of SC. This “short arm”
77 eventually recruits the Aurora B kinase AIR-2, which is required to release cohesion and
78 allow MI segregation (de Carvalho et al., 2008; Ferrandiz et al., 2018; Kaitna et al., 2002;
79 Martinez-Perez et al., 2008; Nabeshima et al., 2005; Rogers et al., 2002; Severson and

80 Meyer, 2014). It has been unclear whether the SC that remains along this arm
81 contributes to regulating cohesion. The hierarchy of steps leading to this remodeling,
82 and particularly the initial trigger for this asymmetry, are also poorly understood.
83 Several recent studies have indicated that structural proteins within assembled
84 SCs are highly mobile (Nadarajan et al., 2017; Pattabiraman et al., 2017; Rog et al.,
85 2017; Voelkel-Meiman et al., 2012). We have also presented evidence that this material
86 likely assembles through regulated phase separation (Rog et al., 2017). When SCs
87 cannot assemble between chromosomes, as in *C. elegans* mutants lacking the
88 essential chromosome axis protein HTP-3, or in budding yeast lacking DSBs, SC
89 proteins self-assemble to form irregularly shaped, but internally structured, nuclear
90 bodies known as polycomplexes (Roth, 1966), which do not appear to be associated
91 with chromosomes. Observations of *C. elegans* polycomplexes *in vivo* revealed that
92 they behave as liquid-like droplets, in that they rapidly change shape and fuse to form
93 larger bodies (Rog et al., 2017). Taken together, these observations indicate that SC
94 proteins self-assemble through regulated coacervation to form a liquid crystalline
95 material – defined as an ordered assembly of molecules that diffuse freely relative to
96 each other. Normally this material preferentially assembles as a bilaterally symmetrical
97 lamina between paired axes, but in the absence of the proper chromosomal substrate, it
98 forms polycomplexes.
99 Growing evidence has implicated the SC in CO regulation, particularly in *C.*
100 *elegans* (Hayashi et al., 2010; Libuda et al., 2013; MacQueen et al., 2002; Rog et al.,
101 2017; Sym and Roeder, 1994). The mobility of proteins within assembled SCs suggests

102 that biochemical signals such as enzymes or posttranslational modifications could move
103 through this material to regulate CO formation along paired chromosomes. In support of
104 this idea, a number of crossover factors and DNA damage repair components have
105 been found to associate with both SCs and polycomplexes. In budding yeast, these
106 include Msh4, Msh5, Spo16, Spo22 (Zip4), Zip2, and Zip3, and the 9-1-1 complex
107 component Mec3 (Shinohara et al., 2015; Tsubouchi et al., 2006). Zip3 is unique among
108 these proteins in that it localizes throughout the body of polycomplexes, suggesting that
109 it has an intrinsic affinity for SC proteins, while all other proteins reported to date appear
110 to localize to a "cap" or focus at the surface of polycomplexes. We observed that ZHP-3,
111 a *C. elegans* homolog of yeast Zip3 (Agarwal and Roeder, 2000), similarly localizes
112 throughout polycomplexes (Rog et al., 2017). Interestingly, ZHP-3 and Zip3 share
113 homology with Hei10 and RNF212, which have been implicated in crossover control
114 across diverse eukaryotes (Chelysheva et al., 2012; De Muyt et al., 2014; Gray and
115 Cohen, 2016; Qiao et al., 2014; Reynolds et al., 2013; Wang et al., 2012; Ward et al.,
116 2007). All of these proteins contain an N-terminal RING finger domain, a central coiled-
117 coil domain, and a C-terminal domain that is predicted to be largely unstructured.
118 Three paralogs of ZHP-3 are expressed in the *C. elegans* germline, but their
119 functions have not previously been described. Here we define essential meiotic roles for
120 these proteins. We report that this family of four paralogs, which we designate as ZHP-
121 1–4, likely act as two heterodimeric complexes to regulate CO formation. Like ZHP-3,
122 the other 3 proteins localize throughout SCs in early prophase, and are also recruited to
123 polycomplexes. Together with other known and unknown factors, these ZHP proteins

124 appear to form a signaling network that acts within the SC to ensure CO formation while
125 limiting the number of CO-designated sites, and may thus mediate both CO assurance
126 and CO interference. In addition, the ZHP proteins in *C. elegans* act upstream of other
127 regulators to direct chromosome remodeling in response to crossover formation, which
128 enables the stepwise removal of cohesion that enables two successive rounds of
129 chromosome segregation during meiosis. Homology between the ZHP proteins and
130 meiotic regulators from other phyla indicate that similar mechanisms likely underlie
131 meiotic CO control in most eukaryotes, and may also play previously-unrecognized
132 roles in regulating sister chromatid cohesion during meiosis.
133

134 ## Results

135 ### A family of meiotic RING finger proteins in *C. elegans*

136 As described in the Introduction, the RING finger protein ZHP-3 was initially identified
137 as a candidate meiotic factor in *C. elegans* based on its homology to Zip3, a component of
138 the "synapsis initiation complex" in yeast (Agarwal and Roeder, 2000). Targeted disruption
139 of *zhp-3* revealed that it is required for CO formation, but dispensable for homolog pairing
140 and synapsis (Jantsch et al., 2004). The *C. elegans* genome includes three additional
141 predicted genes with the same domain structure and significant homology to ZHP-3 (Figure
142 1—figure supplement 1A-B). Several independent analyses indicate that all four genes are
143 expressed in the germline, consistent with a role in meiosis (Lake et al., 2015; S.K. and
144 A.F.D. unpublished).

145 All four predicted proteins have similar N-terminal C3HC4-type RING-finger domains

146 (Figure 1—figure supplement 1A-B), which are usually associated with ubiquitin E3 ligase
147 activity (Deshaies and Joazeiro, 2009). The C-terminal regions of these proteins are
148 divergent and lack obvious structural domains, but contain a number of potential post-
149 translational modification sites (Figure 1—figure supplement 1A). Based on their similarity to
150 each other, and on evidence presented here that they function together to form a regulatory
151 circuit, we have named these genes *zhp-1* (F55A12.10), *zhp-2* (D1081.9) and *zhp-4*
152 (Y39B6A.16) (*zip3* homologous protein). This numbering reflects their physical order in the
153 *C. elegans* genome: *zhp-1, -2,* and *-3* are clustered on Chromosome I, while *zhp-4* is on
154 Chromosome V.

155 To gain insight into the evolution of these proteins, we searched for homologs in
156 other sequenced nematode genomes (Figure 1—figure supplement 1C). Orthologs of each
157 protein can be identified in *C. briggsae* and *C. remanei*, as well as in other nematode
158 genera, indicating that these proteins diversified at least tens to hundreds of millions of
159 years ago (Figure 1—figure supplement 1C-D and data not shown). Their N-terminal regions
160 show homology to the mammalian CO regulator RNF212, and ZHP-1 and ZHP-2 are also
161 recognized by BLAST as homologs of HEI10, which is involved in CO regulation in
162 mammals, plants, and fungi (Chelysheva et al., 2012; De Muyt et al., 2014; Qiao et al., 2014;
163 Rao et al., 2017; Reynolds et al., 2013, and data not shown; Wang et al., 2012; Ward et al.,
164 2007) (data not shown).

165

166 **ZHP proteins exhibit two distinct patterns of dynamic localization during meiosis**

167 To investigate the ZHP proteins, we inserted epitope tags at the C-terminus of each

168 coding sequence; these tagged proteins supported normal meiosis (Supplementary File 1,
169 Table S1) and were readily localized by immunofluorescence with epitope-specific
170 antibodies (Figure 1—figure supplement 2 and Figure 2—figure supplement 2A-B). At
171 meiotic entry the ZHP proteins localized to small polycomplexes, which contain the four
172 known SC structural proteins, SYP-1, -2, -3, and -4 (Goldstein, 2013; Rog et al., 2017; Roth,
173 1966), and once SC assembly initiated, they localized to SCs (Figure 1).

174 As meiosis progressed, the four proteins showed two distinct patterns of localization
175 (Figure 1): From early prophase to mid-pachynema, ZHP-1 and -2 became brighter and
176 more contiguous along the length of SCs, although the intensity of staining was not
177 homogeneous. Upon the appearance of GFP-COSA-1 foci, which mark designated CO sites
178 from mid-pachynema through diplonema (Yokoo et al., 2012), ZHP-1 and -2 became
179 confined to the SC on one side of each CO. Intriguingly, this restriction was observed in
180 pachytene nuclei that retained SC (Figure 1A-B) and the HORMA domain proteins HTP-1/2
181 (data not shown) on both sides of the CO, and represents the earliest known molecular
182 differentiation of the two chromosome domains that will become the long and short arms of
183 the bivalent. ZHP-1 and -2 remained associated with SC proteins along the short arm of
184 each bivalent as the SC disappeared from the long arm, and persisted as long as SC
185 proteins were present along the short arms, through late diakinesis.

186 ZHP-3 and -4 exhibited a similar distribution to ZHP-1 and -2 during early prophase,
187 but showed a distinct pattern starting at mid-pachytene, when crossover designation (the
188 selection of one recombination intermediate as the eventual crossover site for each pair of
189 chromosomes) is thought to occur in *C. elegans* (Figure 1C-D) (Yokoo et al., 2012). Upon

190 the detection of GFP-COSA-1 foci, which mark the subset of recombination intermediates
191 that will become COs, ZHP-3 and -4 both accumulated at these sites and gradually
192 disappeared from the SC along both arms of the chromosomes. These observations are
193 largely consistent with previous characterization of ZHP-3 and a partially functional GFP-
194 ZHP-3 fusion protein (Bhalla et al., 2008; Jantsch et al., 2004).
195

196 **Localization of ZHPs along meiotic chromosomes depends on synaptonemal**
197 **complexes**

198 The SC in *C. elegans* comprises at least 4 proteins, known as SYP-1-4, which are
199 mutually dependent for assembly between chromosomes or as polycomplexes. We found
200 that none of the four ZHP proteins associated along chromosomes in *syp-1* or other *syp*
201 mutants (Figure 1—figure supplement 3A-C, and data not shown). Intriguingly, in the region
202 of the germline that normally corresponds to late pachynema, the 4 ZHP proteins
203 colocalized within nuclear puncta devoid of SC proteins, indicating that the ZHPs can
204 interact with each other in the absence of SCs or polycomplexes (Figure 1—figure
205 supplement 3C, lower panel). These puncta do not coincide with known DSB repair proteins
206 (Figure 1—figure supplement 3D). The ZHP proteins were also less abundant in *syp-1*
207 mutants (Figure 1—figure supplement 3E-K), suggesting that their stability is enhanced by
208 association with SCs, particularly that of ZHP-1 and -2 (Figure 1—figure supplement 3F and
209 J).

210 Because the ZHP proteins relocalized upon CO designation (Figure 1), we examined
211 their distribution under conditions where COs fail to occur. In mutants lacking SPO-11,

212 MSH-5, or COSA-1, ZHPs were detected along the length of SCs through diplonema (data
213 not shown). Thus, relocalization of the ZHPs in late prophase depends on DSBs and CO
214 designation factors.
215
216 **ZHPs likely act as two heterodimeric complexes**
217 To investigate the meiotic functions of the ZHP proteins, we first exploited the auxin-
218 inducible degradation system. Each of the ZHP genes was tagged with a 3xFLAG epitope
219 and a 44-aa degron sequence (hereafter "AID") in a strain that expresses the F-box protein
220 AtTIR1 throughout the germline (Zhang et al., 2015). When adult animals were transferred
221 to plates containing 1 mM auxin, all AID-tagged proteins were robustly depleted within 1-2
222 hours (Figure 2—figure supplement 1A-B). To assess the efficacy of the knockdown, we
223 compared meiotic chromosome segregation in hermaphrodites carrying the previously
224 characterized *zhp-3(jf61)* null allele (Jantsch et al., 2004) to auxin-treated worms expressing
225 ZHP-3-AID-GFP (Figure 2—figure supplement 1C). AID-mediated depletion of ZHP-3
226 quantitatively phenocopied the null allele with respect to both embryonic viability *(Δzhp-3*:
227 2.06 ± 0.62%; *zhp-3::AID*: 1.83 ± 0.82%) and the incidence of males among the self-
228 progeny of hermaphrodites, which reflects X-chromosome nondisjunction (Hodgkin et al.,
229 1979) (*Δzhp-3*: 43.75 ± 27.59 %; *zhp-3::AID*: 37.02 ± 38.12%) (Figure 2—figure supplement
230 1C), indicating that auxin-induced degradation effectively eliminates the function of ZHP-3.
231 To determine the dependence of the ZHP proteins on each other for their localization
232 and stability, we exposed worms to auxin for 24 hours, so that a pool of nuclei had entered
233 and progressed through meiotic prophase in the absence of AID-tagged protein. We found

234 that ZHP-1 and -2 depend on each other for both their chromosome association and stability
235 (Figure 2A-D). ZHP-3 and -4 were also interdependent for their localization to chromosomes
236 (Figure 2E, 2G and Figure 2—figure supplement 2C). ZHP-3 was unstable in the absence of
237 ZHP-4 (Figure 2F) and ZHP-4 levels were somewhat lower when ZHP-3 was depleted
238 (Figure 2H and Figure 2—figure supplement 2D).

239 Other RING finger proteins such as BRCA1/BARD1 are known to act as
240 heterodimers (Brzovic et al., 2001; Metzger et al., 2014; Wu et al., 1996). The similarity and
241 interdependence of localization of ZHP-1 and -2, and of ZHP-3 and -4, suggested that these
242 four proteins might function as two pairs. Using yeast two-hybrid analysis, we found that
243 ZHP-1 and -2 indeed interact with each other, and that ZHP-3 and ZHP-4 also physically
244 interact (Figure 2I and Figure 2—figure supplement 2E). This evidence for specific pairwise
245 physical interactions, together with their physical distributions (above) and functional
246 analysis (below), indicate that ZHP-1 and -2 form a complex, and that ZHP-3 and -4
247 similarly act as a pair. Hereafter we refer to these two dimeric activities as ZHP-1/2 and
248 ZHP-3/4 for simplicity.

249

250 **ZHPs play essential roles in chiasma formation and chromosome segregation**

251 Using a number of established assays, we investigated the meiotic functions of these
252 RING finger proteins. At late diakinesis, association between homologs is normally
253 maintained by chiasmata, and six condensed bivalents can be detected in each wild-type
254 oocyte nucleus. We exposed *zhp-AID* strains to auxin for 24 hours and then analyzed
255 chiasma formation. Depletion of ZHP-1 or ZHP-2 yielded 8-12 DAPI-staining bodies at

256 diakinesis, representing 4-12 univalents and 0-4 bivalents (Figure 3A-B). In contrast,
257 depletion of ZHP-3 or ZHP-4 resulted in a complete failure of chiasma formation, indicated
258 by the appearance of 12 achiasmate chromosomes in each nucleus (Figure 3C-D),
259 consistent with previous characterization of ZHP-3 (Bhalla et al., 2008; Jantsch et al., 2004).
260 Because a few chiasmata were observed when ZHP-1-AID or ZHP-2-AID were
261 depleted, we were concerned that these proteins might not be efficiently degraded. We
262 therefore introduced null mutations in *zhp-1* and *zhp-2* (see Materials and Methods).
263 Homozygous mutants produced few viable progeny and a high incidence of males among
264 the self-progeny of hermaphrodites (Figure 3E), both of which are indicative of meiotic
265 chromosome missegregation. They also showed identical distributions of DAPI-staining
266 bodies at diakinesis to that observed in AID-depleted animals (Figure 3—figure supplement
267 1A-C and data not shown). Additionally, both *zhp-1* and *-2* null mutants produced more
268 viable progeny than *zhp-3* null mutants (***$p<0.001$, two-sided Student's *t*-test) (Figure 3E),
269 consistent with a less absolute dependence of chiasma formation on ZHP-1/2 than on ZHP-
270 3/4.
271 We wondered whether the few chiasmata in hermaphrodites lacking ZHP-1/2 might
272 preferentially occur on the X chromosome, which shows some differences from autosomes
273 in its genetic requirements for DSB induction and CO formation (Yu et al., 2016). To
274 investigate this, we used fluorescence in situ hybridization (FISH) to mark Chromosome V
275 and the X chromosome in *zhp-1* mutants. By examining nuclei at diakinesis, we found that
276 chiasma formation was impaired to a similar degree on both chromosomes. Our
277 observations are quantitatively consistent with a low number of chiasmata distributed evenly

278 among all six chromosome pairs (Figure 3F-G).

279 ZHP-3 was previously found to be dispensable for homologous chromosome pairing,
280 synapsis, and DSB induction (Jantsch et al., 2004). Pairing and synapsis also occurred
281 normally in the absence of ZHP-1, -2, or -4 (Figure 3—figure supplement 2). RAD-51 foci,
282 which mark recombination intermediates and require DSB induction (Colaiacovo et al.,
283 2003), were also abundant in all *zhp* mutants (Figure 3—figure supplement 3A-F). Thus, the
284 high frequency of achiasmate chromosomes in the absence of ZHPs reflects defects in CO
285 recombination downstream of pairing, synapsis, and DSBs.

286 Prior work has established the existence of a "crossover assurance checkpoint" in *C.*
287 *elegans* that delays meiotic progression when recombination intermediates or pro-CO
288 factors are absent on one or more chromosomes due to defects in homolog pairing,
289 synapsis, DSB induction, or recombination (Carlton et al., 2006; Kim et al., 2015; Yu et al.,
290 2016). Activation of this checkpoint prolongs the activity of the CHK-2 kinase, resulting in an
291 extended region and elevated number of RAD-51 foci, and a shift in the pattern of meiotic
292 recombination, but does not perturb CO interference. We observed that phosphorylation of
293 HIM-8 and its paralogs, a marker for CHK-2 activity, was extended when any of the ZHPs
294 was depleted (Figure 3—figure supplement 3G-I), and RAD-51 foci were more abundant
295 (Figure 3—figure supplement 3A-F). Thus, the crossover assurance checkpoint does not
296 require ZHP activity.

297 We noted differences in the dynamics of DNA repair when ZHP-1/2 were depleted as
298 compared to ZHP-3/4 (Figure 3—figure supplement 3A-F). In the absence of ZHP-3/4, RAD-
299 51 foci reached higher peak numbers than in wild-type animals or in the absence of ZHP-1/2,

300 but depletion of ZHP-1/2 caused a greater delay in the both the accumulation and
301 disappearance of RAD-51 foci than depletion of ZHP-3/4. Thus, the two ZHP complexes
302 likely play distinct roles in the processing of recombination intermediates, similar to
303 observations of HEI10 and RNF212 in mouse spermatocytes (Qiao et al., 2014).
304

305 **ZHP-3/4 are essential to stabilize CO intermediates, while ZHP-1/2 restrict pro-CO**
306 **activities and promote CO maturation**

307 To probe the role of ZHPs in recombination, we examined the cytological distributions
308 of MSH-5, which can be detected at sites of early recombination intermediates, and COSA-1,
309 which forms bright foci at sites designated for CO formation (Yokoo et al., 2012). In wild-
310 type and control (non-auxin-treated) worms, ~10-20 MSH-5 foci per nucleus could be
311 detected by mid-pachytene (Figure 4—figure supplement 1A), after which six GFP-COSA-1
312 foci – one per pair of chromosomes – were observed (Figure 4A), and MSH-5 became
313 restricted to these sites (Figure 4 – figure supplement 1), as previously described (Yokoo et
314 al., 2012). In worms depleted of ZHP-3/4, neither MSH-5 nor COSA-1 foci were detected
315 during meiotic prophase (Figure 4B, Figure 4—figure supplement 1B and data not shown).
316 This indicates that ZHP-3/4 are likely required for stable association of MutSγ with early
317 recombination intermediates. In striking contrast, depletion of ZHP-1/2 resulted in
318 appearance of up to ~50 MSH-5 foci and up to ~30 dim but detectable GFP-COSA-1 foci
319 per oocyte nucleus (Figure 4C-D, and Figure 4—figure supplement 1C-D). Notably, the
320 number of detectable foci increased in number as nuclei advanced from mid- to late
321 pachytene, and then rapidly declined (Figure 4D and Figure 4—figure supplement 1D).

322 The dim GFP-COSA-1 foci in ZHP-1/2-depleted worms showed extensive
323 colocalization with MSH-5 foci (Figure 4—figure supplement 1E). Together with prior
324 evidence, this suggested that MSH-5 and COSA-1 colocalize at many recombination
325 intermediates in the absence of ZHP-1/2. Indeed, it is likely that these pro-CO factors
326 initially colocalize at all strand exchange intermediates, and that the difference in the
327 number of detected foci of MSH-5 and COSA-1 is due to the relative sensitivity of the
328 available detection reagents.

329 To validate the idea that these foci correspond to recombination intermediates, we
330 eliminated recombination by disrupting DSB formation. We AID-tagged SPO-11 and either
331 ZHP-1 or ZHP-2 in the same strain, and found that both proteins could be effectively co-
332 depleted by auxin treatment (Figure 4—figure supplement 2A and data not shown). This
333 abolished all MSH-5 and GFP-COSA-1 foci (Figure 4E and data not shown), supporting the
334 idea that the dim foci observed in the absence of ZHP-1/2 are indeed recombination
335 intermediates. Co-depletion of ZHP-1 and ZHP-4 also eliminated GFP-COSA-1 foci (Figure
336 4F and Figure 4—figure supplement 2B) and bivalent formation (Figure 4G), supporting the
337 conclusion that ZHP-3/4 are required to stabilize MutSγ at all recombination intermediates.
338 Depletion of ZHP-1/2 also resulted in persistence of ZHP-3 and -4 throughout SCs in late
339 pachytene nuclei (Figure 4—figure supplement 2C and data not shown). These
340 observations indicate that ZHP-1/2 are required to restrict pro-CO proteins to a single
341 recombination intermediate along each pair of homologs during late prophase.

342 We next sought to understand why oocytes lacking ZHP-1/2 have abundant, dim
343 COSA-1 foci but few bivalent chromosomes. This discrepancy could indicate that the dim

344 foci do not mature as COs, or that they do become COs but fail to give rise to stable
345 chiasmata. To address this, we mapped COs in *zhp-1* null mutants by whole genome
346 sequencing (see Materials and Methods). Using this genetic recombination assay, an
347 average of 2.8 ± 1.8 (SD) COs per oocyte were detected in *zhp-1* mutants, compared to 7.3
348 ± 3.0 (SD) per oocyte (slightly more than the expected number of 6) in wild-type animals
349 (Figure 4H). These data are consistent with the observed number of bivalents (Figure 3 and
350 Figure 3—figure supplement 1), and indicate that only a small fraction of COSA-1-positive
351 foci in *zhp-1/2* mutants mature to become COs and chiasmata.

352 The excess number but weak immunofluorescence of GFP-COSA-1 foci in the
353 absence of ZHP-1/2 suggested that one or more limiting components might be distributed to
354 an excess of recombination intermediates. We therefore wondered whether accumulation of
355 pro-CO factors at specific recombination intermediates could be rescued by restricting the
356 number of these intermediates. Mutations in *dsb-2* cause an age-dependent reduction in
357 meiotic DSBs: very few RAD-51 foci and chiasmata are seen in older (48 h post-L4) *dsb-2*
358 hermaphrodites, while somewhat more RAD-51 foci and chiasmata are seen in younger
359 adults (Rosu et al., 2013). We co-depleted DSB-2 and ZHP-2 using the AID system (Figure
360 5—figure supplement 1A), fixed worms at 24 and 48 hours post-L4, and stained for RAD-51
361 and GFP-COSA-1. Fewer COSA-1 foci and bivalents were observed in animals depleted for
362 both DSB-2 and ZHP-2 than DSB-2 alone, although the number of RAD-51 foci was similar
363 (Figure 5A-C, Figure 5—figure supplement 1B and data not shown). Intriguingly, while
364 younger *dsb-2* mutant animals have more meiotic DSBs (Rosu et al., 2013 and data not
365 shown), we observed fewer bright GFP-COSA-1 foci in young ZHP-2 depleted animals: only

366 11% of nuclei contained a bright GFP-COSA-1 focus, compared to 49% in older animals
367 (Figure 5B-C). The number of bivalents in these animals corresponded well with bright GFP-
368 COSA-1 foci, and only chromosomes with bright COSA-1 foci displayed the normal
369 hallmarks of chromosome remodeling (see below), indicating that only bright COSA-1 foci
370 reliably mature as COs.

371 As another approach to examine how the number of intermediates impacts CO
372 maturation in the absence of ZHP-1/2, we co-depleted ZHP-2 and SPO-11 to abolish
373 programmed meiotic DSBs, and exposed these animals to varying doses of ionizing
374 radiation. When SPO-11 alone was depleted by the AID system, GFP-COSA-1 foci and
375 bivalents were eliminated. Following 10 Gy of radiation, a dose sufficient to ensure CO
376 formation on most chromosomes in the absence of SPO-11, 6 bright GFP-COSA-1 foci were
377 observed in each nucleus, as previously described (Libuda et al., 2013; Yokoo et al., 2012)
378 (Figure 5—figure supplement 1C). When SPO-11 and ZHP-2 were co-depleted, bright GFP-
379 COSA-1 foci were observed following low doses of radiation, but these never exceeded 2
380 per nucleus (Figure 5D). At 10 Gy, only extremely dim GFP-COSA-1 foci were detected
381 (Figure 5D).

382 Taken together, these observations indicate that ZHP-1/2 are dispensable for a
383 single break to become a functional interhomolog CO, but act to limit or focus the activity of
384 ZHP-3/4 and/or other pro-CO factors to select a single recombination intermediate on each
385 chromosome and to ensure CO maturation in the context of excess DSBs. A higher fraction
386 of recombination intermediates become crossovers when breaks are severely reduced, but
387 even when very few DSBs are present, ZHP-1/2 contribute to the accumulation of pro-CO

388 factors, which in turn promotes CO maturation.

389 These results indicate that ZHP-1/2 play dual roles: they restrict the accumulation of
390 pro-CO factors to a subset of recombination intermediates and promote their accumulation
391 at a subset of sites. We tested whether these two functions could be separated by reducing
392 the amount of either protein. When strains carrying AID-tagged ZHP-1 or -2 were exposed
393 to low concentrations of auxin, these proteins could be partially depleted (Figure 5—figure
394 supplement 2A-B and data not shown). At very low protein levels, we saw a reduction in the
395 number of GFP-COSA-1 foci, and never observed more than 6 bright COSA-1 foci per
396 nucleus. Thus, concentrations of ZHP-1/2 required to promote accumulation of pro-CO
397 factors are also sufficient to limit their association with recombination sites (Figure 5—figure
398 supplement 2C and data not shown), indicating that these functions are tightly coupled.

399

400 **ZHP-1/2 mediate chromosome remodeling in response to CO designation**

401 As described in the Introduction, stepwise chromosome segregation in *C. elegans*
402 meiosis requires functional differentiation of the chromosome regions on either side of the
403 crossover. Here we report that even prior to any apparent reorganization of HTP-1/2 or SC
404 proteins, ZHP-1/2 became restricted to the SC on one side of the CO, the presumptive short
405 arm (Figure 1 and data not shown). In addition, depletion of ZHP-1 or -2 resulted in aberrant
406 chromosome remodeling: HTP-1/2 and SYP-1 persisted along most chromosomes, both
407 recombinant and achiasmate (Figure 6—figure supplement 1A-C). These observations
408 suggested that ZHP-1/2 might regulate chromosome remodeling, in addition to their roles in
409 CO control.

410 To further probe the contribution of ZHP-1/2 to remodeling, we examined *dsb-2*
411 mutants, in which some recombination intermediates accumulate pro-CO factors and
412 undergo CO maturation even in the absence of ZHP-1/2. The low number of COs in *dsb-2*
413 mutants also allows direct comparison between recombinant and nonexchange
414 chromosomes in the same nucleus, and thus at the same cell cycle stage. As described
415 above, at 48 h-post L4, most late pachytene nuclei in *dsb-2* mutants had either 0 or 1
416 COSA-1 focus. These foci also accumulated ZHP-3 and ZHP-4, which disappeared from the
417 corresponding SCs on both sides of these sites (Figure 6A and data not shown). SC
418 proteins and the Polo kinase PLK-2 also became enriched along these chromosomes
419 relative to nonexchange chromosomes (Figure 6A and D), as previously described
420 (Machovina et al., 2016; Pattabiraman et al., 2017). We also observed that PLK-2, which
421 plays a poorly characterized role in remodeling (Harper et al., 2011), became co-enriched
422 with ZHP-1/2 on one side of each CO (Figure 6E, upper panel). Similar enrichment of PLK-2
423 along the short arm was observed in wild-type animals (Figure 6—figure supplement 2A-B).
424 This had not been apparent using PLK-2 antibodies, but was readily detected with epitope-
425 tagged PLK-2, as recently reported (Harper et al., 2011; Pattabiraman et al., 2017).
426 When we co-depleted DSB-2 and ZHP-1/2, ZHP-3 still accumulated at the few bright
427 COSA-1 foci and was depleted from the corresponding SCs on both sides of these sites
428 (Figure 6B). This indicates that accumulation of pro-CO factors, rather than ZHP-1/2 activity
429 *per se*, leads to depletion of ZHP-3/4 from the SC. However, none of the other hallmarks of
430 CO-induced remodeling were observed in these animals, including accumulation of SC
431 proteins and PLK-2, and asymmetrical localization of PLK-2, HTP-1/2, and LAB-1 (Figure

432 6B-E and data not shown). Instead, a small focus of PLK-2 was detected at CO sites (Figure
433 6E, lower panel). During diplotene-diakinesis, SC proteins also became restricted to this
434 focus, while HTP-1/2 persisted along all chromosome arms (Figure 6C, lower panel).

435 We also depleted PLK-2 with the AID system (Figure 6F). Under these conditions,
436 both the accumulation of pro-CO factors at a subset of recombination intermediates and the
437 asymmetric localization of ZHP-1/2 were delayed, but still occurred (Figure 6F, lower panel).
438 Thus, ZHP-1/2 are required for the asymmetric localization of PLK-2, but not vice versa,
439 placing ZHP-1/2 upstream of PLK-2 in the remodeling pathway.

440 Because ZHP-3/4 are strictly required for CO formation, we could not analyze their
441 roles in chromosome remodeling. However, prior work has found that a GFP-tagged ZHP-3
442 transgene acts as a separation-of-function allele that is proficient for CO formation but
443 defective for remodeling (Bhalla et al., 2008).

444 This remodeling process ultimately leads to the spatial partitioning of cohesin
445 complexes containing distinct kleisin subunits to reciprocal chromosome domains (Severson
446 et al., 2009; Severson and Meyer, 2014). The most mature oocyte in each gonad arm,
447 referred to as the "-1 oocyte," normally shows enrichment of REC-8 along the long arms of
448 each bivalent, while COH-3/4 are retained along the short arms. In ZHP-1/2 depleted worms,
449 REC-8 persisted along all arms, while COH-3/4 virtually disappeared by the -1 oocyte
450 (Figure 6—figure supplement 2C), consistent with the absence of other "short arm"
451 hallmarks.

452 Taken together, our analysis indicates that the ZHP circuit acts at or near the top of
453 the hierarchy that mediates chromosome remodeling in response to CO designation, and

454 directly couples these two key mechanisms to promote proper chromosome segregation.
455 Our observations also imply that the persistence of SC along the short arm following CO
456 designation plays an important role in remodeling by maintaining ZHP-1/2 and PLK-2
457 activity along this region. Together with previous observations, our findings indicate that a
458 biochemical signaling cascade acts in *cis* within individual SC compartments to mediate and
459 respond to CO designation (Libuda et al., 2013; Machovina et al., 2016).
460

461 **Compartmentalization of CO regulation by the synaptonemal complex**

462 In *C. elegans* lacking the chromosome axis protein HTP-3, large polycomplexes
463 appear shortly after meiotic entry and persist throughout meiotic prophase (Goodyer et al.,
464 2008; Rog et al., 2017; Severson and Meyer, 2014). These polycomplexes recapitulate both
465 the internal order and the liquid-like behavior of SCs, and ZHP-3 concentrates within these
466 bodies (Rog et al., 2017). At mid-prophase, a focus of COSA-1 appears at the surface of
467 each polycomplex. ZHP-3 also accumulates at these foci and gradually disappears from the
468 interior of polycomplexes. Thus, ZHP-3 and COSA-1 recapitulate the dynamic relocalization
469 and interdependence that they show at CO sites on the surface of polycomplexes, even in
470 the absence of DSBs or recombination intermediates (Rog et al., 2017).

471 To investigate this circuitry further, we disrupted *htp-3* in various tagged strains. All 4
472 ZHP proteins localized throughout polycomplexes during early prophase (Figure 7A-B, and
473 data not shown), consistent with the idea that they associate with SC proteins. In contrast to
474 ZHP-3 (Rog et al., 2017), ZHP-1/2 did not accumulate at COSA-1 foci, but instead remained
475 diffusely localized throughout polycomplexes during late prophase (Figure 7A-B and data

476 not shown). COSA-1 foci appeared during late prophase even when ZHP-1/2 were depleted,
477 but under these conditions, ZHP-3 remained distributed throughout polycomplexes in
478 addition to concentrating with COSA-1 (Figure 7C), further indicating that ZHP-1/2 promote
479 the accumulation of ZHP-3/4. We also found that MSH-5 colocalized with ZHP-3/4 and
480 COSA-1 foci on polycomplexes (Figure 7D). PLK-2 localized throughout polycomplexes
481 even prior to the detection of COSA-1 foci, but became noticeably brighter afterwards, in the
482 presence or absence of ZHP-1/2 (Figure 7E-F).

483 Together with the observations of *dsb-2* mutants described above, these findings
484 demonstrate that key aspects of the regulatory circuit that designates a subset of
485 recombination intermediates for CO formation act autonomously within each contiguous SC
486 or polycomplex. Remarkably, our study indicates that this circuit is triggered within
487 polycomplexes in response to progression of nuclei into late prophase, despite the absence
488 of any DSBs or CO intermediates in *htp-3* mutants. These observations indicate that the
489 "designation" of one and only one site per compartment, which mirrors the logic of crossover
490 assurance and interference, is an intrinsic property of this compartmentalized circuitry.
491

492 ## Discussion

493 **Spatial compartmentalization of CO control**

494 Evidence that the SC behaves as a phase-separated, liquid crystalline compartment
495 suggested how this interface might act as a conduit for diffusion of biochemical signals
496 along the interface between paired chromosomes (Rog et al., 2017). Here we provide
497 evidence that CO assurance, CO interference, and CO maturation are coordinately

498 regulated by the ZHP RING finger proteins (Figure 8), all of which are concentrated within
499 the SC. Spatial confinement of the ZHPs within this interface between homologs can explain
500 how each pair of chromosomes in the same nucleus is regulated independently, although
501 CO designation is normally coupled to global cell cycle signals. These results add further
502 support to the idea that CO regulation is mediated through this liquid crystalline medium.

503 CO interference in *C. elegans* normally limits COs to one per homolog pair. This
504 "winner takes all" logic is reminiscent of other well-studied biological symmetry-breaking
505 circuits, such as the selection of a single bud site by growing *S. cerevisiae* cells (Goryachev
506 and Pokhilko, 2008; Howell et al., 2012; Ozbudak et al., 2005). Our evidence indicates that
507 ZHP-1/2 are crucial for both positive feedback that promotes accumulation of pro-CO factors,
508 including ZHP-3/4, at a single recombination intermediate, and negative feedback that
509 depletes these factors from other candidate sites (Figure 8). Similar feedback loops have
510 been proposed in previous work on crossover regulation (Qiao et al., 2014; Rao et al., 2017;
511 Reynolds et al., 2013; Yokoo et al., 2012). Indeed, coupled positive and negative feedback
512 mechanisms are likely essential for any robust, switch-like decision executed by biological
513 circuits (Pfeuty and Kaneko, 2009). A full understanding of CO control will clearly require
514 identification of the substrates of the ZHP ligase family and the effects of their modification.

515 A single crossover site could be selected, and other sites deselected, via a "trigger
516 wave" that moves rapidly through the SC from an initial site of stochastic CO designation
517 and inhibits selection of nearby recombination intermediates (Figure 8A). However, such a
518 mechanism cannot easily be reconciled with observations that pro-crossover factors,
519 including Zip3, accumulate at recombination intermediates even prior to completion of

520 synapsis in budding yeast, and likely in other organisms. Alternatively, coupled positive and
521 negative regulation may give rise to a periodic standing wave, or Turing pattern (Turing,
522 1952), of CO designation potential along each chromosome. This type of patterning requires
523 interaction between two diffusible activities: an activating activity – or "morphogen," to use
524 Turing's term – that acts locally and shows autocatalytic or cooperative behavior, and an
525 inhibitory activity that acts over a greater distance. This type of pattern has intrinsic
526 periodicity that depends on the activities and diffusion rates of the activator and inhibitor.
527 Such a pattern could thus be established prior to full SC assembly, in which case
528 designation of the first CO site would spatially fix one node of the pattern (Figure 8A). A
529 Turing patterning mechanism is also consistent with evidence presented here and in
530 previous studies that stabilization of recombination intermediates and CO patterning are
531 tightly coupled. Evidence that mammalian RNF212 and Arabidopsis HEI10 act as dosage-
532 sensitive modulators of recombination rates (Qiao et al., 2014; Reynolds et al., 2013;
533 Ziolkowski et al., 2017) is compatible with either a temporally-dependent or standing wave
534 model, since an increase or decrease in these activities could alter either the rate of signal
535 propagation or the frequency of a waveform along paired chromosomes.

536 While the SC is an unusual, liquid crystalline material, liquid-liquid phase separation
537 (LLPS) has been implicated in subcellular compartmentalization of diverse signaling
538 mechanisms (Banani et al., 2017). By diffusing and interacting within a spatially confined
539 liquid compartment, biochemical signals could potentially establish a variety of periodic,
540 Turing-type patterns within cells. Analogously, diffusion of signaling molecules within cell
541 membranes can create two-dimensional patterns, which have been proposed to orchestrate

542 polarity decisions (Goryachev and Pokhilko, 2008), as well as more elaborate patterning
543 such as hexagonal arrays of stereocilia (Jacobo and Hudspeth, 2014).
544 Intriguingly, the ZHP proteins and their homologs are very similar to TRIM E3 ligases
545 (tripartite motif: RING, B-box, coiled-coil domain), a very large family of enzymes with
546 diverse cellular roles. The functions of most TRIM ligases are unknown, but like the ZHP
547 proteins, they often form homo-or heterodimers, and many of these proteins appear to
548 localize to cellular compartments, including globular nuclear and cytoplasmic bodies, or to
549 filamentous structures such as microtubules (Rajsbaum et al., 2014; Reymond et al., 2001).
550 Thus, we speculate that compartmentalized regulatory mechanisms with similarities to the
551 circuitry illuminated here may control other spatially-patterned activities within cells.
552
553 **Conservation and divergence of the Zip3/ZHP protein family**
554 RING finger proteins homologous to the ZHP family play important roles in CO
555 formation in diverse eukaryotes. Interestingly, the number of these proteins varies among
556 organisms (Agarwal and Roeder, 2000; Ahuja et al., 2017; Chelysheva et al., 2012; Gray
557 and Cohen, 2016; Lake et al., 2015; Qiao et al., 2014; Rao et al., 2017; Reynolds et al.,
558 2013; Wang et al., 2012; Ward et al., 2007; Zhang et al., 2014a). The cytological
559 distributions and apparent functions of ZHP-3/4 and ZHP-1/2 are very similar to those
560 reported for the mammalian recombination regulators RNF212 and HEI10, respectively. Like
561 ZHP-3/4, mouse RNF212 is required to stabilize recombination intermediates (Reynolds et
562 al., 2013), while HEI10, like ZHP-1/2, is required to limit the number of RNF212/MutSɣ-
563 positive foci along chromosomes and for robust CO maturation (Qiao et al., 2014). Most

564 ZHP homologs also contain predicted coiled-coil domains and localize to the central region
565 of the SC, including Zip3 in budding yeast, which forms foci along chromosomes but
566 localizes throughout polycomplexes. A notable exception is a recently identified homolog
567 required for crossovers in the ciliate *Tetrahymena thermophila*. This protein lacks a coiled-
568 coil domain, likely related to the fact that this organism lacks SCs (Shodhan et al., 2017).

569 HEI10 in *Sordaria* and *Arabidopsis*, and Zip3 in budding yeast, may be bifunctional
570 proteins with roles similar to both ZHP-1/2 and ZHP-3/4, as suggested by their localization
571 to CO sites and the apparent absence of RNF212 in these clades (Agarwal and Roeder,
572 2000; Chelysheva et al., 2012; De Muyt et al., 2014). We speculate that they could play dual
573 roles by partnering with multiple E2 conjugating enzymes, or perhaps with distinct substrate-
574 recognition factors.

575 In mammals, RNF212 and HEI10 are thought to mediate opposing pro- and anti-
576 crossover activities through SUMOylation and SUMO-dependent ubiquitylation, respectively
577 (Qiao et al., 2014; Rao et al., 2017; Reynolds et al., 2013); a similar "SUMO-ubiquitin switch"
578 has been proposed based on findings in Sordaria (De Muyt et al., 2014). In budding yeast,
579 Sordaria, and mice, SUMOylation is essential for SC assembly, and thus for CO regulation
580 (De Muyt et al., 2014; Hooker and Roeder, 2006; Klug et al., 2013; Leung et al., 2015; Lin et
581 al., 2010; Rao et al., 2017; Voelkel-Meiman et al., 2013). In *C. elegans* we do not detect
582 SUMO cytologically either along the SC or at CO sites, even with highly sensitive tools such
583 as epitope-tagged SUMO transgenes (Pelisch and Hay, 2016; data not shown). Further,
584 genetic analysis has indicated that SMO-1 (SUMO) and its E2 conjugating enzyme UBC-9
585 are dispensable for synapsis and CO control in *C. elegans*, although they play key roles

586 downstream of COs to mediate meiotic chromosome segregation in oocytes (Bhalla et al.,
587 2008; Pelisch et al., 2017). Taken together, we favor the idea that each pair of ZHP proteins
588 acts as a ubiquitin ligase, like the "lion's share" of RING finger proteins (Deshaies and
589 Joazeiro, 2009).

590 Our analysis also reveals that the *C. elegans* ZHP proteins likely function as
591 heterodimers, or perhaps as higher order oligomers. It will be interesting to determine
592 whether ZHP homologs in other organisms also have obligate partners, or perhaps
593 homooligomerize, since this knowledge may help to illuminate their *in vivo* activities and
594 substrates.

595

596 **Regulation of sister chromatid cohesion by the ZHP family**

597 In addition to their roles in CO control, the ZHP family also link COs to chromosome
598 remodeling, which enables the stepwise release of cohesion during the MI and MII divisions
599 (Figure 8). Specifically, we find that CO designation results in enrichment of ZHP-1/2 along
600 one chromosome arm, which in turn promotes concentration of PLK-2 within this domain,
601 asymmetric disassembly of the SC, and spatial regulation of cohesin function.

602 It is not clear whether sister chromatid cohesion during meiosis is regulated in the
603 same fashion in other organisms. In budding and fission yeasts, Drosophila, diverse plants,
604 and mammals, cohesion near centromeres is specifically retained during the first division
605 (Duro and Marston, 2015). Cohesin complexes containing the meiosis-specific kleisin Rec8
606 are enriched in pericentromeric heterochromatin and sometimes at centromere cores, and
607 Shugoshin/MEI-S332, a Rec8-specific protective factor, is also recruited to these regions. In

608 principle, programmed release of cohesion along arms and its retention near centromeres
609 could suffice to allow homologs to segregate in MI while maintaining a link between sisters
610 until MII. However, experimental evidence from several organisms indicates that CO
611 formation leads to a local disruption of cohesion, which can predispose chromosomes to
612 missegregate when COs occur close to centromeres (Brar and Amon, 2008). In light of
613 other similarities between ZHP-1/2 and HEI10, this raises the possibility that HEI10 may
614 also influence sister chromatid cohesion, perhaps via spatial control of Polo-like kinases,
615 which promote release of cohesion in mitosis and meiosis (Archambault and Glover, 2009).
616 If so, HEI10 activity may directly impact chromosome missegregation in human oocytes,
617 which has been attributed to compromised cohesion, and also – very recently – to inefficient
618 CO maturation (Wang et al., 2017), another process that involves HEI10.
619

620 # Materials and methods

621 ## Key Resources Table

Reagent type (species) or resource	Designation	Source or reference	Identifiers	Additional information
gene (*Caenorhabditis elegans*)	*zhp-1*	Wormbase/This paper	Wormbase ID: F55A12.10; WBGene00018867	
gene (*Caenorhabditis elegans*)	*zhp-2*	Wormbase/This paper	Wormbase ID: D1081.9; WBGene00008387	
gene (*Caenorhabditis elegans*)	*zhp-3*	Wormbase/(Jantsch et al., 2004) PMID: 15340062	Wormbase ID: K02B12.8b; WBGene00006976	
gene (*Caenorhabditis elegans*)	*zhp-4*	Wormbase/This paper	Wormbase ID: Y39B6A.16; WBGene00012678	
gene (*Caenorhabditis elegans*)	*S. cerevisiae*: MaV203	Invitrogen	Cat#11445012	
gene (*Caenorhabditis elegans*)	For *C. elegans* allele and strain information, see Supplementary File 1, Tables S2 and S4.	This paper	N/A	
gene (*Caenorhabditis elegans*)	For CRISPR/Cas9 reagents, see sequence-based reagent and peptide, recombinant protein.	This paper	N/A	
gene (*Caenorhabditis elegans*)	Rabbit polyclonal anti-SYP-1	(MacQueen et al., 2002) PMID: 12231631	N/A	(1:500 IF)
gene (*Caenorhabditis elegans*)	Rabbit polyclonal anti-SYP-2	(Colaiácovo et al., 2003) PMID: 12967565	N/A	(1:500 IF)
gene (*Caenorhabditis elegans*)	Rabbit polyclonal anti-HTP-1	(Martinez-Perez et al., 2008) PMID: 18923085	N/A	(1:500 IF)

gene (*Caenorhabditis elegans*)	Rabbit polyclonal anti-RAD-51	Novus Biologicals	Cat#29480002	(1:5,000 IF)
gene (*Caenorhabditis elegans*)	Rabbit polyclonal anti-pHIM-8/ZIMs	(Kim et al., 2015) PMID: 26506311	N/A	(1:500 IF)
gene (*Caenorhabditis elegans*)	Rabbit polyclonal anti-ZHP-3	ModENCODE/SDIX; (Rog et al., 2017) PMID: 28045371	Cat#SDQ3956	(1:5,000 IF)
gene (*Caenorhabditis elegans*)	Rabbit polyclonal anti-MSH-5	ModENCODE/SDIX	Cat#SDQ2376	(1:5,000 IF)
gene (*Caenorhabditis elegans*)	Rabbit polyclonal anti-REC-8	ModENCODE/SDIX	Cat#SDQ0802	(1:5,000 IF)
gene (*Caenorhabditis elegans*)	Rabbit polyclonal anti-COH-3	ModENCODE/SDIX	Cat#SDQ3972	(1:5,000 IF)
gene (*Caenorhabditis elegans*)	Rat polyclonal anti-HIM-8	(Phillips et al., 2005) PMID: 16360035	N/A	(1:500 IF)
gene (*Caenorhabditis elegans*)	Goat polyclonal anti-SYP-1	(Harper et al., 2011) PMID: 22018922	N/A	(1:300 IF)
gene (*Caenorhabditis elegans*)	Chicken polyclonal anti-HTP-3	(MacQueen et al., 2005) PMID: 16360034	N/A	(1:500 IF)
gene (*Caenorhabditis elegans*)	Guinea pig polyclonal anti-HTP-3	(MacQueen et al., 2005) PMID: 16360034	N/A	(1:500 IF) (1:1,500 WB)
gene (*Caenorhabditis elegans*)	Guinea pig polyclonal anti-PLK-2	(Harper et al., 2011) PMID: 22018922	N/A	(1:100 IF)
gene (*Caenorhabditis elegans*)	Rabbit polyclonal anti-V5	Sigma-Aldrich	Cat#V8137; RRID:AB_261889	(1:250 IF)
gene (*Caenorhabditis elegans*)	Mouse monoclonal anti-V5	Thermo Fisher Scientific	Cat#R960-25; RRID:AB_2556564	(1:500 IF) (1:1,000 WB)

gene (*Caenorhabditis elegans*)	Mouse monoclonal anti-FLAG M2	Sigma-Aldrich	Cat#F1804; RRID:AB_262044	(1:500 IF) (1:1,000 WB)
gene (*Caenorhabditis elegans*)	Mouse monoclonal anti-HA, clone 2-2.2.14	Thermo Fisher Scientific	Cat#26183; RRID:AB_10978021	(1:400 IF) (1:1,000 WB)
gene (*Caenorhabditis elegans*)	Mouse monoclonal anti-GFP	Roche	Cat#11814460001; RRID:AB_390913	(1:500 IF) (1:1,000 WB)
gene (*Caenorhabditis elegans*)	Mouse monoclonal anti-α-tubulin, clone DM1A	Millipore	Cat#05-829; RRID:AB_310035	(1:5,000 WB)
gene (*Caenorhabditis elegans*)	eft-3p::AID::GFP::unc-54 3'UTR	(Zhang et al., 2015) PMID: 26552885; Addgene	pLZ29; Addgene plasmid #71719	
gene (*Caenorhabditis elegans*)	cDNA zhp-1	Wormbase	Wormbase ID: F55A12.10; WBGene00018867	
gene (*Caenorhabditis elegans*)	cDNA zhp-2	Wormbase	Wormbase ID: D1081.9; WBGene00008387	
gene (*Caenorhabditis elegans*)	cDNA zhp-3	Wormbase	Wormbase ID: K02B12.8b; WBGene00006976	
gene (*Caenorhabditis elegans*)	cDNA zhp-4	Wormbase (codon-optimized by Integrated DNA Technologies to facilitate gBlock synthesis)	Wormbase ID: Y39B6A.16; WBGene00012678	
gene (*Caenorhabditis elegans*)	Plasmid: pDEST32-zhp-1-V5	This paper	N/A	
gene (*Caenorhabditis elegans*)	Plasmid: pDEST32-zhp-2-3xFLAG	This paper	N/A	
gene (*Caenorhabditis elegans*)	Plasmid: pDEST32-zhp-3-3xFLAG	This paper	N/A	

gene (*Caenorhabditis elegans*)	Plasmid: pDEST32-zhp-4-HA	This paper	N/A	
gene (*Caenorhabditis elegans*)	Plasmid: pDEST22-zhp-1-V5	This paper	N/A	
gene (*Caenorhabditis elegans*)	Plasmid: pDEST22-zhp-2-3xFLAG	This paper	N/A	
gene (*Caenorhabditis elegans*)	Plasmid: pDEST22-zhp-3-3xFLAG	This paper	N/A	
gene (*Caenorhabditis elegans*)	Plasmid: pDEST22-zhp-4-HA	This paper	N/A	
gene (*Caenorhabditis elegans*)	FISH probe to the right arm of chromosome V (5S rDNA)	(Dernburg et al., 1998) PMID: 9708740	N/A	
gene (*Caenorhabditis elegans*)	FISH Probe to the right arm of X chromosome	(Philips et al., 2005) PMID: 16360035	N/A	
gene (*Caenorhabditis elegans*)	CRISPR tracrRNA	Integrated DNA Technologies	Cat#1072534	
gene (*Caenorhabditis elegans*)	For crRNAs, repair templates and genotyping primers, see Supplementary File 1, Table S3	This paper	N/A	
gene (*Caenorhabditis elegans*)	S. pyogenes Cas9-NLS purified protein	QB3 MacroLab at UC Berkeley	N/A	
gene (*Caenorhabditis elegans*)	Auxin: 1H-Indole-3-acetic acid	ACROS ORGANICS	Cat#122160250; CAS:87-51-4	
gene (*Caenorhabditis elegans*)	NuSieve 3:1 agarose	Lonza	Cat#50090	
gene (*Caenorhabditis*	Nuclease-Free Duplex Buffer	Integrated DNA Technologies	Cat#11-01-03-01	

elegans)				
gene (*Caenorhabditis elegans*)	SuperSignal West Femto Maximum Sensitivity Substrate kit	Thermo Fisher Scientific	Cat #34095	
gene (*Caenorhabditis elegans*)	SoftWorx package	Applied Precision; GE Healthcare Life Sciences	http://www.gelifesciences.com/webapp/wcs/stores/servlet/productById/en/GELifeSciences-us/29065728	
gene (*Caenorhabditis elegans*)	ImageJ	NIH	https://imagej.nih.gov/ij/	
gene (*Caenorhabditis elegans*)	Adobe Photoshop CC 2014	Adobe	http://www.adobe.com/products/photoshop.html	
gene (*Caenorhabditis elegans*)	T-COFFEE	Swiss Institute of Bioinformatics; (Notredame et al., 2000) PMID: 10964570	http://tcoffee.vital-it.ch/apps/tcoffee/index.html	
gene (*Caenorhabditis elegans*)	IBS_1.0.1	(Liu et al., 2015) PMID: 26069263	http://ibs.biocuckoo.org/download.php	
gene (*Caenorhabditis elegans*)	Clustal Omega	EMBL-EBI	http://www.clustal.org/omega/	
gene (*Caenorhabditis elegans*)	Graphpad Prism	Graphpad Software, Inc	http://www.graphpad.com/	
gene (*Caenorhabditis elegans*)	MSG software package	(Andolfatto et al., 2011) PMID: 21233398	https://github.com/JaneliaSciComp/msg	

622

623 **Generation of transgenic worm strains**

624 All *C. elegans* strains were maintained on nematode growth medium (NGM) plates

625 seeded with OP50 bacteria at 20°C. All epitope-tagged genes used in this study were fully

626 functional, as indicated by their ability to support normal meiosis (Supplementary File 1,
627 Table S1). New alleles and their detailed information are listed in Supplementary File 1,
628 Tables S2 and S3. Unless otherwise indicated, new alleles in this study were generated by
629 genome editing, by injection of Cas9-gRNA RNP complexes, using *dpy-10* Co-CRISPR to
630 enrich for edited progeny (Arribere et al., 2014; Paix et al., 2015). Cas9-NLS protein was
631 produced by the MacroLab at UC Berkeley. The protein was complexed *in vitro* with
632 equimolar quantities of duplexed tracrRNA and target-specific crRNAs, purchased from
633 Integrated DNA Technologies (IDT). Repair templates were single- or double-stranded
634 amplicons generated by asymmetric or standard PCR, respectively, or Ultramer
635 oligonucleotides purchased from IDT. Each 10 μl of injection mixture contained: 16 μM
636 [Cas9 protein + gRNA] (target gene + *dpy-10*), plus 0.16-2μM long and/or 6μM
637 oligonucleotide repair templates. In cases where Unc worms were injected (*e.g.,* to tag *zhp*
638 genes in a *syp-1(me17)/nT1* strain), plasmids encoding green fluorescent reporter proteins
639 were co-injected to enrich for edited progeny.

640 Injected animals were transferred to individual plates and incubated at 20˚C. After 4
641 days, F1 Rol or Dpy progeny (*dpy-10* heterozygotes or homozygotes, respectively) from
642 "jackpot" broods containing multiple Rol/Dpy animals were picked to individual plates,
643 allowed to produce self-progeny, then lysed and screened by PCR.

644 Disruption of the *zhp-1* gene was accomplished by inserting the sequence
645 TAAGCTCGAG after the 6th codon, introducing a stop codon, a frameshift, and an Xho I
646 restriction site. Three independent alleles of the same sequence were generated: *ie43* and
647 *ie44* in the N2 strain background, and *ie46* in the CB4856 strain. The *zhp-2* gene was

648 similarly disrupted by insertion of TAATAATTAATTAG after the 7th codon, resulting in
649 multiple stop codons and a frameshift.

650 See Supplementary File 1, Table S4 for a full list of strains used. Unless otherwise
651 indicated, young adults were used for both immunofluorescence and Western blotting
652 assays. Synchronized young adults were obtained by picking L4 larvae and culturing them
653 for 20-24 h at 20°C.

654

655 **Auxin-mediated protein depletion**

656 To deplete AID-tagged proteins in a strain expressing the *AtTIR1* transgene, animals
657 were treated with auxin (indole acetic acid, IAA) as previously described (Zhang et al., 2015).
658 Briefly, NGM agar was supplemented with 1mM IAA just before pouring plates. *E. coli* OP50
659 bacteria cultures were concentrated and spread on plates, which were allowed to dry before
660 transferring *C. elegans* onto the plates.

661 We note that two major advantages of the AID system have facilitated our study of
662 these proteins in meiosis: i) this approach enables temporal control and germline-specific
663 degradation of proteins; ii) complex strains that combine various mutations and epitope-
664 tagged alleles can be constructed far more easily, since balancer chromosomes are not
665 required to maintain conditional alleles of genes essential for reproduction. Additionally,
666 control experiments can be performed using the same strains without auxin treatment.

667

668 **Viability and fertility**

669 To quantify brood size and males among self-progeny, L4 hermaphrodites were

670 picked onto individual plates and transferred to new plates daily over 4 days. Eggs were
671 counted every day. Viable progeny and males were counted when the F1 reached the L4 or
672 adult stages. To analyze viability and fertility in the presence of auxin, L1s were transferred
673 onto auxin plates and grown to the L4 stage. Hermaphrodites were then transferred onto
674 fresh auxin plates, transferred daily over 4 days, and progeny were scored as described
675 above.
676

677 **Recombination mapping by whole-genome sequencing**

678 The *zhp-1* gene was disrupted by CRISPR/Cas9-based genome editing in both the
679 N2 Bristol and CB4856 Hawaiian strain backgrounds, as described above (allele
680 designations: *ie43* and *ie46*, respectively). By crossing animals carrying these mutations, we
681 generated N2/CB4856 hybrids lacking *zhp-1.* To map meiotic COs that occurred during
682 oogenesis in these animals, hybrid hermaphrodites were backcrossed to (*zhp-1*$^{+}$) CB4856
683 males. Hermaphrodite progeny from this cross were picked to individual 60mm plates and
684 allowed to produce self-progeny until the plates were starved. Genomic DNA was extracted
685 from these pools of progeny using Gentra Puregene Tissue Kit (Qiagen), and quantified by
686 Qubit (Invitrogen). Sequencing libraries were constructed in the Functional Genomics Lab
687 (FGL), a QB3-Berkeley Core Research Facility at UC Berkeley. DNA was Fragmented with
688 an S220 Focused-Ultrasonicator (Covaris), then cleaned & concentrated with the MinElute®
689 PCR Purification kit (QIAGEN). Library preparation was done on an Apollo 324™ with
690 PrepX™ ILM 32i DNA Library Kits (WaferGen Biosystems, Fremont, CA). 9 cycles of PCR
691 amplification were used. The average insert size of libraries was 380bp. 150PE sequencing

692 at approximately 9x coverage was carried out on an Illumina Hiseq 2500 by the Vincent J.
693 Coates Genomics Sequencing Laboratory at UC Berkeley. Two libraries for each of the
694 parental strains (N2 and CB4856) were prepared in parallel, sequenced at 30x coverage,
695 and aligned to the reference genome sequences available through Wormbase (Thompson
696 et al., 2015). To map COs, the data were analyzed using the MSG software package
697 (https://github.com/JaneliaSciComp/msg) (Andolfatto et al., 2011).
698

699 **Yeast two-hybrid analysis**

700 To test for interactions among the ZHP proteins using the yeast two-hybrid system,
701 coding sequences for ZHP-1-V5, ZHP-2-3xFLAG, ZHP-3-3xFLAG and ZHP-4-HA were
702 synthesized as gBlocks by Integrated DNA Technologies (IDT). Epitope tags were
703 appended to the protein sequences so that expression in yeast could be monitored. The
704 coding sequence for ZHP-4 was codon-optimized by IDT to facilitate gBlock synthesis and
705 expression in yeast. Each of these sequences was fused to both the GAL4 DNA binding
706 domain and the GAL4 activation domain by insertion into pDEST32 and pDEST22,
707 respectively, using the Gateway cloning system, following the manufacturer's instructions
708 (Invitrogen).

709 All possible pairwise combinations of the four ZHP proteins, including potential
710 homodimers, were tested using the ProQuest™ Two-Hybrid System (Invitrogen). Briefly,
711 each pair of bait and prey plasmids was co-transformed into yeast strain MaV203 using
712 standard LiAc-mediated transformation. To test for specific interactions, 2-4 independent
713 clones of each strain were assayed for *HIS3*, *URA3* and *LacZ* induction. Negative and

714 positive controls provided with the ProQuest™ kit (Cat. Series 10835) were run in parallel.

715

716 **Microscopy**

717 Immunofluorescence experiments were performed as previously described (Zhang et al.,
718 2015), except that samples were mounted in Prolong Diamond mounting medium with DAPI
719 (Life Technologies). Primary antibodies were obtained from commercial sources or have
720 been previously described, and were diluted as follows: Rabbit anti-SYP-1 [1:500,
721 (MacQueen et al., 2002)], Rabbit anti-SYP-2 [1:500, (Colaiacovo et al., 2003)], Rabbit anti-
722 HTP-1 [1:500, (Martinez-Perez et al., 2008)], Rabbit anti-RAD-51 (1:5,000, Novus
723 Biologicals, #29480002), Rabbit anti-pHIM-8/ZIMs [1:500, (Kim et al., 2015)], Rabbit MSH-5
724 [1:5,000, modENCODE/SDIX, #SDQ2376, (Yokoo et al., 2012)], Rabbit anti-REC-8 (1:5,000,
725 modENCODE/SDIX, #SDQ0802), Rabbit anti-COH-3 (1:5,000, modENCODE/SDIX,
726 #SDQ3972), Guinea pig anti-PLK-2 [1:100, (Harper et al., 2011)], Goat anti-SYP-1 [1:300,
727 (Harper et al., 2011)], Chicken anti-HTP-3 [1:500, (MacQueen et al., 2005)], Rabbit anti-
728 ZHP-3 [1:5,000, modENCODE/SDIX, #SDQ3956, (Rog et al., 2017)], Rat anti-HIM-8 [1:500,
729 (Phillips et al., 2005)], Mouse anti-FLAG (1:500, Sigma, #F1804), Mouse anti-HA (1:400,
730 Thermo Fisher, #26183), Mouse anti-V5 (1:500, Thermo Fisher, #R960-25), Rabbit anti-V5
731 (1:250, Sigma, #V8137), Mouse anti-GFP (1:500, Roche, #11814460001). Secondary
732 antibodies labeled with Alexa 488, Cy3 or Cy5 were purchased from Jackson
733 ImmunoResearch and used at 1:500.

734 Chromosomal *in situ* hybridization was performed as previously described (Dernburg
735 et al., 1998) with modifications. Briefly, worms were dissected and fixed essentially

736 according to the immunofluorescence protocol described above. Fixed worm gonads were
737 then washed with 2xSSCT and incubated in 50% formamide/2xSSCT overnight at 37°C.
738 Tissue and probes were denatured at 91°C for 2 min, then hybridized overnight at 37˚C.
739 Hybridized gonads were then washed and stained with DAPI. Two chromosome-specific
740 probes were used: an oligonucleotide targeting a short repetitive sequence on the X
741 chromosome (Lieb et al., 2000; Phillips et al., 2005) and the 5S rDNA repeat on the right
742 arm of chromosome V (Dernburg et al., 1998). FISH probes were labeled with aminoallyl-
743 dUTP (Sigma) by terminal transferase-mediated 3' end-labeling, followed by conjugation to
744 Alexa 488-NHS-ester (Molecular Probes) or Cy3-NHS-ester (Amersham), as previously
745 described (Dernburg, 2011)
746 All images were acquired as z-stacks through 8-μm depth at intervals of 0.2 μm using
747 a DeltaVision Elite microscope (GE) with a 100x, 1.4 N.A. oil-immersion objective. Iterative
748 3D deconvolution, image projection and colorization were carried out using the SoftWoRx
749 package and Adobe Photoshop CC 2014.
750

751 **Western blotting**

752 Adult worms were picked into SDS sample buffer and lysed by boiling for 30 min, a
753 single freeze/thaw cycle in liquid nitrogen, and occasionally vortexing. Whole worm lysates
754 were separated on 4-12% polyacrylamide gradient gels and blotted with indicated antibodies:
755 Mouse anti-GFP (1:1,000, Roche, #11814460001), Mouse anti-FLAG (1:1,000, Sigma,
756 #F1804), Mouse anti-HA (1:1,000, Thermo Fisher, #26183), Mouse anti-V5 (1:1,000,
757 Thermo Fisher, #R960-25), Mouse anti-α-tubulin (1:5,000, EMD MILLIPORE, #05-829),

758 Guinea pig anti-HTP-3 [1:1,500, (MacQueen et al., 2005)]. HRP-conjugated secondary
759 antibodies (Jackson Laboratory, #115-035-068) and SuperSignal West Femto Maximum
760 Sensitivity Substrate (Thermo Fisher, #34095) were used for detection.

761 To quantify Western blots, TIF images were collected for each blot using a Chemidoc
762 system (Bio-Rad). Integrated intensities for relevant bands were then calculated using
763 ImageJ. To normalize for sample loading, the indicated band intensity was divided by the
764 corresponding α-tubulin or HTP-3 band intensity. Each normalized band intensity is
765 expressed as the percentage of the intensity at t=0 or in a control sample.

766

767 **Quantification and statistical analysis**

768 Quantification methods and statistical parameters are indicated in the legend of each figure,
769 including error calculations (SD or SEM), *n* values, statistical tests, and p-values. $p<0.05$
770 was considered to be significant.

771

772 **Acknowledgements**

773 This work was supported by funding from the National Institutes of Health
774 (GM065591) and the Howard Hughes Medical Institute to AFD. Some strains were provided
775 by the CGC, which is funded by NIH Office of Research Infrastructure Programs (P40
776 OD010440). Genome sequencing was performed in the Vincent J. Coates Genomics
777 Sequencing Laboratory at UC Berkeley, supported by NIH S10 Instrumentation Grants
778 S10RR029668 and S10RR027303. We are grateful to Ed Ralston for assistance with the
779 irradiator and to Anne Villeneuve for the SYP-2 antiserum. We thank members of the

Dernburg lab for helpful discussions during the course of this work and for critical reading of the manuscript, Mike Rosen for pointing us to work on TRIM ligases, Leonid Mirny for calling our attention to the pioneering work of Alan Turning, and anonymous reviewers for their constructive suggestions.

Competing interests

The authors declare that no competing interests exist.

References

Agarwal, S., and Roeder, G.S. (2000). Zip3 provides a link between recombination enzymes and synaptonemal complex proteins. Cell *102*, 245-255.

Ahuja, J.S., Sandhu, R., Mainpal, R., Lawson, C., Henley, H., Hunt, P.A., Yanowitz, J.L., and Borner, G.V. (2017). Control of meiotic pairing and recombination by chromosomally tethered 26S proteasome. Science *355*, 408-411.

Andolfatto, P., Davison, D., Erezyilmaz, D., Hu, T.T., Mast, J., Sunayama-Morita, T., and Stern, D.L. (2011). Multiplexed shotgun genotyping for rapid and efficient genetic mapping. Genome Res *21*, 610-617.

Archambault, V., and Glover, D.M. (2009). Polo-like kinases: conservation and divergence in their functions and regulation. Nat Rev Mol Cell Biol *10*, 265-275.

Arribere, J.A., Bell, R.T., Fu, B.X., Artiles, K.L., Hartman, P.S., and Fire, A.Z. (2014). Efficient marker-free recovery of custom genetic modifications with CRISPR/Cas9 in Caenorhabditis elegans. Genetics *198*, 837-846.

Banani, S.F., Lee, H.O., Hyman, A.A., and Rosen, M.K. (2017). Biomolecular condensates: organizers of cellular biochemistry. Nat Rev Mol Cell Biol.

Bhalla, N., Wynne, D.J., Jantsch, V., and Dernburg, A.F. (2008). ZHP-3 acts at crossovers to couple meiotic recombination with synaptonemal complex disassembly and bivalent formation in C. elegans. PLoS Genet *4*, e1000235.

Brar, G.A., and Amon, A. (2008). Emerging roles for centromeres in meiosis I chromosome segregation. Nat Rev Genet *9*, 899-910.

Brzovic, P.S., Rajagopal, P., Hoyt, D.W., King, M.C., and Klevit, R.E. (2001). Structure of a BRCA1-BARD1 heterodimeric RING-RING complex. Nat Struct Biol *8*, 833-837.

Carlton, P.M., Farruggio, A.P., and Dernburg, A.F. (2006). A link between meiotic prophase progression and crossover control. PLoS Genet *2*, e12.

Chelysheva, L., Vezon, D., Chambon, A., Gendrot, G., Pereira, L., Lemhemdi, A., Vrielynck, N., Le Guin, S., Novatchkova, M., and Grelon, M. (2012). The Arabidopsis HEI10 is a new ZMM protein related to Zip3. PLoS Genet *8*, e1002799.

Colaiacovo, M.P., MacQueen, A.J., Martinez-Perez, E., McDonald, K., Adamo, A., La Volpe, A., and Villeneuve, A.M. (2003). Synaptonemal complex assembly in C. elegans is dispensable for loading strand-exchange proteins but critical for proper completion of recombination. Dev Cell *5*, 463-474.

de Carvalho, C.E., Zaaijer, S., Smolikov, S., Gu, Y., Schumacher, J.M., and Colaiacovo, M.P. (2008). LAB-1 antagonizes the Aurora B kinase in C. elegans. Genes Dev *22*, 2869-2885.

De Muyt, A., Zhang, L., Piolot, T., Kleckner, N., Espagne, E., and Zickler, D. (2014). E3 ligase Hei10: a multifaceted structure-based signaling molecule with roles within and beyond meiosis. Genes Dev *28*, 1111-1123.

Dernburg, A.F. (2011). Fragmentation and labeling of probe DNA for whole-mount FISH in Drosophila. Cold Spring Harb Protoc *2011*, 1527-1530.

Dernburg, A.F., McDonald, K., Moulder, G., Barstead, R., Dresser, M., and Villeneuve, A.M. (1998). Meiotic recombination in C. elegans initiates by a conserved mechanism and is dispensable for homologous chromosome synapsis. Cell *94*, 387-398.

830 Deshaies, R.J., and Joazeiro, C.A. (2009). RING domain E3 ubiquitin ligases. Annu Rev
831 Biochem *78*, 399-434.
832 Duro, E., and Marston, A.L. (2015). From equator to pole: splitting chromosomes in mitosis and
833 meiosis. Genes Dev *29*, 109-122.
834 Ferrandiz, N., Barroso, C., Telecan, O., Shao, N., Kim, H.M., Testori, S., Faull, P., Cutillas, P.,
835 Snijders, A.P., Colaiacovo, M.P.*, et al.* (2018). Spatiotemporal regulation of Aurora B
836 recruitment ensures release of cohesion during C. elegans oocyte meiosis. Nat Commun *9*,
837 834.
838 Goldstein, P. (2013). Multiple synaptonemal complexes (polycomplexes) in wild-type
839 hermaphroditic Caenorhabditis elegans and their absence in males. Russ J Nematol *21*, 73-
840 81.
841 Goodyer, W., Kaitna, S., Couteau, F., Ward, J.D., Boulton, S.J., and Zetka, M. (2008). HTP-3
842 links DSB formation with homolog pairing and crossing over during C. elegans meiosis.
843 Developmental cell *14*, 263-274.
844 Goryachev, A.B., and Pokhilko, A.V. (2008). Dynamics of Cdc42 network embodies a Turing-
845 type mechanism of yeast cell polarity. FEBS Lett *582*, 1437-1443.
846 Gray, S., and Cohen, P.E. (2016). Control of Meiotic Crossovers: From Double-Strand Break
847 Formation to Designation. Annu Rev Genet *50*, 175-210.
848 Harper, N.C., Rillo, R., Jover-Gil, S., Assaf, Z.J., Bhalla, N., and Dernburg, A.F. (2011). Pairing
849 centers recruit a Polo-like kinase to orchestrate meiotic chromosome dynamics in C.
850 elegans. Dev Cell *21*, 934-947.
851 Hayashi, M., Mlynarczyk-Evans, S., and Villeneuve, A.M. (2010). The synaptonemal complex
852 shapes the crossover landscape through cooperative assembly, crossover promotion and
853 crossover inhibition during Caenorhabditis elegans meiosis. Genetics *186*, 45-58.
854 Hodgkin, J., Horvitz, H.R., and Brenner, S. (1979). Nondisjunction Mutants of the Nematode
855 CAENORHABDITIS ELEGANS. Genetics *91*, 67-94.
856 Hooker, G.W., and Roeder, G.S. (2006). A Role for SUMO in meiotic chromosome synapsis.
857 Curr Biol *16*, 1238-1243.
858 Howell, A.S., Jin, M., Wu, C.F., Zyla, T.R., Elston, T.C., and Lew, D.J. (2012). Negative
859 feedback enhances robustness in the yeast polarity establishment circuit. Cell *149*, 322-333.
860 Jacobo, A., and Hudspeth, A.J. (2014). Reaction-diffusion model of hair-bundle morphogenesis.
861 Proc Natl Acad Sci U S A *111*, 15444-15449.
862 Jantsch, V., Pasierbek, P., Mueller, M.M., Schweizer, D., Jantsch, M., and Loidl, J. (2004).
863 Targeted gene knockout reveals a role in meiotic recombination for ZHP-3, a Zip3-related
864 protein in Caenorhabditis elegans. Mol Cell Biol *24*, 7998-8006.
865 Kaitna, S., Pasierbek, P., Jantsch, M., Loidl, J., and Glotzer, M. (2002). The aurora B kinase
866 AIR-2 regulates kinetochores during mitosis and is required for separation of homologous
867 Chromosomes during meiosis. Curr Biol *12*, 798-812.
868 Keeney, S. (2008). Spo11 and the Formation of DNA Double-Strand Breaks in Meiosis. Genome
869 Dyn Stab *2*, 81-123.
870 Keeney, S., Giroux, C.N., and Kleckner, N. (1997). Meiosis-specific DNA double-strand breaks
871 are catalyzed by Spo11, a member of a widely conserved protein family. Cell *88*, 375-384.
872 Kelly, K.O., Dernburg, A.F., Stanfield, G.M., and Villeneuve, A.M. (2000). Caenorhabditis
873 elegans msh-5 is required for both normal and radiation-induced meiotic crossing over but
874 not for completion of meiosis. Genetics *156*, 617-630.

875 Kim, Y., Kostow, N., and Dernburg, A.F. (2015). The Chromosome Axis Mediates Feedback
876 Control of CHK-2 to Ensure Crossover Formation in C. elegans. Dev Cell *35*, 247-261.
877 Kleckner, N., Zickler, D., Jones, G.H., Dekker, J., Padmore, R., Henle, J., and Hutchinson, J.
878 (2004). A mechanical basis for chromosome function. Proc Natl Acad Sci U S A *101*, 12592-
879 12597.
880 Klug, H., Xaver, M., Chaugule, V.K., Koidl, S., Mittler, G., Klein, F., and Pichler, A. (2013). Ubc9
881 sumoylation controls SUMO chain formation and meiotic synapsis in Saccharomyces
882 cerevisiae. Mol Cell *50*, 625-636.
883 Lake, C.M., Nielsen, R.J., Guo, F., Unruh, J.R., Slaughter, B.D., and Hawley, R.S. (2015). Vilya,
884 a component of the recombination nodule, is required for meiotic double-strand break
885 formation in Drosophila. Elife *4*, e08287.
886 Leung, W.K., Humphryes, N., Afshar, N., Argunhan, B., Terentyev, Y., Tsubouchi, T., and
887 Tsubouchi, H. (2015). The synaptonemal complex is assembled by a polySUMOylation-
888 driven feedback mechanism in yeast. J Cell Biol *211*, 785-793.
889 Libuda, D.E., Uzawa, S., Meyer, B.J., and Villeneuve, A.M. (2013). Meiotic chromosome
890 structures constrain and respond to designation of crossover sites. Nature *502*, 703-706.
891 Lieb, J.D., de Solorzano, C.O., Rodriguez, E.G., Jones, A., Angelo, M., Lockett, S., and Meyer,
892 B.J. (2000). The Caenorhabditis elegans dosage compensation machinery is recruited to X
893 chromosome DNA attached to an autosome. Genetics *156*, 1603-1621.
894 Lin, F.M., Lai, Y.J., Shen, H.J., Cheng, Y.H., and Wang, T.F. (2010). Yeast axial-element protein,
895 Red1, binds SUMO chains to promote meiotic interhomologue recombination and
896 chromosome synapsis. EMBO J *29*, 586-596.
897 Machovina, T.S., Mainpal, R., Daryabeigi, A., McGovern, O., Paouneskou, D., Labella, S., Zetka,
898 M., Jantsch, V., and Yanowitz, J.L. (2016). A Surveillance System Ensures Crossover
899 Formation in C. elegans. Curr Biol *26*, 2873-2884.
900 MacQueen, A.J., Colaiacovo, M.P., McDonald, K., and Villeneuve, A.M. (2002). Synapsis-
901 dependent and -independent mechanisms stabilize homolog pairing during meiotic prophase
902 in C. elegans. Genes Dev *16*, 2428-2442.
903 MacQueen, A.J., Phillips, C.M., Bhalla, N., Weiser, P., Villeneuve, A.M., and Dernburg, A.F.
904 (2005). Chromosome sites play dual roles to establish homologous synapsis during meiosis
905 in C. elegans. Cell *123*, 1037-1050.
906 Martinez-Perez, E., and Colaiacovo, M.P. (2009). Distribution of meiotic recombination events:
907 talking to your neighbors. Curr Opin Genet Dev *19*, 105-112.
908 Martinez-Perez, E., Schvarzstein, M., Barroso, C., Lightfoot, J., Dernburg, A.F., and Villeneuve,
909 A.M. (2008). Crossovers trigger a remodeling of meiotic chromosome axis composition that
910 is linked to two-step loss of sister chromatid cohesion. Genes Dev *22*, 2886-2901.
911 Mercier, R., Mezard, C., Jenczewski, E., Macaisne, N., and Grelon, M. (2015). The molecular
912 biology of meiosis in plants. Annu Rev Plant Biol *66*, 297-327.
913 Metzger, M.B., Pruneda, J.N., Klevit, R.E., and Weissman, A.M. (2014). RING-type E3 ligases:
914 master manipulators of E2 ubiquitin-conjugating enzymes and ubiquitination. Biochim
915 Biophys Acta *1843*, 47-60.
916 Muller, H.J. (1916). The mechanism of crossing-over. Am Nat *50*, 193-221.
917 Nabeshima, K., Villeneuve, A.M., and Colaiacovo, M.P. (2005). Crossing over is coupled to late
918 meiotic prophase bivalent differentiation through asymmetric disassembly of the SC. J Cell
919 Biol *168*, 683-689.

920 Nadarajan, S., Lambert, T.J., Altendorfer, E., Gao, J., Blower, M.D., Waters, J.C., and
921 Colaiacovo, M.P. (2017). Polo-like kinase-dependent phosphorylation of the synaptonemal
922 complex protein SYP-4 regulates double-strand break formation through a negative
923 feedback loop. Elife *6*.
924 Notredame, C., Higgins, D.G., and Heringa, J. (2000). T-Coffee: A novel method for fast and
925 accurate multiple sequence alignment. J Mol Biol *302*, 205-217.
926 Ozbudak, E.M., Becskei, A., and van Oudenaarden, A. (2005). A system of counteracting
927 feedback loops regulates Cdc42p activity during spontaneous cell polarization.
928 Developmental cell *9*, 565-571.
929 Page, S.L., and Hawley, R.S. (2003). Chromosome choreography: the meiotic ballet. Science
930 *301*, 785-789.
931 Paix, A., Folkmann, A., Rasoloson, D., and Seydoux, G. (2015). High Efficiency, Homology-
932 Directed Genome Editing in Caenorhabditis elegans Using CRISPR-Cas9 Ribonucleoprotein
933 Complexes. Genetics *201*, 47-54.
934 Pattabiraman, D., Roelens, B., Woglar, A., and Villeneuve, A.M. (2017). Meiotic recombination
935 modulates the structure and dynamics of the synaptonemal complex during C. elegans
936 meiosis. PLoS Genet *13*, e1006670.
937 Pelisch, F., and Hay, R.T. (2016). Tools to Study SUMO Conjugation in Caenorhabditis elegans.
938 Methods Mol Biol *1475*, 233-256.
939 Pelisch, F., Tammsalu, T., Wang, B., Jaffray, E.G., Gartner, A., and Hay, R.T. (2017). A SUMO-
940 Dependent Protein Network Regulates Chromosome Congression during Oocyte Meiosis.
941 Mol Cell *65*, 66-77.
942 Pfeuty, B., and Kaneko, K. (2009). The combination of positive and negative feedback loops
943 confers exquisite flexibility to biochemical switches. Phys Biol *6*, 046013.
944 Phillips, C.M., Wong, C., Bhalla, N., Carlton, P.M., Weiser, P., Meneely, P.M., and Dernburg,
945 A.F. (2005). HIM-8 binds to the X chromosome pairing center and mediates chromosome-
946 specific meiotic synapsis. Cell *123*, 1051-1063.
947 Qiao, H., Prasada Rao, H.B., Yang, Y., Fong, J.H., Cloutier, J.M., Deacon, D.C., Nagel, K.E.,
948 Swartz, R.K., Strong, E., Holloway, J.K.*, et al.* (2014). Antagonistic roles of ubiquitin ligase
949 HEI10 and SUMO ligase RNF212 regulate meiotic recombination. Nat Genet *46*, 194-199.
950 Rajsbaum, R., Garcia-Sastre, A., and Versteeg, G.A. (2014). TRIMmunity: the roles of the TRIM
951 E3-ubiquitin ligase family in innate antiviral immunity. J Mol Biol *426*, 1265-1284.
952 Rao, H.B., Qiao, H., Bhatt, S.K., Bailey, L.R., Tran, H.D., Bourne, S.L., Qiu, W., Deshpande, A.,
953 Sharma, A.N., Beebout, C.J.*, et al.* (2017). A SUMO-ubiquitin relay recruits proteasomes to
954 chromosome axes to regulate meiotic recombination. Science *355*, 403-407.
955 Reymond, A., Meroni, G., Fantozzi, A., Merla, G., Cairo, S., Luzi, L., Riganelli, D., Zanaria, E.,
956 Messali, S., Cainarca, S.*, et al.* (2001). The tripartite motif family identifies cell
957 compartments. EMBO J *20*, 2140-2151.
958 Reynolds, A., Qiao, H., Yang, Y., Chen, J.K., Jackson, N., Biswas, K., Holloway, J.K., Baudat,
959 F., de Massy, B., Wang, J.*, et al.* (2013). RNF212 is a dosage-sensitive regulator of
960 crossing-over during mammalian meiosis. Nat Genet *45*, 269-278.
961 Rog, O., Kohler, S., and Dernburg, A.F. (2017). The synaptonemal complex has liquid
962 crystalline properties and spatially regulates meiotic recombination factors. Elife *6*.
963 Rogers, E., Bishop, J.D., Waddle, J.A., Schumacher, J.M., and Lin, R. (2002). The aurora
964 kinase AIR-2 functions in the release of chromosome cohesion in Caenorhabditis elegans
965 meiosis. J Cell Biol *157*, 219-229.

966 Rosu, S., Zawadzki, K.A., Stamper, E.L., Libuda, D.E., Reese, A.L., Dernburg, A.F., and
967 Villeneuve, A.M. (2013). The C. elegans DSB-2 protein reveals a regulatory network that
968 controls competence for meiotic DSB formation and promotes crossover assurance. PLoS
969 Genet *9*, e1003674.
970 Roth, T.F. (1966). Changes in Synaptinemal Complex during Meiotic Prophase in Mosquito
971 Oocytes. Protoplasma *61*, 346-&.
972 Severson, A.F., Ling, L., van Zuylen, V., and Meyer, B.J. (2009). The axial element protein HTP-
973 3 promotes cohesin loading and meiotic axis assembly in C. elegans to implement the
974 meiotic program of chromosome segregation. Genes Dev *23*, 1763-1778.
975 Severson, A.F., and Meyer, B.J. (2014). Divergent kleisin subunits of cohesin specify
976 mechanisms to tether and release meiotic chromosomes. Elife *3*, e03467.
977 Shinohara, M., Hayashihara, K., Grubb, J.T., Bishop, D.K., and Shinohara, A. (2015). DNA
978 damage response clamp 9-1-1 promotes assembly of ZMM proteins for formation of
979 crossovers and synaptonemal complex. J Cell Sci *128*, 1494-1506.
980 Shodhan, A., Kataoka, K., Mochizuki, K., Novatchkova, M., and Loidl, J. (2017). A Zip3-like
981 protein plays a role in crossover formation in the SC-less meiosis of the protist Tetrahymena.
982 Mol Biol Cell *28*, 825-833.
983 Sturtevant, A.H. (1915). Castle and Wright on Crossing over in Rats. Science *42*, 342.
984 Sym, M., and Roeder, G.S. (1994). Crossover interference is abolished in the absence of a
985 synaptonemal complex protein. Cell *79*, 283-292.
986 Thompson, O.A., Snoek, L.B., Nijveen, H., Sterken, M.G., Volkers, R.J., Brenchley, R., Van't Hof,
987 A., Bevers, R.P., Cossins, A.R., Yanai, I.*, et al.* (2015). Remarkably Divergent Regions
988 Punctuate the Genome Assembly of the Caenorhabditis elegans Hawaiian Strain CB4856.
989 Genetics *200*, 975-989.
990 Tsubouchi, T., Zhao, H., and Roeder, G.S. (2006). The meiosis-specific zip4 protein regulates
991 crossover distribution by promoting synaptonemal complex formation together with zip2.
992 Developmental cell *10*, 809-819.
993 Turing, A.M. (1952). The Chemical Basis of Morphogenesis. Philos T Roy Soc B *237*, 37-72.
994 Voelkel-Meiman, K., Moustafa, S.S., Lefrancois, P., Villeneuve, A.M., and MacQueen, A.J.
995 (2012). Full-length synaptonemal complex grows continuously during meiotic prophase in
996 budding yeast. PLoS Genet *8*, e1002993.
997 Voelkel-Meiman, K., Taylor, L.F., Mukherjee, P., Humphryes, N., Tsubouchi, H., and Macqueen,
998 A.J. (2013). SUMO localizes to the central element of synaptonemal complex and is
999 required for the full synapsis of meiotic chromosomes in budding yeast. PLoS Genet *9*,
1000 e1003837.
1001 Wang, K., Wang, M., Tang, D., Shen, Y., Miao, C., Hu, Q., Lu, T., and Cheng, Z. (2012). The
1002 role of rice HEI10 in the formation of meiotic crossovers. PLoS Genet *8*, e1002809.
1003 Wang, S., Hassold, T., Hunt, P., White, M.A., Zickler, D., Kleckner, N., and Zhang, L. (2017).
1004 Inefficient Crossover Maturation Underlies Elevated Aneuploidy in Human Female Meiosis.
1005 Cell *168*, 977-989 e917.
1006 Ward, J.O., Reinholdt, L.G., Motley, W.W., Niswander, L.M., Deacon, D.C., Griffin, L.B.,
1007 Langlais, K.K., Backus, V.L., Schimenti, K.J., O'Brien, M.J.*, et al.* (2007). Mutation in mouse
1008 hei10, an e3 ubiquitin ligase, disrupts meiotic crossing over. PLoS Genet *3*, e139.
1009 Wu, L.C., Wang, Z.W., Tsan, J.T., Spillman, M.A., Phung, A., Xu, X.L., Yang, M.C., Hwang, L.Y.,
1010 Bowcock, A.M., and Baer, R. (1996). Identification of a RING protein that can interact in vivo
1011 with the BRCA1 gene product. Nat Genet *14*, 430-440.

1012 Yokoo, R., Zawadzki, K.A., Nabeshima, K., Drake, M., Arur, S., and Villeneuve, A.M. (2012).
1013 COSA-1 reveals robust homeostasis and separable licensing and reinforcement steps
1014 governing meiotic crossovers. Cell *149*, 75-87.

1015 Yu, Z., Kim, Y., and Dernburg, A.F. (2016). Meiotic recombination and the crossover assurance
1016 checkpoint in Caenorhabditis elegans. Semin Cell Dev Biol *54*, 106-116.

1017 Zalevsky, J., MacQueen, A.J., Duffy, J.B., Kemphues, K.J., and Villeneuve, A.M. (1999).
1018 Crossing over during Caenorhabditis elegans meiosis requires a conserved MutS-based
1019 pathway that is partially dispensable in budding yeast. Genetics *153*, 1271-1283.

1020 Zhang, L., Espagne, E., de Muyt, A., Zickler, D., and Kleckner, N.E. (2014a). Interference-
1021 mediated synaptonemal complex formation with embedded crossover designation. Proc Natl
1022 Acad Sci U S A *111*, E5059-5068.

1023 Zhang, L., Liang, Z., Hutchinson, J., and Kleckner, N. (2014b). Crossover patterning by the
1024 beam-film model: analysis and implications. PLoS Genet *10*, e1004042.

1025 Zhang, L., Ward, J.D., Cheng, Z., and Dernburg, A.F. (2015). The auxin-inducible degradation
1026 (AID) system enables versatile conditional protein depletion in C. elegans. Development *142*,
1027 4374-4384.

1028 Ziolkowski, P.A., Underwood, C.J., Lambing, C., Martinez-Garcia, M., Lawrence, E.J.,
1029 Ziolkowska, L., Griffin, C., Choi, K., Franklin, F.C., Martienssen, R.A.*, et al.* (2017). Natural
1030 variation and dosage of the HEI10 meiotic E3 ligase control Arabidopsis crossover
1031 recombination. Genes Dev *31*, 306-317.

1032

1033

1034 ## Figure legends

1035 **Figure 1. ZHP proteins exhibit two distinct patterns of dynamic localization.**

1036 (A-D) Projection images showing immunofluorescent localization of 3xFLAG tagged
1037 ZHP-1 (A), ZHP-2 (B), ZHP-3 (C) and ZHP-4 (D) relative to SCs (marked by SYP-1) and
1038 CO sites (marked by GFP-COSA-1) from mitosis to early diakinesis in the germ line.
1039 Insets in each panel show representative images of ZHP localization in (left to right)
1040 early pachytene (EP), mid-pachytene (MP), late pachytene (LP) and diplotene (Di)
1041 nuclei. Inserts with higher magnification images highlight of the localization patterns of
1042 ZHPs (red) from MP to Di. Gray lines, blue line and green focus represent the
1043 chromosome axis, central region of the synaptonemal complex (SC) and CO site,
1044 respectively. ZHP-1 and ZHP-2 show identical dynamics: they localize to assembling
1045 SCs, and upon the appearance of COSA-1 foci they become restricted to the short arm
1046 of each bivalent. ZHP-3 and ZHP-4 also mirror each other, localizing initially throughout
1047 the SC, and then accumulating at one site along each chromosome pair, concomitant
1048 with the appearance of COSA-1 at these sites. By late pachynema, 100% of GFP-
1049 COSA-1 foci colocalize with ZHP-4 puncta (n= 2,700 COSA-1 foci in 450 nuclei from 8
1050 gonads [11 rows of cells per gonad] were scored). 3F indicates 3xFLAG. Scale bars,
1051 5μm.

1052

1053

1054 **Figure 1—figure supplement 1. Sequence alignment of *C. elegans* ZHPs, and the**
1055 **evolution of ZHPs in nematodes.**

1056 (A) Sequence alignment of *C. elegans* F55A12.10 (ZHP-1), D1081.9 (ZHP-2), K02B12.8
1057 (ZHP-3) and Y39B6A.16 (ZHP-4) generated with T-Coffee (Notredame et al., 2000).
1058 Dark and gray shading indicate identical and similar residues, respectively. Asterisks
1059 indicate residues involved in zinc coordination. (B) Schematic showing the domain
1060 organization of the four ZHP proteins. RING: RING finger domain; CC: coiled coil.
1061 Numbers indicate amino acid positions. (C) Phylogenetic relationship of ZHPs from
1062 different Caenorhabditids: *Ce, C. elegans, Cb, C. briggsae; Cr, C. remanei.* (D)
1063 Sequence alignment of the C-terminal domain of the four ZHPs from Caenorhabditids.
1064 The C-termini of the same ZHP protein from different nematodes are much more
1065 conserved than the C-termini of the different ZHPs from the same nematode. CT: C-
1066 terminus. Dark and gray shading indicate identical and similar residues, respectively.
1067

1068 **Figure 1—figure supplement 2. Absence of nonspecific staining with anti-FLAG**
1069 **antibodies in the *C. elegans* germline.**
1070 Projection images showing *C. elegans* germline immunostained with anti-3xFLAG
1071 epitope antibody (red) and anti-SYP-1 antibody (indicating synaptonemal complex (SC),
1072 blue). Insets in each panel show representative nuclei (left to right) in early pachytene
1073 (EP), mid-pachytene (MP), late pachytene (LP) and diplotene (Di). Anti-FLAG antibody
1074 staining shows no obvious unspecific signal in the germline. Mitotic and TZ indicate
1075 Mitotic zone and Transition Zone, respectively. WT: wild-type. Scale bars, 5μm.
1076

1077 **Figure 1—figure supplement 3. Localization of the ZHPs along meiotic**

1078 **chromosomes depends on SCs.**

1079 (A,B) Projection images of mid- and late pachytene nuclei, showing the localization of
1080 ZHP-2-HA (A) and ZHP-4-HA (B) in *syp-1* mutant hermaphrodites and heterozygous
1081 controls. Chromosome axes are marked by HTP-3 (red). (C) Projection images of mid-
1082 and late pachytene nuclei showing the localization of ZHP-1-V5 (green) and ZHP-3-
1083 3xFLAG (cyan) in *syp-1* mutants and control animals. Chromosome axes are marked by
1084 HTP-3 (red). Association of ZHPs along chromosomes was abolished in the absence of
1085 synapsis. (D) Projection images of mid- and late pachytene nuclei showing the
1086 localization of ZHP-3-3xFLAG (cyan) and RAD-51 (green) in *syp-1* mutants.
1087 Chromosome axes are marked by HTP-3 (red). The nuclear puncta of ZHP-3 do not
1088 colocalize with DSB repair sites. Scale bars, 5μm. (E,G,I) Western blots showing the
1089 abundance of ZHP proteins in *syp-1* mutants and control worms. Protein from an equal
1090 number of animals was loaded in each lane, and HTP-3 was blotted as a loading control.
1091 (F,H,J,K) Quantification of Western blots. The ZHP band intensity was normalized
1092 against HTP-3 and expressed as percentage of the intensity in a control sample. Data
1093 are presented as mean±SD protein levels from three independent experiments.

1094

1095 **Figure 2. ZHPs likely act as two heterodimeric protein complexes.**

1096 (A-H) Projection images of mid-pachytene and diplotene nuclei, showing the localization
1097 of ZHPs (green), with corresponding Western blots to assess protein levels in the
1098 presence and absence of their partners. SCs are marked by SYP-1 (red). Tubulin was
1099 blotted as a loading control. Localization of each ZHP to SCs was abolished when its

1100 partner was depleted by auxin treatment for 24 h. In the absence of their partners, the
1101 ZHPs were also destabilized. Scale bars, 5μm. (I) Yeast 2-hybrid interactions monitored
1102 by β-galactosidase expression reveal specific interactions between ZHP-1 and ZHP-2,
1103 and ZHP-3 and ZHP-4, respectively. No interactions were detected for other
1104 combinations. "Empty" indicates the same vector with no insert. None control: pPC97
1105 and pPC86 with no insert; weak control: pPC97-human RB amino acids 302-928 and
1106 pPC86-human E2F1 amino acids 342-437; moderate control: pPC97-*Drosophila* DP
1107 amino acids 1-377 and pPC86-*Drosophila* E2F amino acids 225-433; and strong control:
1108 pPC97-rat cFos amino acids 132-211 and pPC86-mouse cJun amino acids 250-325.
1109

1110 **Figure 2—figure supplement 1. Depletion of ZHP proteins using the AID system.**
1111 (A) Western blots showing robust, rapid degradation of AID-tagged ZHP proteins in
1112 animals exposed to 1 mM auxin. Blots were done with anti-FLAG and anti-tubulin
1113 antibodies, respectively. Tubulin was blotted as a loading control. 3F: 3xFLAG. (B)
1114 Degradation kinetics of AID-tagged ZHPs. Proteins were quantified by Western blotting,
1115 normalized against tubulin controls. The graph shows the mean±SD protein levels from
1116 three independent experiments. (C) Frequencies of males and viable embryos observed
1117 among whole broods for the indicated genotypes and conditions. No meiotic defects
1118 were observed in animals expressing ZHP-3-AID under standard culture conditions, but
1119 in the presence of 1mM auxin this strain quantitatively phenocopies a *zhp-3(jf61)* null
1120 mutant. Reported viability of >100% is a consequence of failing to count some embryos.
1121

1122 **Figure 2—figure supplement 2. Additional antibody validation, ZHP-4 in *zhp-3***
1123 **mutants, and yeast 2-hybrid analysis of ZHP protein interactions.**
1124 (A,B) Projection images showing dissected *C. elegans* gonads stained with anti-HA
1125 antibodies (green) (A) or anti-V5 antibodies (green) (B), and anti-SYP-1 antibodies (red).
1126 Anti-epitope antibodies do not appear to detect endogenous proteins in wild-type *C.*
1127 *elegans*. WT: wild-type. Scale bars, 5*μ*m. (C) Projection images of pachytene and
1128 diplotene nuclei in *zhp-3* null mutants, revealing that the localization of ZHP-4 (green) to
1129 SCs depends on ZHP-3. Chromosome axes are marked by HTP-3 (red). Scale bars,
1130 5*μ*m. (D) Western blot showing protein levels of ZHP-4 in *zhp-3* null mutants and
1131 controls. (E) The yeast two-hybrid assay reveals specific interactions between ZHP-1
1132 and -2, and ZHP-3 and -4. No interactions were detected among other combinations of
1133 ZHP proteins. Summary of the interactions derived from β-galactosidase, HIS+3AT, and
1134 URA expression assays are shown in this table. ++ indicates a moderately strong
1135 interaction.
1136
1137 **Figure 3. ZHP proteins play a central role in chiasma formation and meiotic**
1138 **chromosome segregation.**
1139 (A-D) Upper: DAPI-stained oocyte nuclei at late diakinesis. Each panel shows a
1140 representative nucleus. Lower: Graphs indicating the distribution of DAPI-staining
1141 bodies observed at diakinesis. ZHPs tagged with AID in a $P_{sun\text{-}1}$*::TIR1* background were
1142 treated with or without auxin for 24 h. In the absence of auxin, each nucleus contains six
1143 bivalents (homolog pairs held together by chiasmata). Depletion of ZHP-1 or -2 leads to

1144 a marked decrease in bivalents per nucleus (8-12 DAPI-staining bodies, or 0-4
1145 bivalents), while depletion of ZHP-3 or -4 results in a complete loss of bivalents (12
1146 DAPI-staining bodies). *n* is the number of nuclei scored for each condition or genotype.
1147 Depletion of ZHP-1, -2, -3 or -4 significantly increase the number of DAPI-staining
1148 bodies (***$p < 0.0001$ by Chi-square test for trend). The difference between ZHP-1
1149 depletion and ZHP-2 depletion or ZHP-3 depletion and ZHP-4 depletion is not significant
1150 ($p = 0.7537$ and 0.9760, respectively, by Chi-square test for trend). The difference
1151 between depletion of ZHP-1 or ZHP-2 and depletion of ZHP-3 or ZHP-4 is significant
1152 (***$p < 0.0001$ by Chi-square test for trend). (E) Frequencies of males and viable
1153 embryos observed among the whole broods in wild-type, *zhp-1*, *zhp-2* and *zhp-3* null
1154 mutant hermaphrodites. (F-G) Sex chromosomes and autosomes show a similar
1155 reduction in chiasma formation in the absence of ZHP-1. (F) High magnification images
1156 of nuclei at late diakinesis from *zhp-1* heterozygous controls and null mutant
1157 hermaphrodites, hybridized with FISH probes recognizing either the right end of X-
1158 chromosome or 5s rDNA on chromosome V, and stained with DAPI. (G) Graph showing
1159 the frequency of bivalents observed for Chromosome V and the X chromosome.
1160 "Expected value" is the frequency for any single chromosome, given the average
1161 number of bivalents we observed, and assuming that they were distributed equally
1162 among 6 chromosome pairs. Data were derived from the number of DAPI-staining
1163 bodies in *zhp-1* heterozygotes and null mutants. Data are represented as mean ±SEM
1164 from three independent experiments ($n = 103$ and 145 nuclei, respectively). Significance
1165 was tested using the two-sided Student's *t*-test. Scale bars, 5μm.

1166

1167 **Figure 3—figure supplement 1. Chiasma formation in *zhp-1* or *zhp-3* null mutants.**

1168 (A-C) Null mutations in *zhp-1* and *zhp-3* quantitatively recapitulate the effects of AID-

1169 mediated depletion. Upper: Representative examples of DAPI-stained oocyte nuclei at

1170 diakinesis. Lower: Graphs indicating the distribution of nuclei containing various

1171 numbers of DAPI-staining bodies. Note: the observed number of DAPI-staining bodies,

1172 on average, is slightly lower than the true mean, since occasionally univalent or bivalent

1173 chromosomes in the same nucleus cannot be clearly resolved. (A) Auxin treatment does

1174 not impair chiasma formation in wild-type hermaphrodites ($p = 0.8670$ by Chi-square

1175 test for trend). (B) A few bivalents are detected in *zhp-1* null mutants, as in *zhp-1::AID*

1176 animals treated with 1 mM auxin. (C) No bivalents are observed in *zhp-3* null mutants,

1177 as in *zhp-3::AID* hermaphrodites exposed to auxin. The difference in bivalents observed

1178 in *zhp-1* and zhp-3 null mutants is significant ($p < 0.0001$ by Chi-square test for trend). *n*

1179 is the number of nuclei scored for each condition or genotype. Scale bars, 5μm.

1180

1181 **Figure 3—figure supplement 2. ZHP are dispensable for homolog pairing and**

1182 **synapsis.**

1183 (A) Projection images of representative pachytene nuclei stained for SYP-1 (green) and

1184 HTP-3 (red), revealing normal synapsis in ZHP-depleted worms. Animals expressing the

1185 indicated transgene, along with germline-expressed TIR1 protein (Zhang et al., 2015)

1186 were incubated on plates with or without 1mM auxin for 24 h before dissection. Scale

1187 bars, 5μm. (B) Images of representative early prophase nuclei stained for HIM-8

1188 (yellow), which specifically marks the pairing center region of the X chromosome
1189 (Phillips et al., 2005), and DNA (blue). Robust pairing of HIM-8 foci in early meiotic
1190 prophase is observed. Homologous pairing at other chromosomal loci was confirmed by
1191 FISH (data not shown). Scale bars, 5μm. (C) Diagram of a hermaphrodite gonad,
1192 indicating the four zones in which homolog pairing was scored. (D-G) Quantification of
1193 the pairing of X chromosomes. Gonads were divided into four zones of equal length,
1194 spanning the meiotic entry through late pachytene region. Pairing was evaluated as
1195 previously described (Harper et al., 2011). The average percentage of nuclei with paired
1196 X chromosomes is plotted for each zone. Data are presented as mean±SD (n = 3
1197 gonads for each genotype or condition). No pairing defects were detected following
1198 depletion of ZHP-1, -2, -3, or -4 (p = 0.7059, 0.3631, 0.6188, 0.3064, 0.0554, 0.5515,
1199 0.2639, 0.4158, 0.1893, 0.9247, 0.8599, 0.3740, 0.7631, 0.1672, 0.7879 and 0.2935,
1200 respectively, from zone 1 to zone 4, and *zhp-1::AID* to *zhp-4::AID*, two-sided Student *t*-
1201 test).
1202
1203 **Figure 3—figure supplement 3. ZHP are dispensable for DSB induction and the**
1204 **crossover assurance checkpoint.**
1205 (A) Projection images of mid-pachytene nuclei stained for RAD-51 (yellow) and DNA
1206 (blue), showing accumulation of DSB repair intermediates in the absence of ZHP-1 or
1207 ZHP-4. Scale bars, 5μm. (B) Diagram of a hermaphrodite gonad, indicating the six
1208 zones in which RAD-51 foci were scored. (C-F) Quantification of RAD-51 foci. Gonads
1209 were divided into six zones of equal length, spanning the premeiotic through late

1210 pachytene region. The number of RAD-51 foci in each nucleus is presented for each
1211 zone. *n* = 167, 229, 160, 200, 133, 209, 100, 131, 87, 87, 44, 62, 222, 258, 227, 274,
1212 190, 173, 158, 151, 109, 100, 68, 68, 352, 251, 283, 296, 197, 172, 167, 138, 124, 119,
1213 76, 103, 338, 317, 281, 290, 227, 171, 194, 111, 134, 102, 74 and 102 nuclei,
1214 respectively, from zone 1 to zone 6, and *zhp-1::AID* to *zhp-4::AID*. 4 gonads were
1215 scored for each genotype or condition. **p = 0.0084 and 0.0028, respectively, ***p <
1216 0.0001, Mann-Whitney test. (G-I) CHK-2 activity is extended in the absence of ZHP
1217 proteins. Low magnification images of gonads stained for pHIM-8/pZIMs (yellow) and
1218 DNA (blue). The upper gonad in each panel is a non-auxin treated control, while lower
1219 panels show gonads from animals depleted of ZHP-1 (G) or ZHP-4 (H) for ~24 h. Scale
1220 bars, 5*μ*m. (I) Quantification of the 'CHK-2 active zone,' defined as the length of the
1221 region of pHIM-8/ZIM staining as a fraction of the region from meiotic onset to the end of
1222 pachytene before nuclei form a single file. *n* = number of gonads scored for each
1223 genotype or condition. *p = 0.0199, **p = 0.0018 and 0.0021, respectively, ***p < 0.0001,
1224 two-sided Student *t*-test.
1225

1226 **Figure 4. ZHP-3/4 are required to stabilize recombination intermediates, while**
1227 **ZHP-1/2 promote accumulation of pro-CO factors at a subset of intermediates**
1228 **during late prophase.**

1229 (A-F) Low-magnification images of mid- and late pachytene nuclei stained for GFP-
1230 COSA-1 (green) and SYP-1 (red). Insets on the right showing corresponding nuclei at
1231 late pachynema. (A) Representative *zhp-4::AID;* $P_{sun\text{-}1}$*::TIR1* germline showing 6 sites

1232 per nucleus marked by bright GFP-COSA-1 foci in the absence of auxin treatment. (B)
1233 Depletion of ZHP-4 by auxin treatment for 24 h resulted in an absence of COSA-1 foci.
1234 (C) Control *zhp-1::AID;* $_{Psun\text{-}1}$*::TIR1* worm showing 6 bright GFP-COSA-1 foci per
1235 nucleus. (D) Depletion of ZHP-1 by auxin treatment for 24 h results in a large number of
1236 recombination intermediates marked by dim GFP-COSA-1 foci. Image acquisition and
1237 display were adjusted to allow the dim foci to be visualized. (E, F) Co-depletion of ZHP-
1238 1 and SPO-11 (E) or of ZHP-1 and ZHP-4 (F) results in an absence of COSA-1 foci. (G)
1239 Left: Oocyte nuclei at late diakinesis, fixed and stained with DAPI. Each panel indicates
1240 a single representative nucleus. Right: Graphs of the distribution of DAPI-staining
1241 bodies at diakinesis. Co-depletion of ZHP-1 and ZHP-4 eliminates bivalents (12 DAPI-
1242 staining bodies). The number of nuclei scored for each condition was: n = 84 and 104,
1243 respectively. (H) Quantification of COs in wild type and *zhp-1* null mutant oocytes by
1244 whole genome sequencing. n = 8 oocytes for each genotype. **p = 0.0072, Mann-
1245 Whitney test. Scale bars, 5μm.
1246

1247 **Figure 4—figure supplement 1. ZHP-3/4 are required for the appearance of MSH-5**
1248 **foci, while ZHP-1/2 limit the number of foci during late prophase.**
1249 (A-D) Recombination intermediates visualized by immunolocalization of MSH-5. Low-
1250 magnification images of pachytene nuclei stained for MSH-5 (green) and SYP-1 (red).
1251 Larger magnification insets on the right show indicated nuclei at mid-or late pachynema.
1252 (A, C) MSH-5 foci normally peak at mid-pachytene, when 10-20 can be detected per
1253 nucleus (B) No MSH-5 foci were detected when ZHP-4 was depleted for 24h. (D)

1254 Depletion of ZHP-1 caused a large increase in the number of MSH-5-positive
1255 recombination intermediates. ~40-50 foci were detected in most nuclei at late
1256 pachynema. (E) The same gonad as in (D) showing the colocalization of dim GFP-
1257 COSA-1 foci with MSH-5 foci in the absence of ZHP-1. Scale bars, 5 μm.
1258

1259 **Figure 4—figure supplement 2. Robust protein co-depletion by the AID system**
1260 **and persistence of ZHP-3 throughout SCs following ZHP-1/2 depletion.**
1261 (A) Images of representative pachytene nuclei stained for ZHP-1-AID-3xFLAG (green),
1262 RAD-51 (cyan) and SYP-1 (red). ZHP-1 and recombination intermediates were
1263 undetectable following treatment with auxin for 24 h. Scale bars, 5 μm. (B) Western
1264 blotting showing efficient co-depletion of ZHP-1 and ZHP-4. Blots were probed with anti-
1265 FLAG and anti-tubulin antibodies, respectively. Tubulin was blotted as a loading control.
1266 3F: 3xFLAG. (C) Depletion of ZHP-2 by auxin treatment for 24 h resulted in persistence
1267 of ZHP-3 throughout SCs in late pachytene nuclei. Scale bars, 5 μm.
1268

1269 **Figure 5. CO designation in the absence of ZHP-1/2.**
1270 (A) Projection images of representative late pachytene nuclei stained for GFP-COSA-1
1271 (green) and SYP-1 (red). In the absence of DSB-2 at 24 h post-L4, an average of 3
1272 bright GFP-COSA-1 foci are detected in each nucleus. However, very few bright GFP-
1273 COSA-1 foci are observed when ZHP-2 is co-depleted. By 48 h post-L4, only ~2 bright
1274 GFP-COSA-1 foci are observed per nucleus in the absence of DSB-2, and most nuclei
1275 display 0-1 bright GFP-COSA-1 focus when ZHP-2 is also depleted. (B) Quantification

1276 of bright GFP-COSA-1 foci at late pachynema, 24 h post-L4. Worms of the indicated
1277 genotypes were maintained in the presence or in the absence of 1 auxin for 24 h and
1278 then dissected for analysis. Data were derived from 4-8 gonads for each genotype or
1279 condition. *n* = 165, 348, 172 and 377 nuclei, respectively. The number of GFP-COSA-1
1280 foci differed significantly between *dsb-2::AID* and *zhp-2::AID; dsb-2::AID* following auxin
1281 treatment (***$p < 0.0001$ by Chi-square test for trend). (C) Quantification of bright GFP-
1282 COSA-1 foci in late pachytene nuclei 48 h post-L4. Data were derived from 4-8 gonads
1283 for each genotype or condition. *n* = 252, 558, 263 and 416 nuclei, respectively.
1284 Depletion of ZHP-2 significantly reduces the number of GFP-COSA-1 foci in the
1285 absence of DSB-2 (***$p<0.0001$ by Chi-square test for trend). The distribution of GFP-
1286 COSA-1 foci is also significantly different between 24 h and 48 h post-L4 for auxin
1287 treated *zhp-2::AID; dsb-2::AID* hermaphrodites (***$p<0.0001$ by Chi-square test for
1288 trend). (D) Representative images of late pachytene nuclei stained for RAD-51 (yellow),
1289 GFP-COSA-1 (green), SYP-1 (red), and DNA (blue). GFP-COSA-1 foci in the absence
1290 of ZHP-1/2 was visualized following exposure of SPO-11-depleted worms to varying
1291 doses of ionizing radiation. L4 worms were maintained in the presence or in the
1292 absence of 1 mM auxin for 24 h, followed by irradiation at the indicated dosage, and
1293 then incubated for additional 8 h to allow irradiated nuclei to progress to late pachynema.
1294 Scale bars, 5 μm.
1295
1296 **Figure 5—figure supplement 1. Validation of protein depletion, and further**
1297 **characterization of ZHP-1/2.**

1298 (A) Western blot showing efficient auxin-mediated depletion of DSB-2 alone, or co-
1299 depletion of ZHP-2 and DSB-2. Blots were probed with anti-FLAG and anti-tubulin
1300 antibodies, respectively. Tubulin was blotted as a loading control. 3F: 3xFLAG. (B) Low
1301 magnification images of gonads from worms at 48 h post-L4 stained for RAD-51 (yellow),
1302 GFP-COSA-1 (green), SYP-1 (red) and DNA (blue). RAD-51 staining in the upper panel
1303 indicates that few DSBs are induced in the absence of DSB-2. The lower panel shows
1304 GFP-COSA-1 and SYP-1 staining in the same gonad. A few bright GFP-COSA-1 foci
1305 are detected in the absence of ZHP-2 when the number of DSBs is limited by DSB-2
1306 depletion. Insets show enlargements of corresponding regions of the gonad. (C) SPO-
1307 11 activity is effectively abrogated by AID-mediated depletion. Projection images of
1308 pachytene nuclei stained for RAD-51 (yellow), GFP-COSA-1 (green), SYP-1 (red), and
1309 DNA (blue). DSBs were induced by ionizing radiation following depletion of SPO-11. No
1310 COSA-1 foci were observed in unirradiated animals, but CO designation was rescued
1311 following 10 Gy of irradiation. Scale bars, 5 μm.
1312
1313 **Figure 5—figure supplement 2. Partial depletion fails to separate the roles of**
1314 **ZHP-1/2 in limiting late recombination intermediates and promoting crossover**
1315 **maturation.**
1316 (A) Western blots showing partial depletion of AID-tagged ZHP-2 in animals exposed to
1317 low concentrations of auxin. Blots were probed with anti-FLAG and anti-tubulin
1318 antibodies, respectively. Tubulin was blotted as a loading control. 3F: 3xFLAG. (B)
1319 Quantification of ZHP-2 depletion. The intensity of ZHP-2 bands were normalized

1320 against the corresponding tubulin band, and expressed as percentage of the intensity in
1321 a control sample. The graph shows the mean±SD protein levels from three independent
1322 experiments. (C) Low-magnification images of late pachytene nuclei stained for GFP-
1323 COSA-1 (green) and SYP-1 (red). Insets on the right show representative oocyte nuclei
1324 at late diakinesis under the same conditions. In the presence of 3 μM auxin for 24 h,
1325 *zhp-2:AID;* $P_{sun\text{-}1}$*:TIR1* germline still show 6 designated CO sites per nucleus marked by
1326 bright GFP-COSA-1 foci. At 10 μM auxin, a reduced number of bright GFP-COSA-1
1327 were detected. Nuclei with more than 6 bright foci were not observed under any
1328 depletion conditions. Similar results were obtained when ZHP-1-AID was depleted (data
1329 not shown) Scale bars, 5 μm.
1330
1331 **Figure 6. ZHP-1/2 act at the top of a hierarchy of chromosome remodeling factors.**
1332 (A) Late pachytene nuclei in a *dsb-2* mutant at 48 h post-L4, stained for ZHP-3-V5
1333 (green) and SYP-2 (red). ZHP-3 is depleted and SYP-2 is enriched specifically along
1334 SCs with bright ZHP-3 foci. Boxed areas indicate nuclei shown at higher magnification
1335 to the right. Arrowheads in inset images indicate designated CO sites. (B) Late
1336 pachytene nuclei stained for ZHP-3-V5 (green), SYP-2 (red) and GFP-COSA-1 (blue). In
1337 the absence of ZHP-2 and DSB-2, ZHP-3 was still depleted from CO-designated SCs.
1338 However, enrichment of SYP proteins was not observed, (C) Higher-magnification
1339 images of diplotene nuclei from hermaphrodites depleted of DSB-2 alone or in
1340 combination with ZHP-2. The tissue was stained with antibodies against SYP-1 (green),
1341 HTP-1 (red) and GFP-COSA-1 (blue). In the absence of DSB-2 alone, SYP-1 and HTP-

1342 1 localized to reciprocal chromosome domains of bivalent chromosomes, as previously
1343 described (Machovina et al., 2016; Martinez-Perez et al., 2008). In worms depleted of
1344 both ZHP-2 and DSB-2, SYP-1 was restricted to CO sites at diplotene-diakinesis, while
1345 HTP-1/2 were retained on both short and long arms of bivalents. Asterisk indicates
1346 nuclear envelope staining due to cross-reactivity of our SYP-1 antibody, which becomes
1347 more prominent in late prophase. (D and E) Representative nuclei from the same
1348 genotypes as in (C), stained for PLK-2-HA (green), anti-SYP-2 (red) and GFP-COSA-1
1349 (blue). In the absence of DSB-2, PLK-2 became enriched on CO-designated
1350 chromosomes, after which it relocalized to the short arm of CO-designated SCs at late
1351 pachynema, as recently described (Pattabiraman et al., 2017). However, when ZHP-2
1352 and DSB-2 were co-depleted, PLK-2 was not enriched along CO-designated
1353 chromosomes, although foci were observed at CO sites. (F) Representative late
1354 pachytene and diplotene nuclei from hermaphrodites depleted of PLK-2, stained for
1355 ZHP-2-HA (green), SYP-1 (red) and GFP-COSA-1 (blue). In the absence of PLK-2, CO
1356 designation and asymmetric localization of ZHP-2 were delayed, and asymmetric
1357 disassembly of the SC was severely impaired, as previously described (Harper et al.,
1358 2011), but ZHP-2 still relocalized to the presumptive short arm during late prophase.
1359 Arrowheads indicate designated CO sites. Scale bars, 5 μm.
1360
1361 **Figure 6—figure supplement 1. ZHP-1/2 are required for chromosome remodeling.**
1362 (A-C) Images of late pachytene nuclei stained for SYP-1 (green) and HTP-1 (red). (A) In
1363 *zhp-1* heterozygotes, SYP-1 and HTP-1 show normal, reciprocal localization in late

1364 prophase. (B) In *dsb-2* null mutants 48 h post-L4, most late prophase nuclei display 2-4
1365 bright COSA-1 foci. Although disassembly of SYP-1 and HTP-1 are delayed due to
1366 activation of the CO assurance checkpoint, these proteins eventually show reciprocal
1367 localization on these CO-designated chromosomes, while univalent chromosomes
1368 retain HTP-1 but not SYP-1. (C) In *zhp-1* null mutants, SYP-1 and HTP-1 remain
1369 colocalized with each other on most chromosomes, despite the appearance of ~2-3
1370 bright COSA-1 foci at late pachytene and a similar number of bivalents at diakinesis.
1371 Univalent chromosomes also show persistent staining with both HTP-1 and SYP-1.
1372 Insets showing enlarged views of the indicated nuclei. Scale bars, 5 μm.
1373
1374 **Figure 6—figure supplement 2. ZHP-1/2 are required for chromosome remodeling.**
1375 (A,B) ZHP-2 are required for asymmetric localization of PLK-2 following crossover
1376 designation. (A) In wild-type nuclei, and in animals expressing ZHP-AID in the absence
1377 of auxin, PLK-2 (red) concentrates along the presumptive short arms during late meiotic
1378 prophase. (B) When ZHP-2 is depleted, PLK-2 localizes to a subset of recombination
1379 intermediates, but does not show asymmetric localization along the SCs. (C) High-
1380 magnification images of maturing oocytes stained for the kleisin proteins REC-8 or
1381 COH-3 and the HORMA domain protein HTP-3, which persists along all arms of
1382 bivalents. Worms were treated with or without auxin for 48 h. In the most mature, or "–1"
1383 (relative to the spermatheca) oocyte in each arm of the gonad, REC-8 normally
1384 becomes enriched on the long arms, while COH-3 is retained on short arms. In the
1385 absence of ZHP-2, removal of REC-8 from short arms was defective and retention of

1386 COH-3 was rarely observed. Scale bars, 5 μm. Scale bar for insets, 1 μm

1387

1388 **Figure 7. Compartmentalization of CO signaling within polycomplexes.**

1389 Polycomplexes assemble from SC proteins in meiotic nuclei of *htp-3* mutants. During
1390 late meiotic prophase, a single focus containing COSA-1 and ZHP-3 appears on each
1391 polycomplex (Rog et al., 2017 and data not shown). (A) ZHP-1 (not shown) and ZHP-2
1392 (green) localize throughout polycomplexes (red) both before and after the appearance
1393 of COSA-1 foci (blue). Insets show higher magnification images of the indicated
1394 polycomplexes without (left) and with (right) COSA-1 foci. (B,C) Late prophase nuclei
1395 showing polycomplexes in the presence and absence of ZHP-2 (minus and plus auxin
1396 treatment, respectively). Insets show higher magnification views of the indicated
1397 polycomplexes. (B) In the presence of ZHP-2, ZHP-3 (green) colocalize with COSA-1
1398 foci (cyan) in late meiotic prophase and become depleted from the body of
1399 polycomplexes (red). (C) In the absence of ZHP-2, ZHP-3 (green) colocalize with GFP-
1400 COSA-1, but also remain diffusely localized throughout polycomplexes. (D) Late
1401 prophase nuclei from *htp-3* mutants showing colocalization of MSH-5 (red) with GFP-
1402 COSA-1 foci (green) on the surface of polycomplexes (blue). (E,F) Late prophase nuclei
1403 from the same genotypes depicted in (B,C). (E) PLK-2 (green) localizes throughout
1404 polycomplexes (red) prior to the appearance of GFP-COSA-1 foci (blue), but staining
1405 becomes more intense in late prophase. (F) Depletion of ZHP-2 does not affect the
1406 localization of PLK-2 to polycomplexes. Scale bars in lower magnification images, 5 μm;
1407 in insets, 1 μm.

1408 **Figure 8. Schemata for crossover control and chromosome remodeling.**

1409 (A) Spatial regulation of CO designation by ZHP proteins. In early prophase, all 4 ZHPs
1410 concentrate within SCs at the interface between homologous chromosomes. DSBs are
1411 induced and homologous recombination is initiated through strand invasion.
1412 Recruitment or stabilization of MutSɣ and COSA-1 at these early intermediates
1413 depends on the presence of ZHP-3/4 within the SC. As nuclei progress through mid-
1414 prophase, one such intermediate along each chromosome stochastically crosses a
1415 threshold activity level. [We note that this is analogous to a "cracking" event posited in a
1416 beam-film model for crossover interference (Kleckner et al., 2004; Zhang et al., 2014b)].
1417 This event triggers positive and negative feedback to promote accumulation of COSA-1,
1418 MutSɣ, and ZHP-3/4 at this site and are depletion from other sites along the same SC
1419 compartment. Pro-CO activities may accumulate at a single site per chromosome pair
1420 through a winner-takes-all mechanism, or are distributed in a periodic pattern along
1421 paired chromosomes. In either scenario, diffusion of proteins within the SC permits
1422 coordinated behavior of potential CO sites along each pair of chromosomes. (B) A
1423 circuit diagram for CO control and chromosome remodeling, incorporating the findings
1424 of this work. Coupled positive and negative feedback mechanisms mediated by ZHPs
1425 and other factors lead to accumulation of pro-CO factors at a single designated
1426 crossover site. ZHP-1/2 also act at the top of a hierarchy that leads to PLK-2 enrichment
1427 on one side of the crossover and retention of the SC within this domain, creating
1428 another positive feedback loop, although how ZHP-1/2 become enriched on one side of
1429 the crossover is currently unknown. Activities within the SC antagonize the retention of

1430 HTP-1/2 and associated factors along the axis, and vice versa, resulting in the
1431 differentiation of two distinct chromosome domains. This leads to eventual removal of
1432 REC-8 from the short arm and its retention on the long arm, promoting accurate,
1433 stepwise meiotic chromosome separation.

1434 **Supplemental File 1**

1435 This file includes four tables (**Table S1-S4**). Table S1 reports analysis of the progeny
1436 produced by animals expressing epitope-tagged proteins described in this work. In all
1437 cases, animals homozygous for these epitope-tagged alleles show no reduction in
1438 embryonic viability or increase in male production, indicating that the epitope tags used
1439 to detect various proteins do not impair their meiotic functions. **Table S2** provides a list
1440 of all new alleles generated in this work, with details about the genome editing methods
1441 used to introduce epitope tags or mutations. **Table S3** includes the sequences of RNA
1442 and DNA sequences used for genome editing, including synthetic CRISPR RNAs
1443 (crRNAs), repair templates, and DNA primers used for detecting or genotyping these
1444 mutations. In cases where restriction digests were used for genotyping, fragment sizes
1445 for wild-type and mutant alleles are also provided. **Table S4** lists new worm strains
1446 constructed in the course of this work, as well as previously referenced strains.

Figure 1

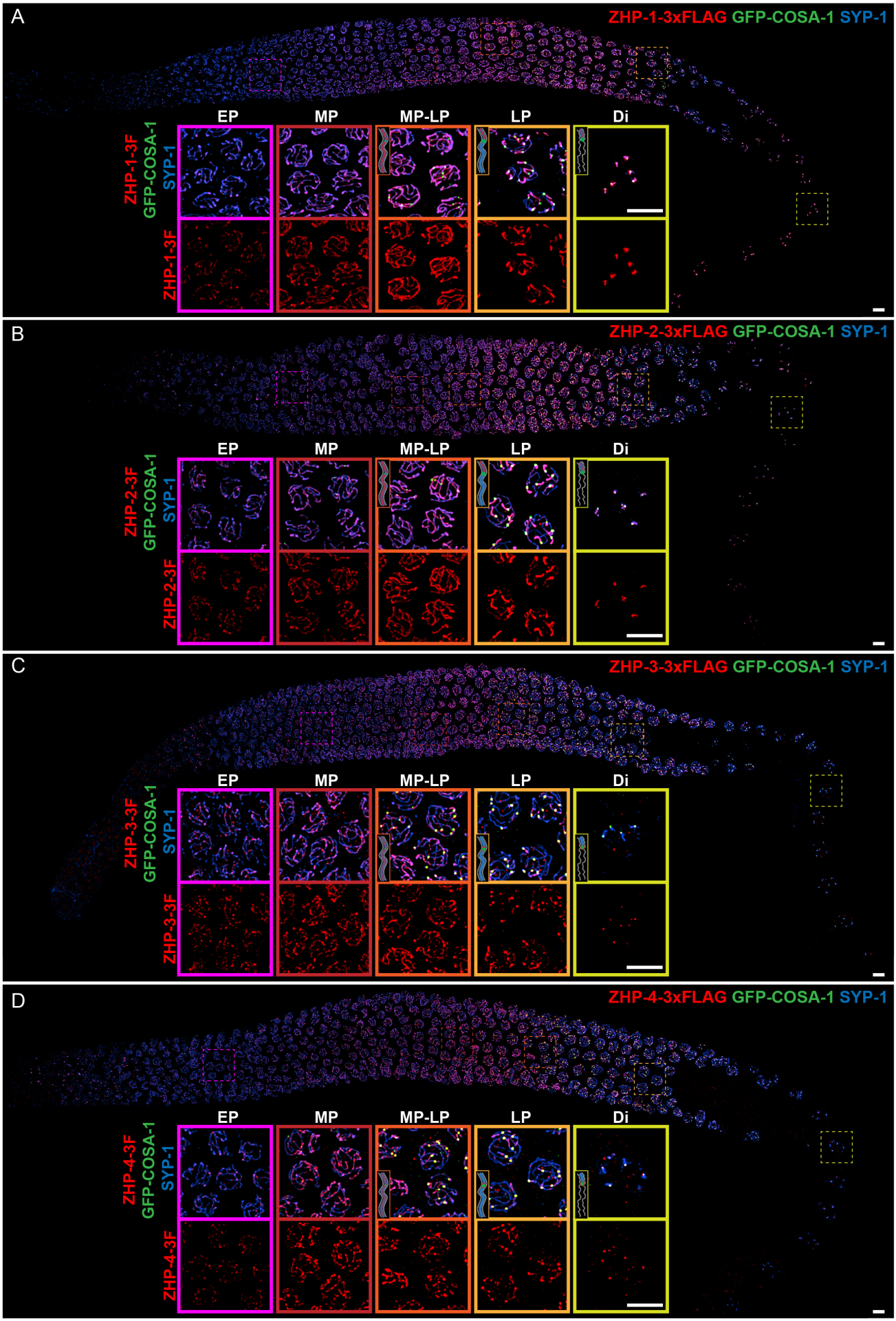
A
ZHP-1-3xFLAG GFP-COSA-1 SYP-1
EP
MP
MP-LP
LP
Di
ZHP-1-3F
GFP-COSA-1
SYP-1
ZHP-1-3F
B
ZHP-2-3xFLAG GFP-COSA-1 SYP-1
EP
MP
MP-LP
LP
Di
ZHP-2-3F
GFP-COSA-1
SYP-1
ZHP-2-3F
C
ZHP-3-3xFLAG GFP-COSA-1 SYP-1
EP
MP
MP-LP
LP
Di
ZHP-3-3F
GFP-COSA-1
SYP-1
ZHP-3-3F
D
ZHP-4-3xFLAG GFP-COSA-1 SYP-1
EP
MP
MP-LP
LP
Di
ZHP-4-3F
GFP-COSA-1
SYP-1
ZHP-4-3F

Figure 2

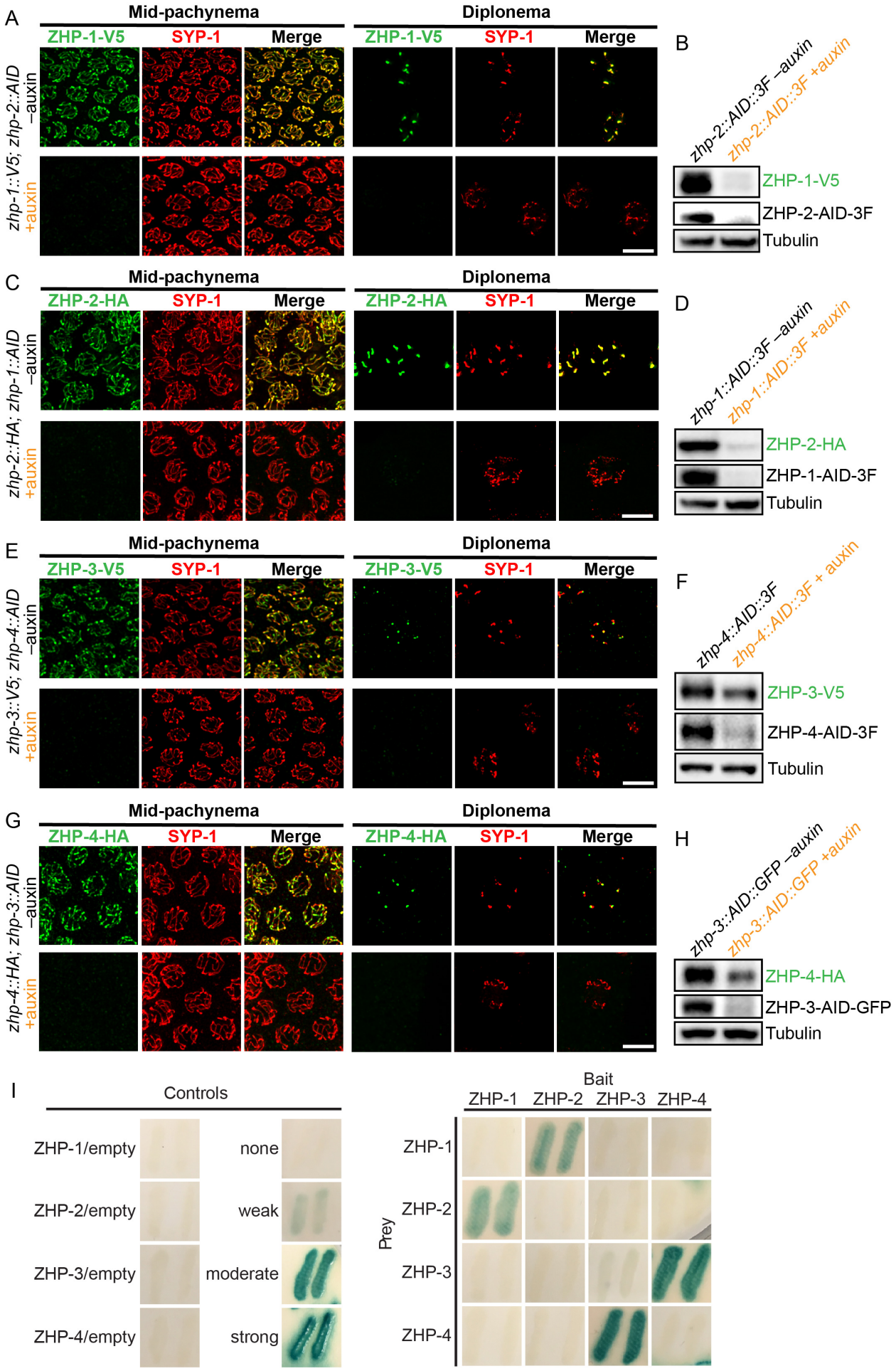
A
Mid-pachynema
Diplonema
ZHP-1-V5
SYP-1
Merge
zhp-1::V5; zhp-2::AID
–auxin
+auxin
B
zhp-2::AID::3F –auxin
zhp-2::AID::3F +auxin
ZHP-1-V5
ZHP-2-AID-3F
Tubulin
C
ZHP-2-HA
zhp-2::HA; zhp-1::AID
D
zhp-1::AID::3F –auxin
zhp-1::AID::3F +auxin
ZHP-2-HA
ZHP-1-AID-3F
E
ZHP-3-V5
zhp-3::V5; zhp-4::AID
F
zhp-4::AID::3F
zhp-4::AID::3F + auxin
ZHP-3-V5
ZHP-4-AID-3F
G
ZHP-4-HA
zhp-4::HA; zhp-3::AID
H
zhp-3::AID::GFP –auxin
zhp-3::AID::GFP +auxin
ZHP-4-HA
ZHP-3-AID-GFP
I
Controls
ZHP-1/empty
ZHP-2/empty
ZHP-3/empty
ZHP-4/empty
none
weak
moderate
strong
Bait
ZHP-1
ZHP-2
ZHP-3
ZHP-4
Prey

Figure 3

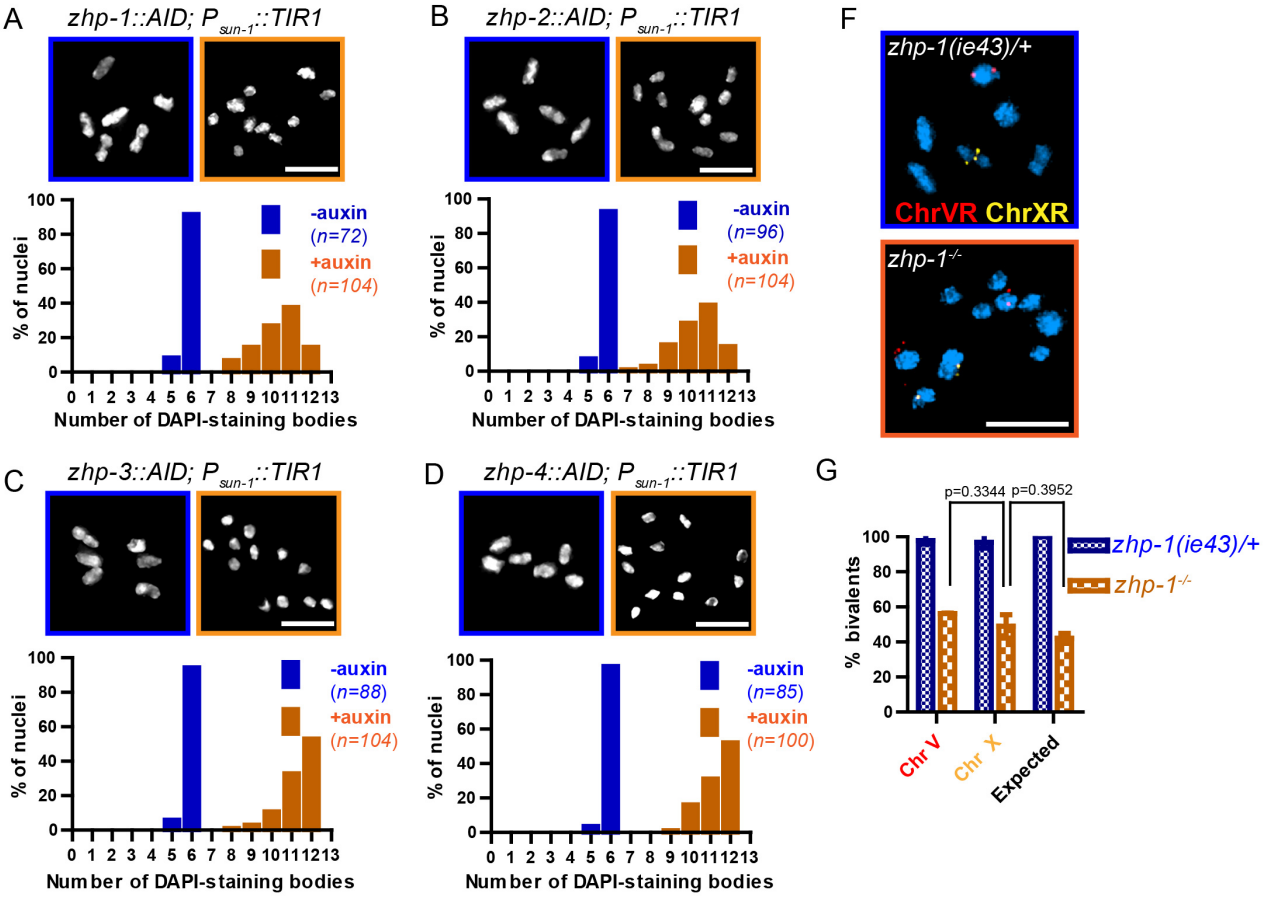

E

Strains	Eggs laid (±SD) (5-11 Hermaphrodites)	Egg viability (±SD) (%)	Male progeny (±SD) (%)
WT[a]	281.6 (±35.96)	109.24 (±3.47)	0.07 (±0.16)
zhp-1(ie43)	219.73 (±32.78)	3.79 (±1.24)	37.06 (±13.57)
zhp-2(ie45)	205.1 (±47.21)	5.11 (±1.61)	38.41 (±15.24)
zhp-3(jf61)[a]	221 (±49.64)	2.06 (±0.62)	43.75 (±27.59)

a. These data are also included in the table in Figure S3C.

Figure 4

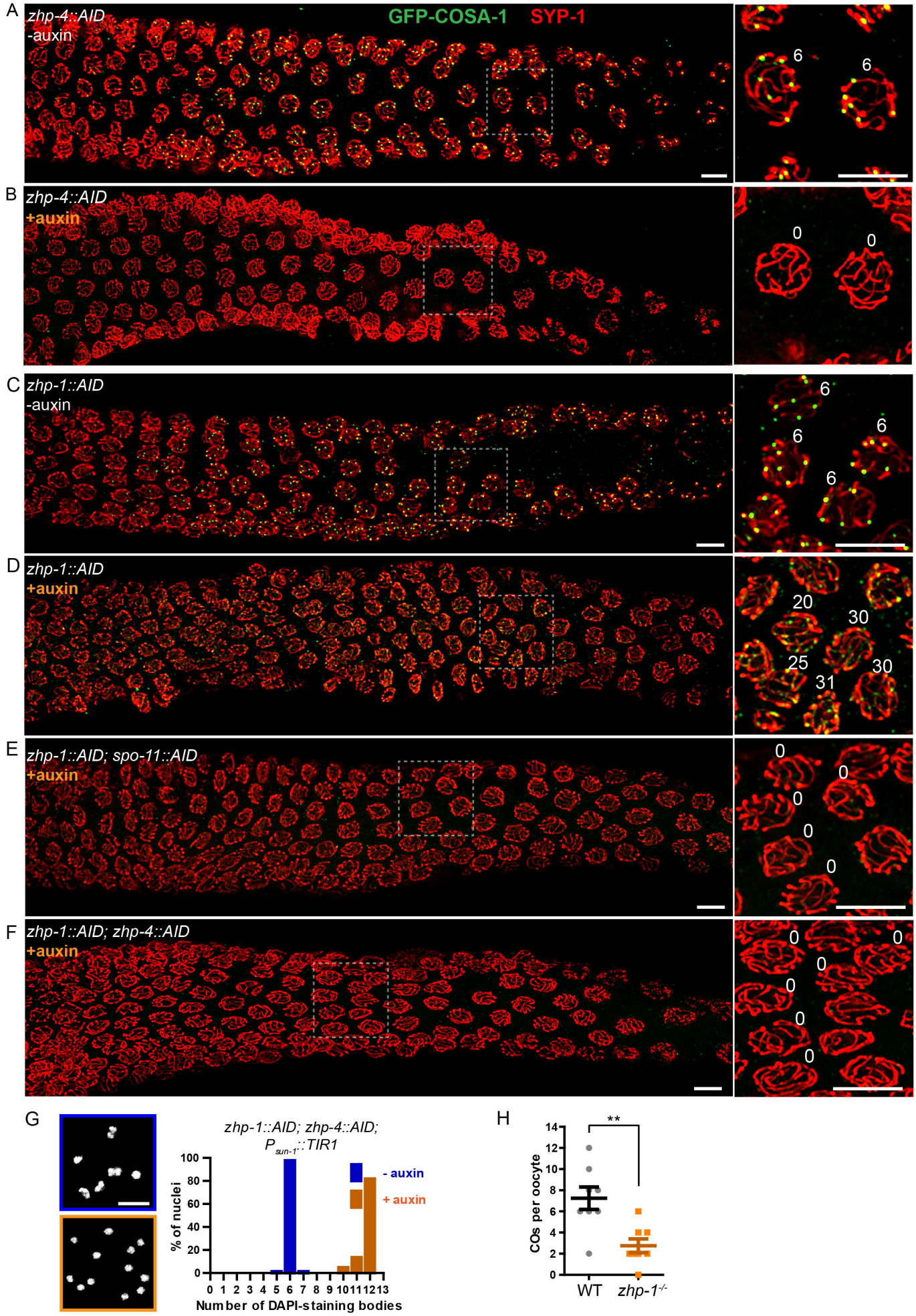
A
zhp-4::AID
-auxin
GFP-COSA-1
SYP-1
6
6
B
zhp-4::AID
+auxin
0
0
C
zhp-1::AID
-auxin
6
6
6
6
D
zhp-1::AID
+auxin
20
30
25
31
30
E
zhp-1::AID; spo-11::AID
+auxin
0
0
0
0
0
F
zhp-1::AID; zhp-4::AID
+auxin
0
0
0
0
0
0
G
zhp-1::AID; zhp-4::AID;
P sun-1::TIR1
% of nuclei
100
80
60
40
20
0
0 1 2 3 4 5 6 7 8 9 10 11 12 13
Number of DAPI-staining bodies
- auxin
+ auxin
H
**
COs per oocyte
14
12
10
8
6
4
2
0
WT
zhp-1-/-

Figure 5

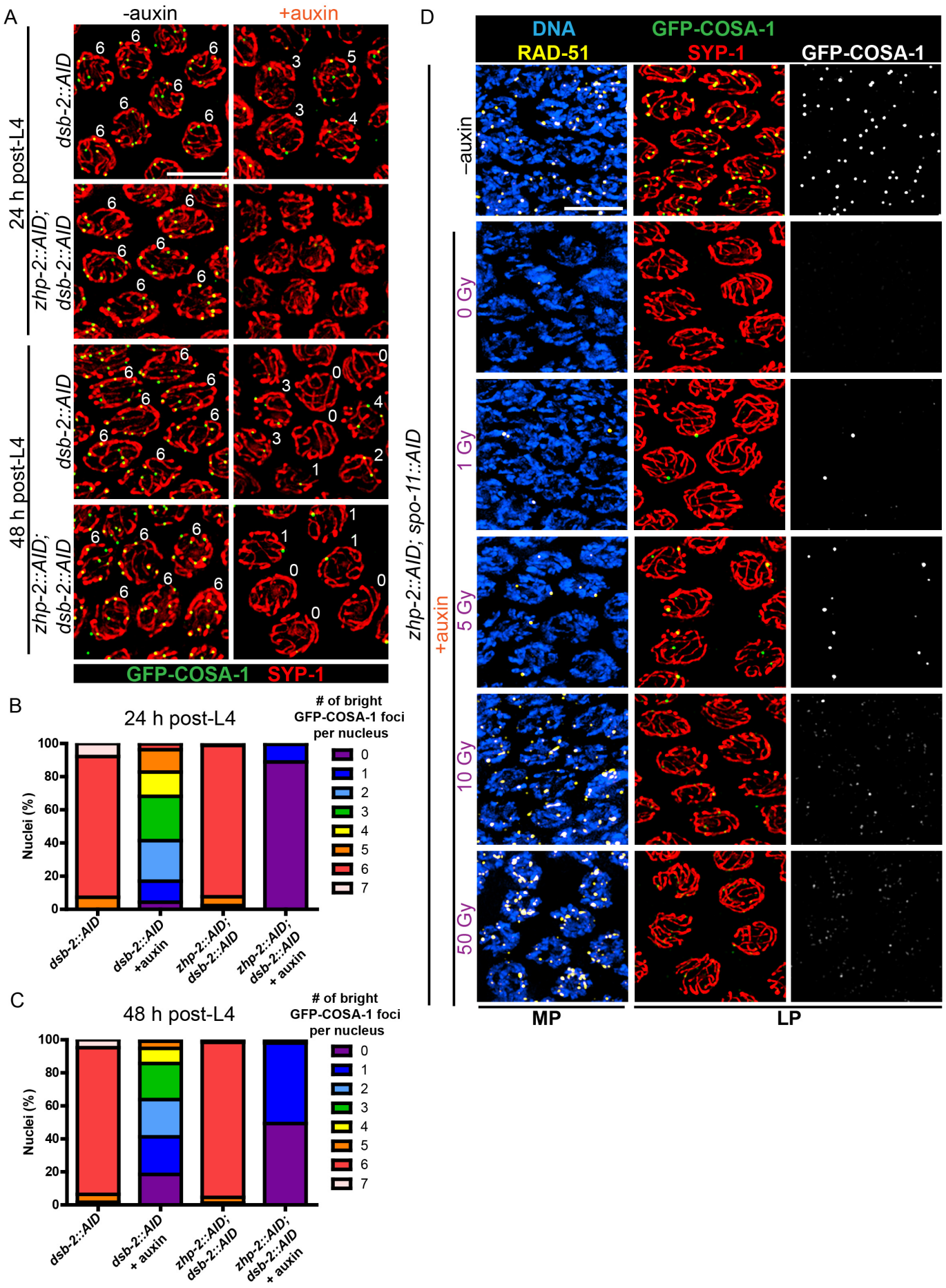
A
-auxin
+auxin
24 h post-L4
48 h post-L4
dsb-2::AID
zhp-2::AID; dsb-2::AID
GFP-COSA-1
SYP-1
B
24 h post-L4
# of bright GFP-COSA-1 foci per nucleus
Nuclei (%)
dsb-2::AID
dsb-2::AID +auxin
zhp-2::AID; dsb-2::AID
zhp-2::AID; dsb-2::AID + auxin
C
48 h post-L4
D
DNA
RAD-51
GFP-COSA-1
SYP-1
zhp-2::AID; spo-11::AID
+auxin
–auxin
0 Gy
1 Gy
5 Gy
10 Gy
50 Gy
MP
LP

Figure 6

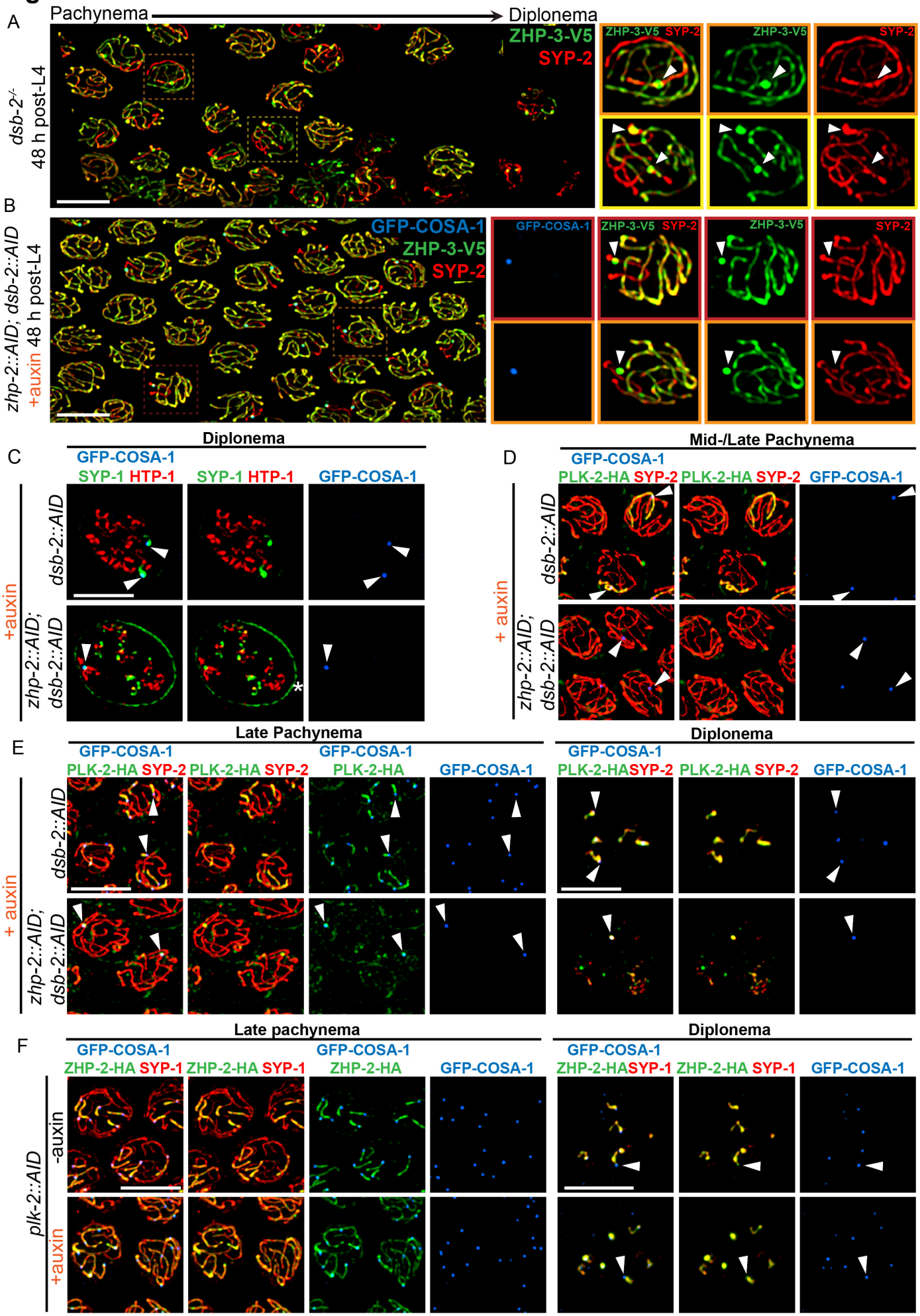
A
Pachynema
Diplonema
ZHP-3-V5
SYP-2
dsb-2-/-
48 h post-L4
B
GFP-COSA-1
ZHP-3-V5
SYP-2
zhp-2::AID; dsb-2::AID
+auxin 48 h post-L4
C
Diplonema
GFP-COSA-1
SYP-1 HTP-1
SYP-1 HTP-1
GFP-COSA-1
+auxin
dsb-2::AID
zhp-2::AID;
dsb-2::AID
D
Mid-/Late Pachynema
GFP-COSA-1
PLK-2-HA SYP-2
PLK-2-HA SYP-2
GFP-COSA-1
+ auxin
dsb-2::AID
zhp-2::AID;
dsb-2::AID
E
Late Pachynema
Diplonema
GFP-COSA-1
PLK-2-HA SYP-2
PLK-2-HA
GFP-COSA-1
+ auxin
dsb-2::AID
zhp-2::AID;
dsb-2::AID
F
Late pachynema
Diplonema
GFP-COSA-1
ZHP-2-HA SYP-1
ZHP-2-HA
GFP-COSA-1
plk-2::AID
-auxin
+auxin

Figure 7

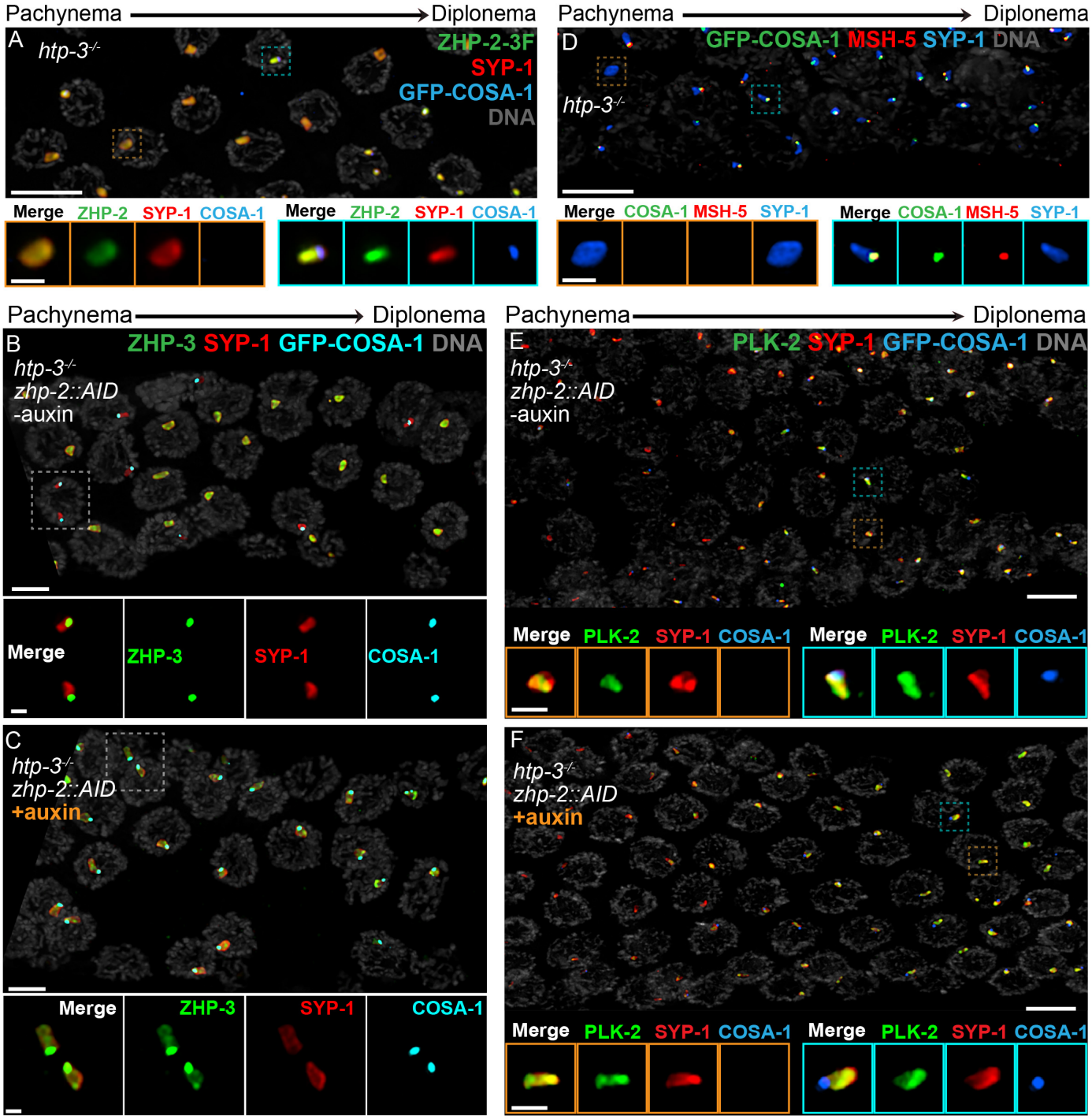
Pachynema
Diplonema
A
htp-3-/-
ZHP-2-3F
SYP-1
GFP-COSA-1
DNA
Merge
ZHP-2
SYP-1
COSA-1
D
GFP-COSA-1
MSH-5
SYP-1
DNA
htp-3-/-
COSA-1
B
ZHP-3
htp-3-/-
zhp-2::AID
-auxin
C
+auxin
E
PLK-2
F

Figure 8

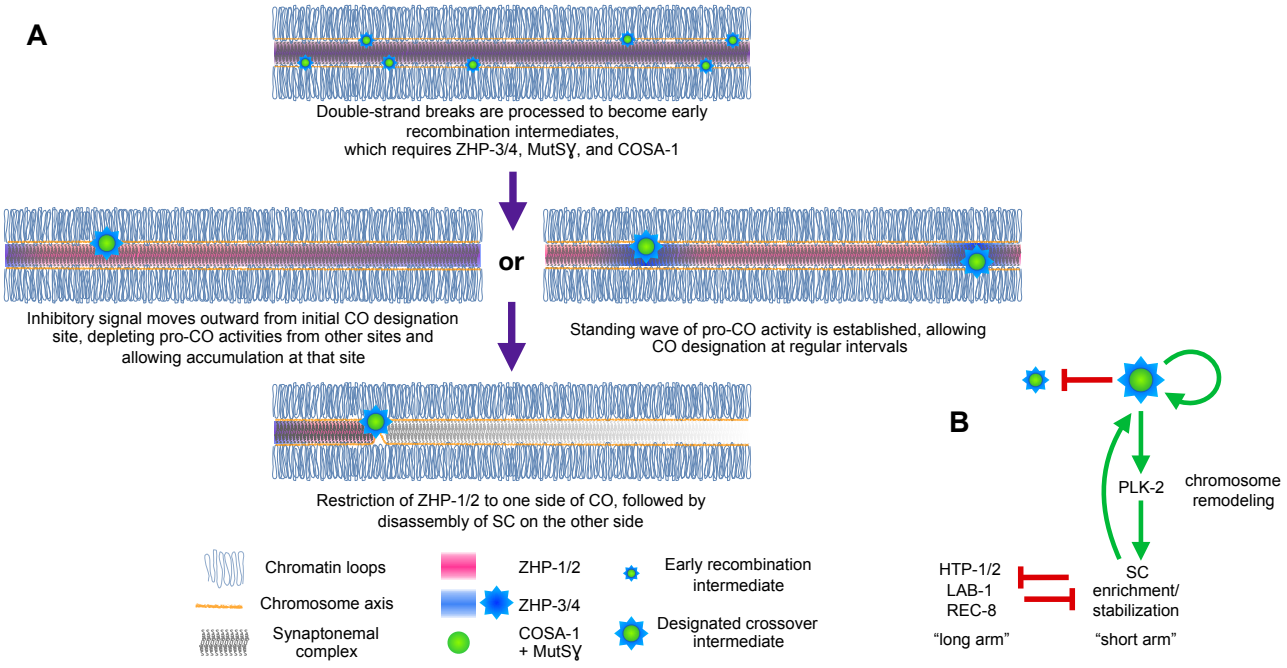
A
Double-strand breaks are processed to become early recombination intermediates, which requires ZHP-3/4, MutSɣ, and COSA-1
or
Inhibitory signal moves outward from initial CO designation site, depleting pro-CO activities from other sites and allowing accumulation at that site
Standing wave of pro-CO activity is established, allowing CO designation at regular intervals
Restriction of ZHP-1/2 to one side of CO, followed by disassembly of SC on the other side
Chromatin loops
Chromosome axis
Synaptonemal complex
ZHP-1/2
ZHP-3/4
COSA-1 + MutSɣ
Early recombination intermediate
Designated crossover intermediate
B
PLK-2
chromosome remodeling
HTP-1/2
LAB-1
REC-8
SC enrichment/ stabilization
"long arm"
"short arm"

Figure 1—figure supplement 1

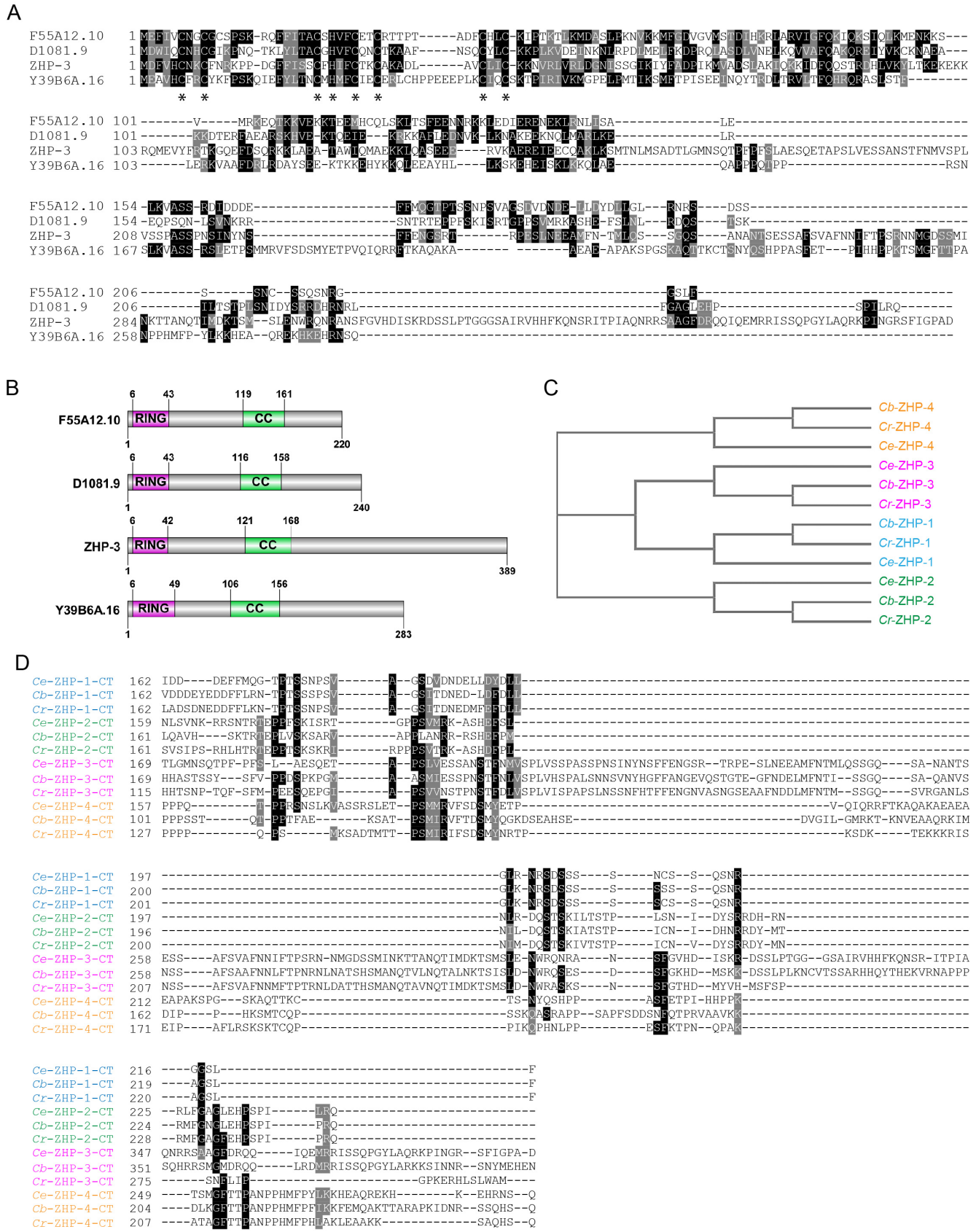

Figure 1—figure supplement 2

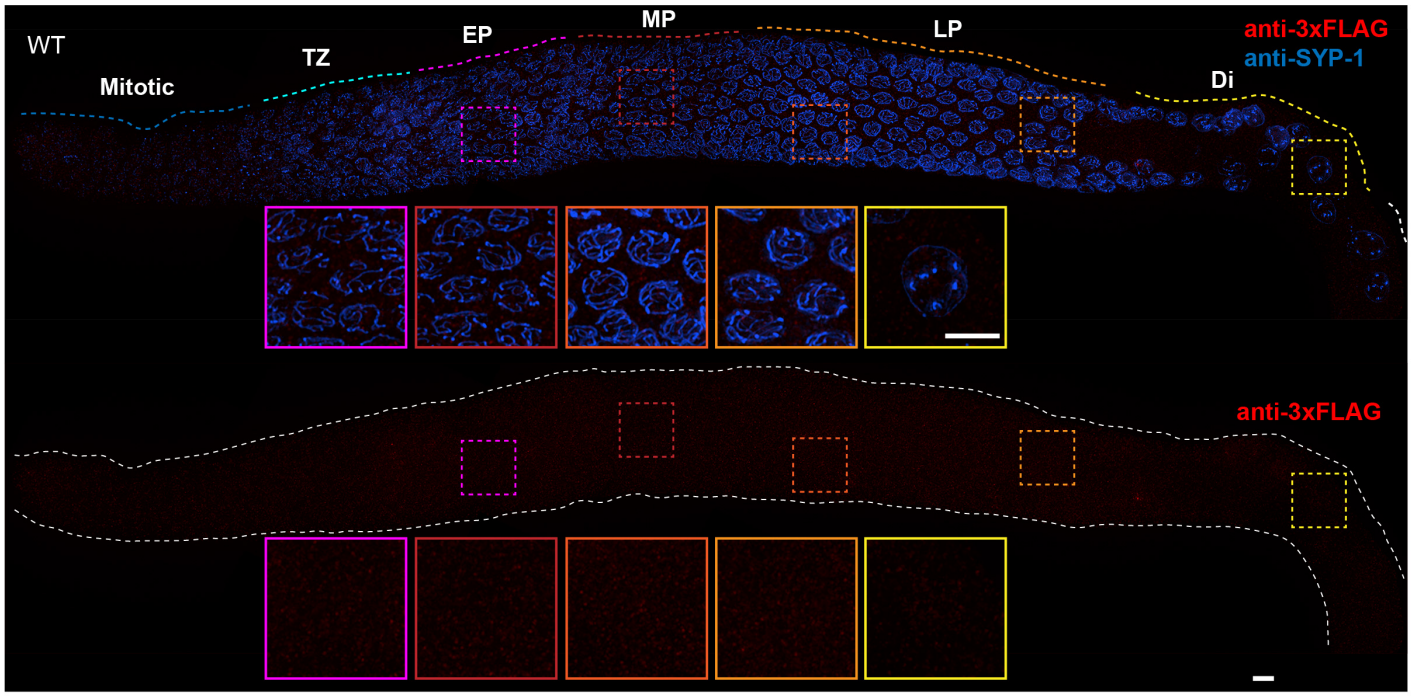

Figure 1—figure supplement 3

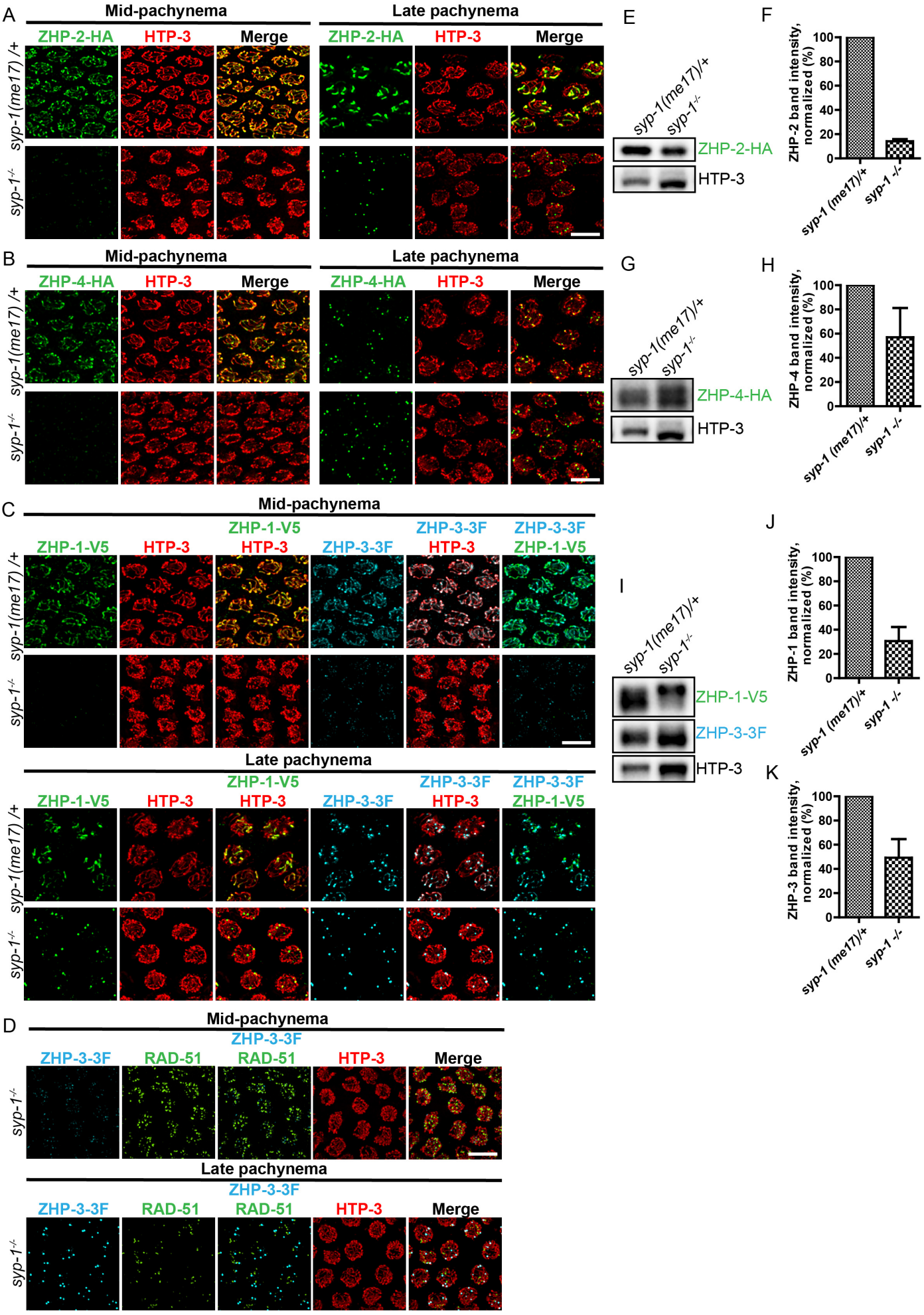

Figure 2—figure supplement 1

A

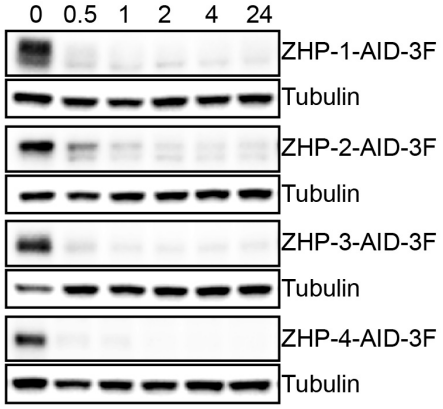

B

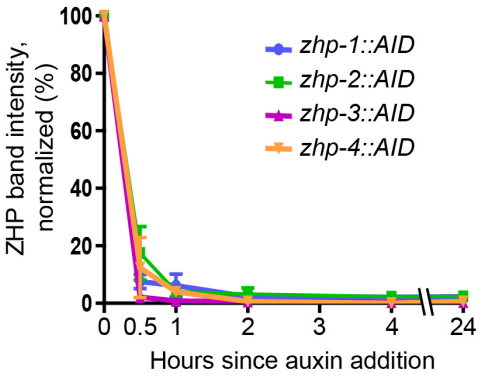

C

Strains	Auxin	Eggs laid (±SD) (3-10 Hermaphrodites)	Egg viability (±SD) (%)	Male progeny (±SD) (%)
WT[a]	-	281.6 (±35.96)	109.24 (±3.47)	0.07 (±0.16)
WT[a]	+	230.2 (±10.47)	115.47 (±6.06)	0.07 (±0.16)
zhp-3(jf61)/+	-	235.17 (±26.35)	31.57 (±3.07)	0.00 (±0.00)
zhp-3(jf61)[a]	-	221 (±49.64)	2.06 (±0.62)	43.75 (±27.59)
zhp-3::AID::GFP; P_{sun-1}*::TIR1*	-	302.67 (±26.27)	102.00 (±5.17)	0.62 (±0.57)
zhp-3::AID::GFP; P_{sun-1}*::TIR1*	+	202 (±21.29)	1.83 (±0.82)	37.02 (±38.12)

a. These data are also included in the table in Figure 3E.

Figure 2—figure supplement 2

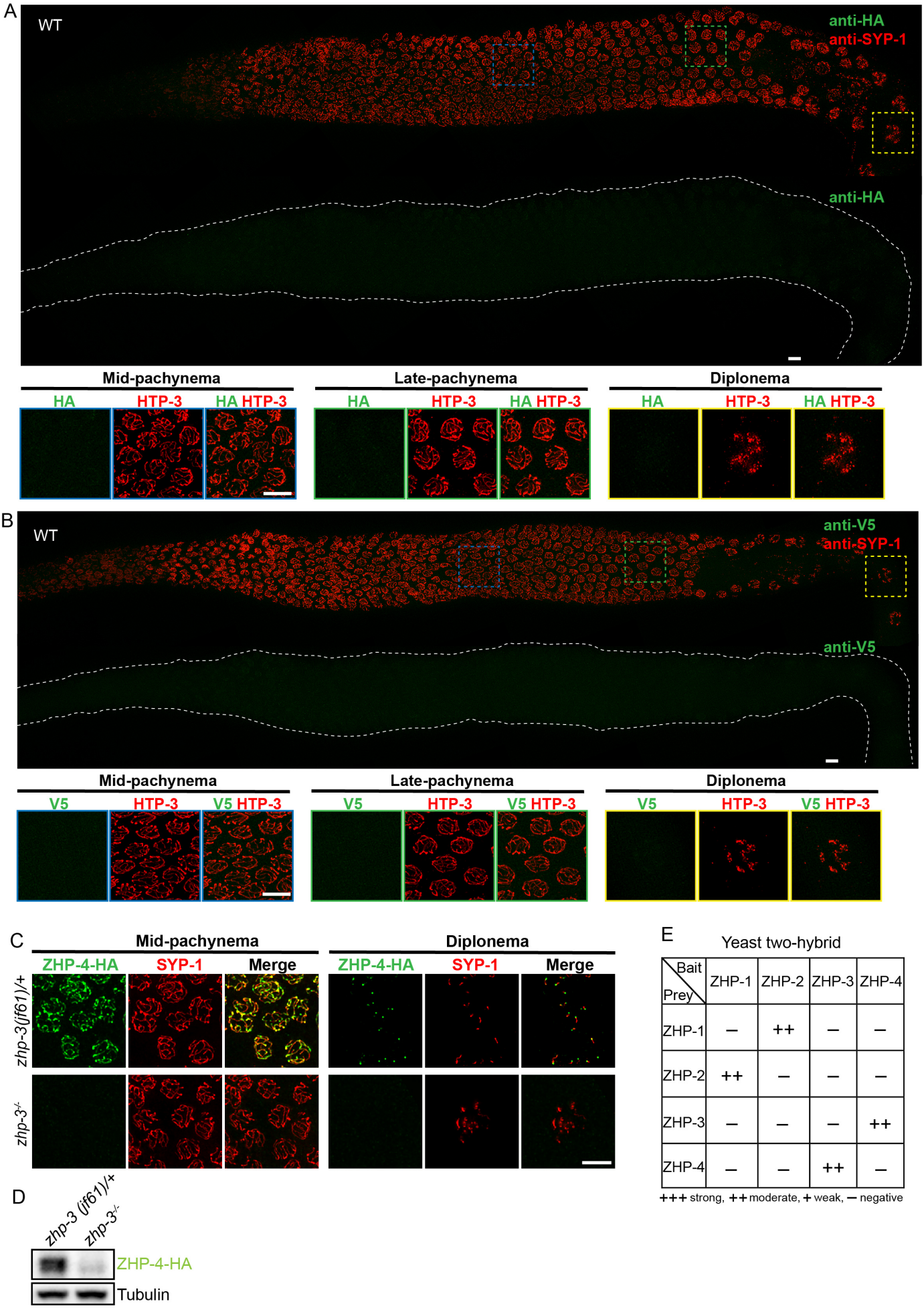

E

Yeast two-hybrid

Prey \ Bait	ZHP-1	ZHP-2	ZHP-3	ZHP-4
ZHP-1	–	++	–	–
ZHP-2	++	–	–	–
ZHP-3	–	–	–	++
ZHP-4	–	–	++	–

+++ strong, ++ moderate, + weak, – negative

Figure 3—figure supplement 1

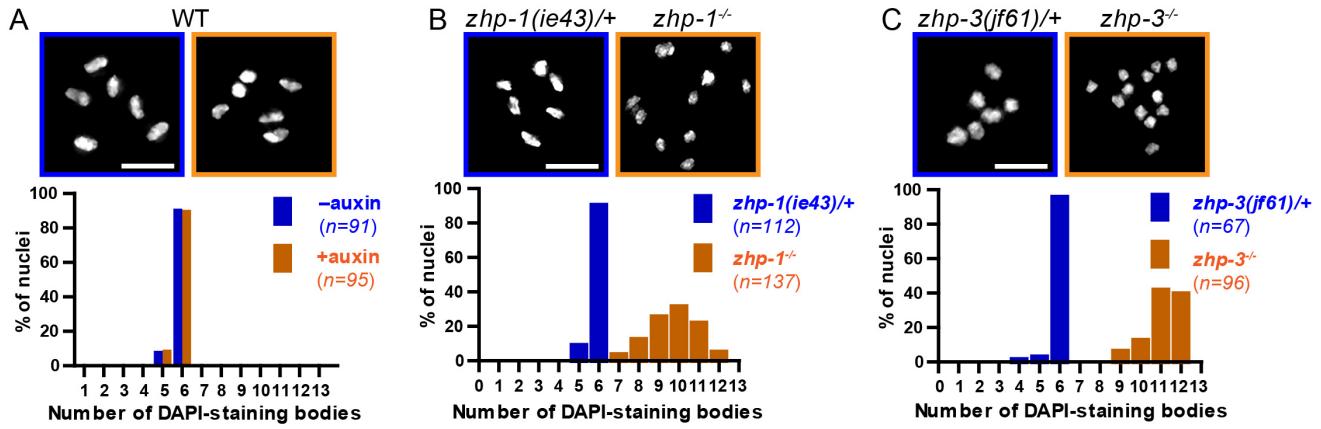

Figure 3—figure supplement 2

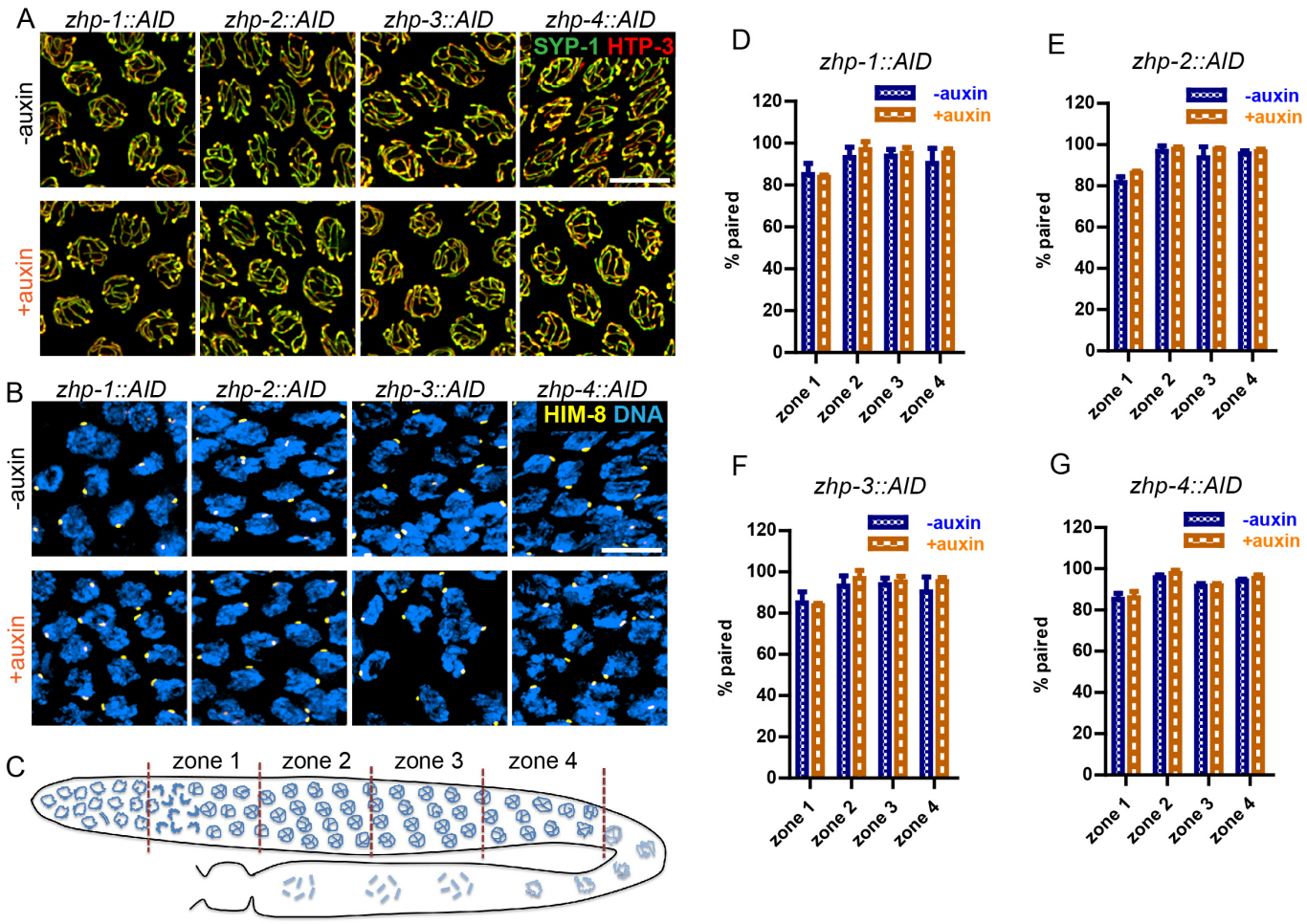

Figure 3—figure supplement 3

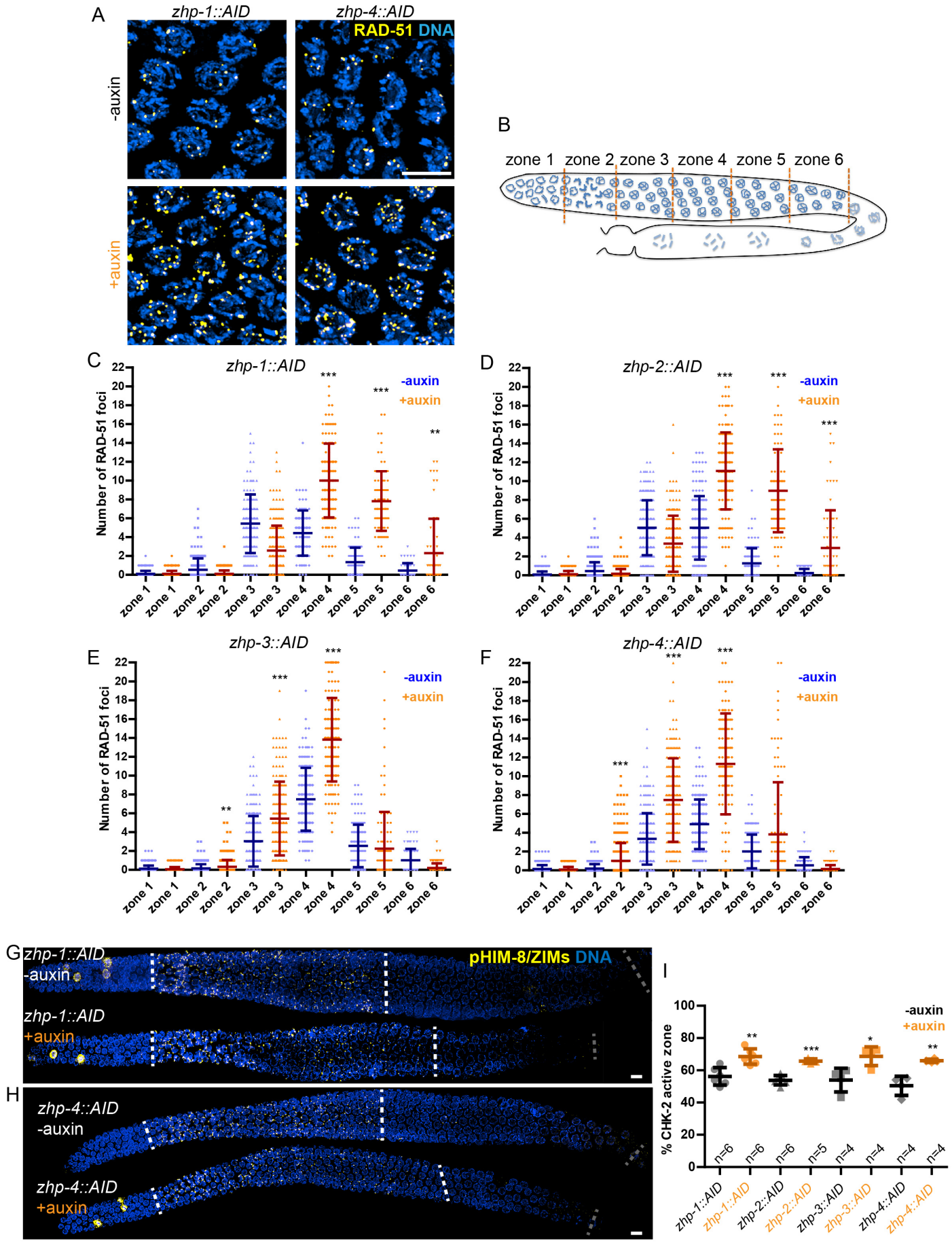

Figure 4—figure supplement 1

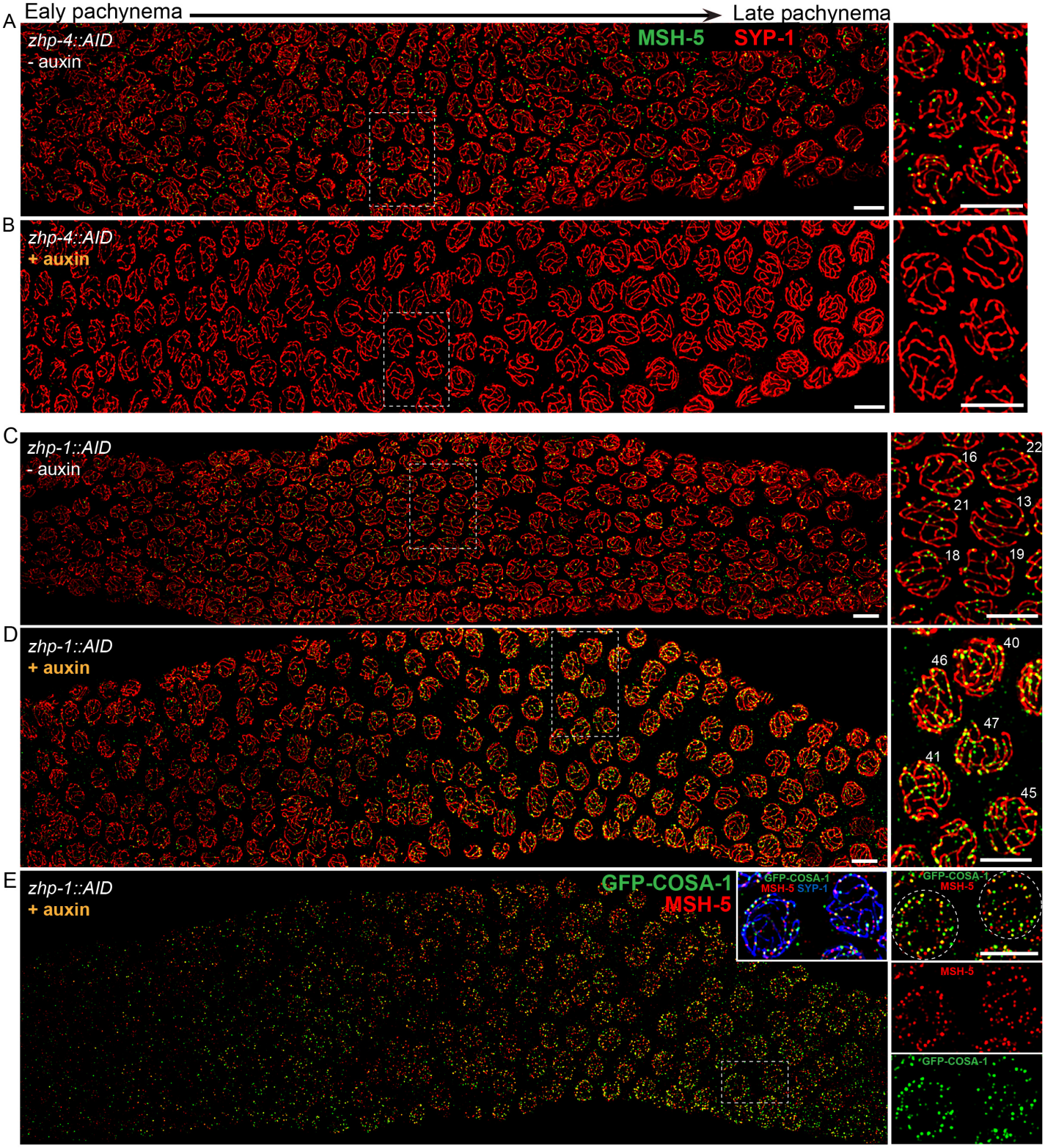

Figure 4—figure supplement 2

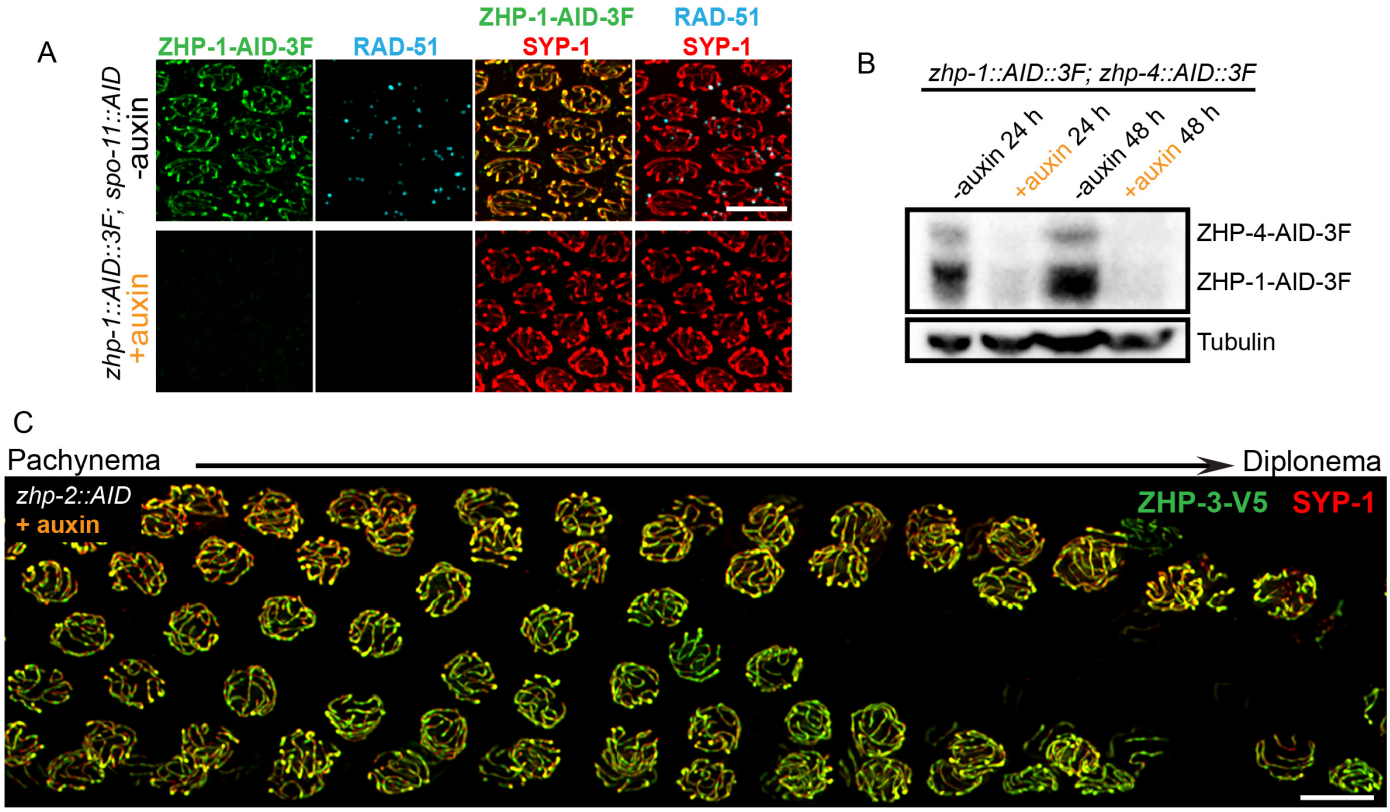

Figure 5—figure supplement 1

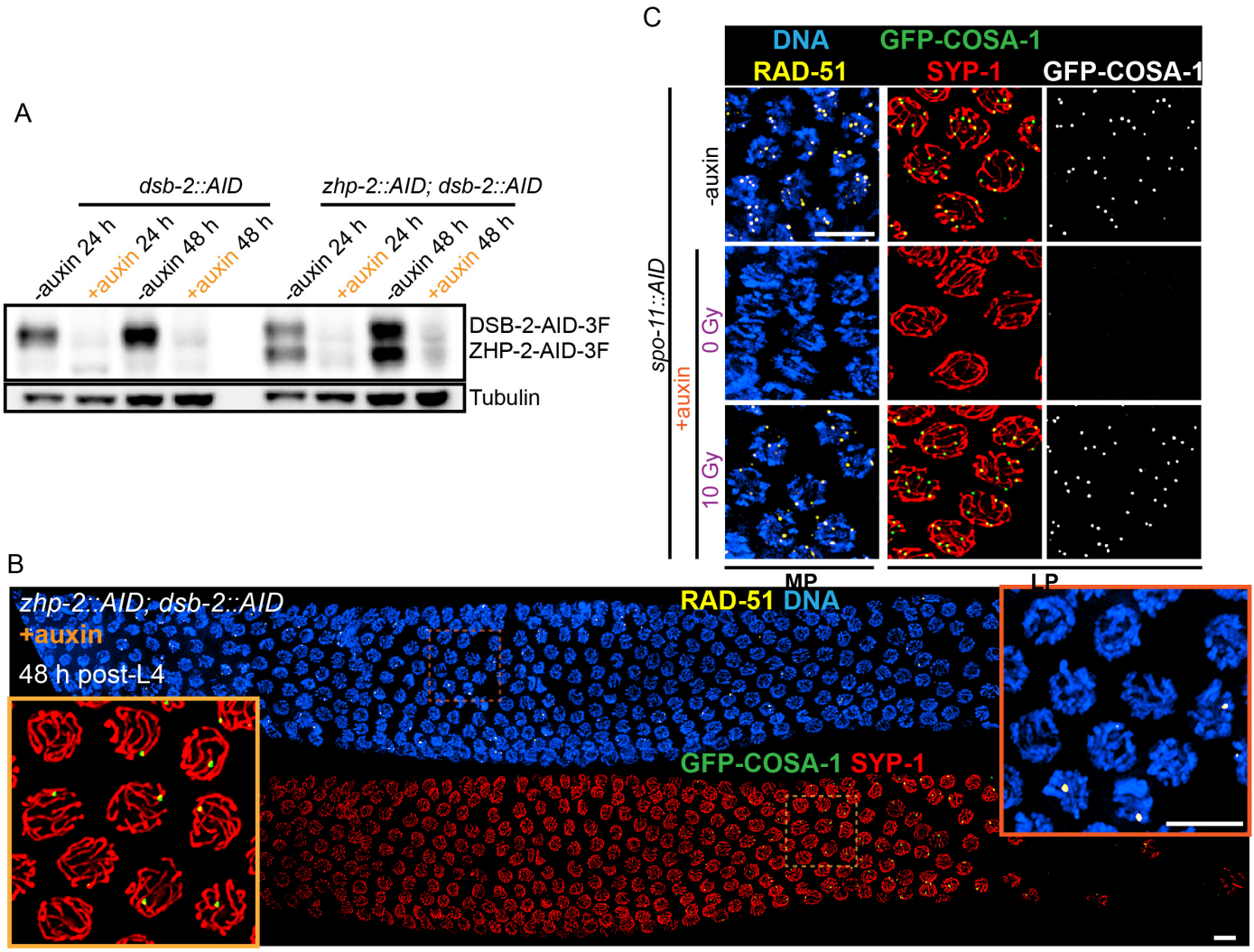

Figure 5—figure supplement 2

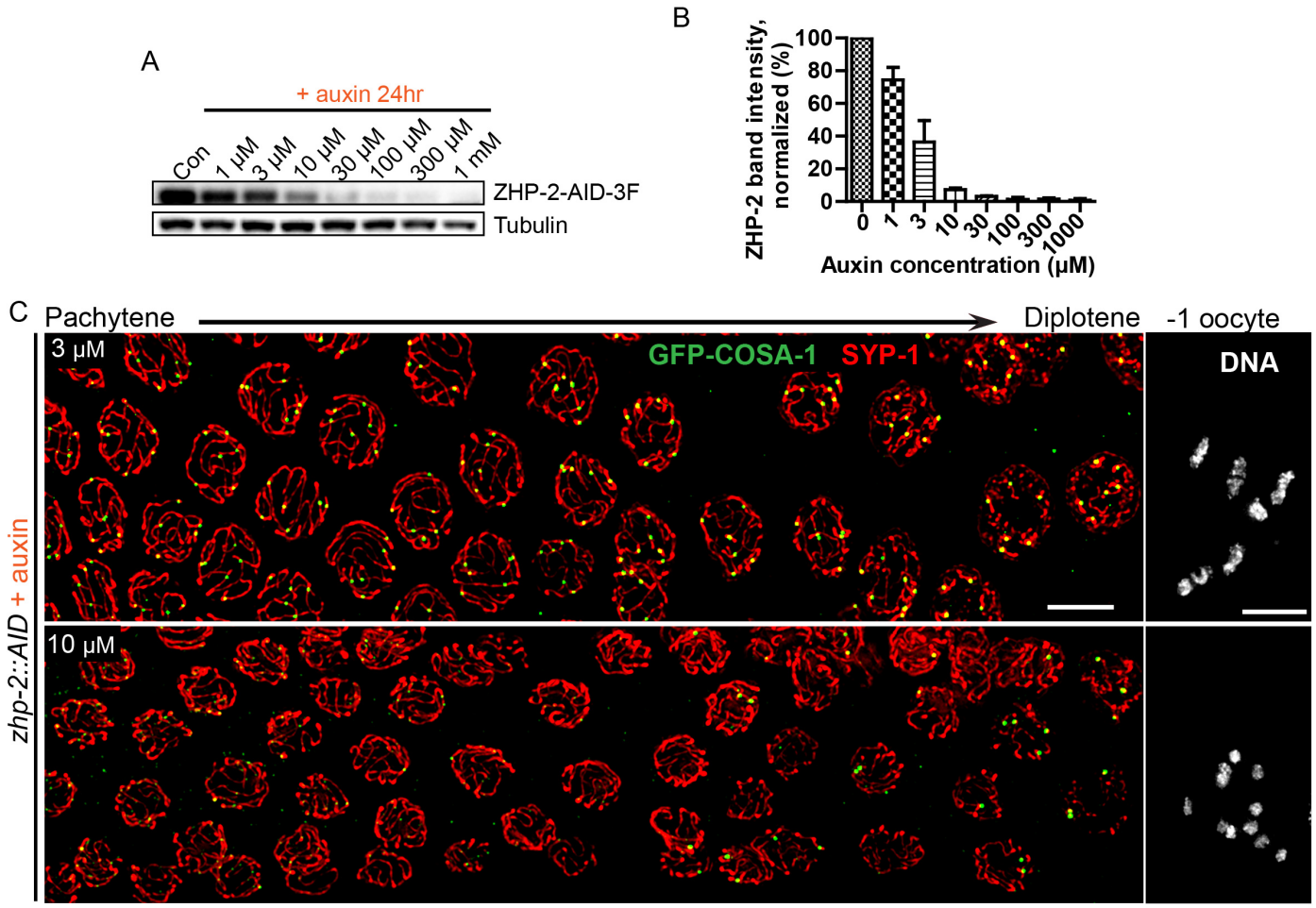

Figure 6—figure supplement 1

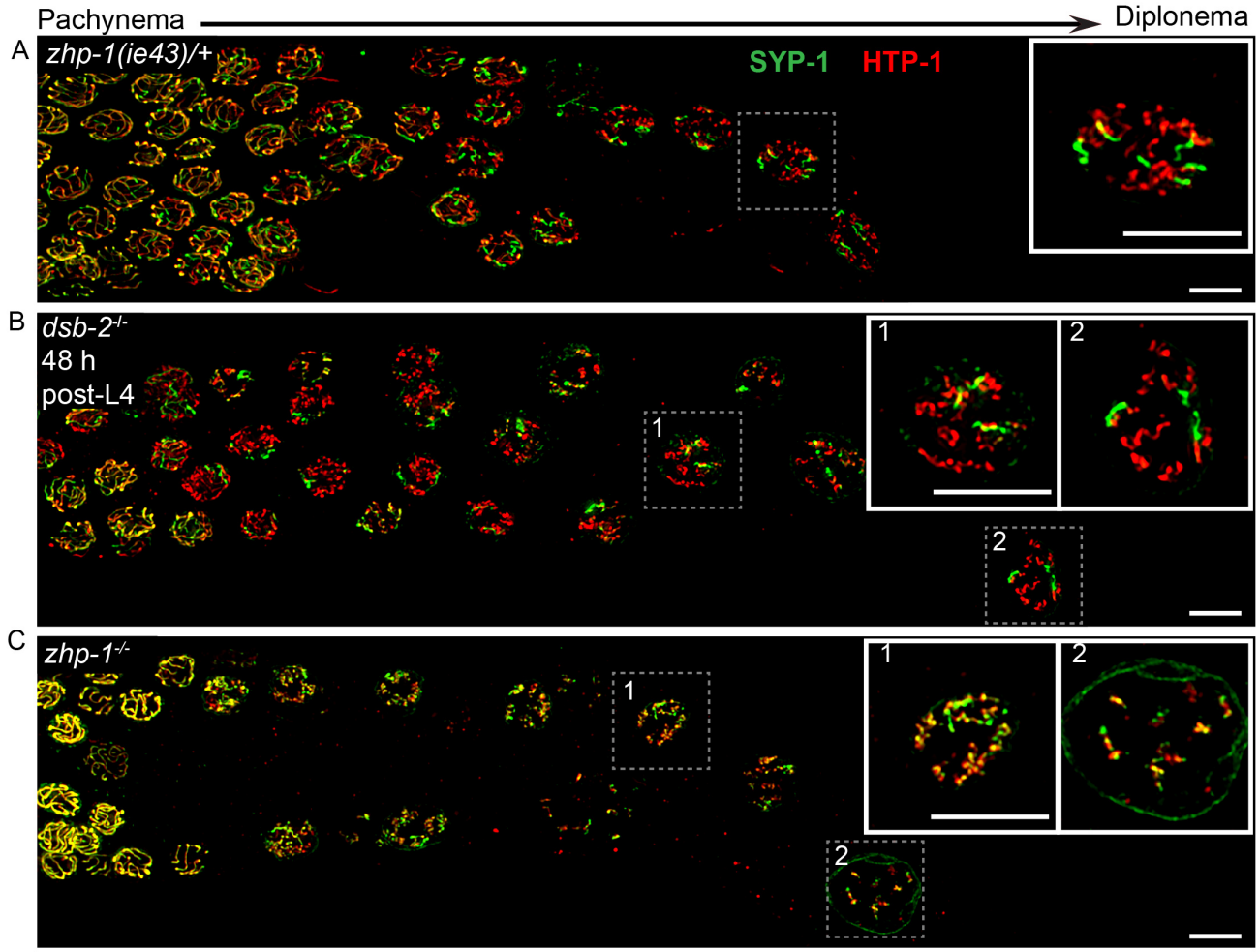

Figure 6—figure supplement 2

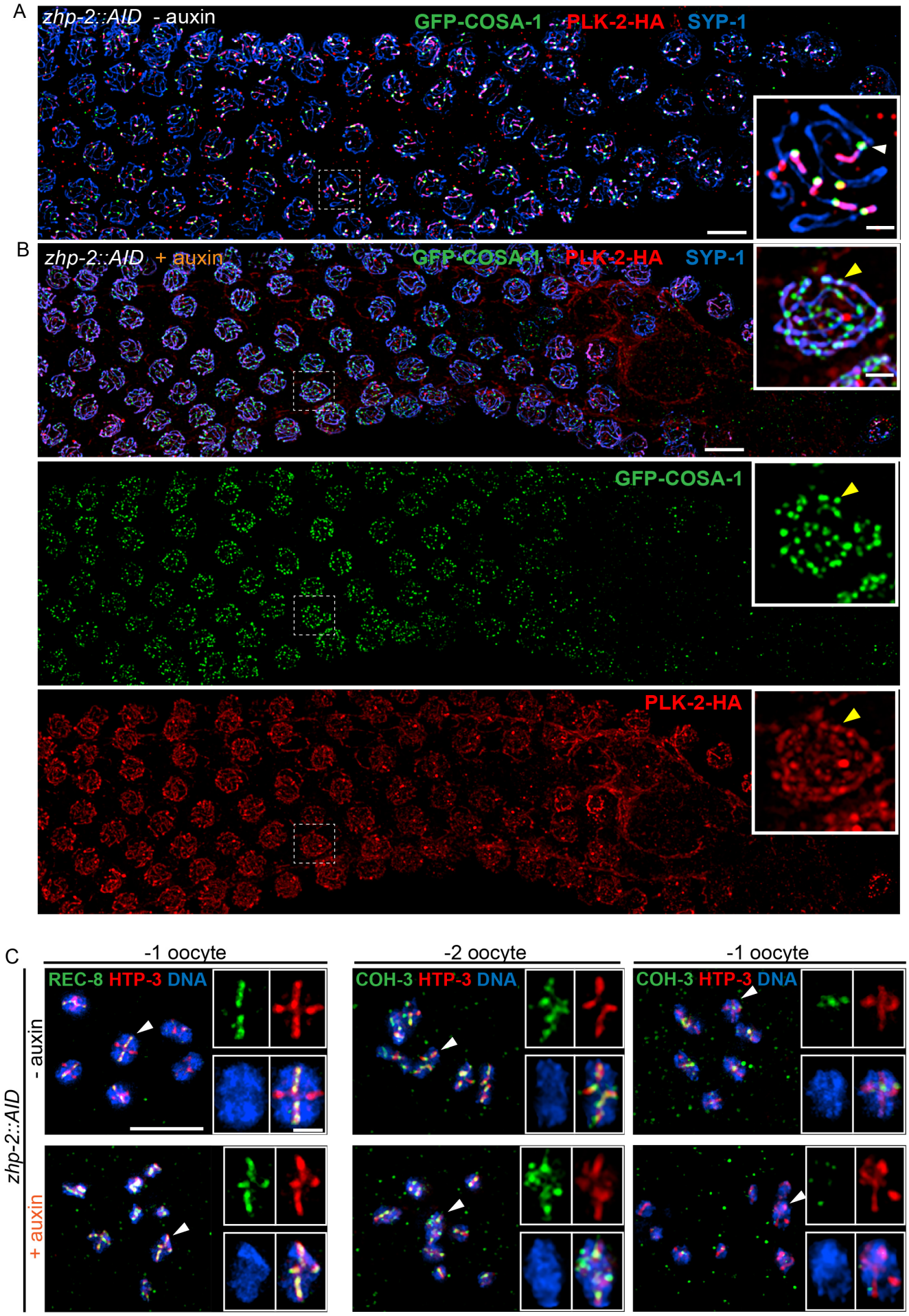

Supplementary File 1

Table S1

Viability and fertility of representative transgenic worm strains

Strains	Eggs laid (±SD) (6 Hermaphrodites)	Egg viability (±SD) (%)	Male progeny (±SD) (%)
WT	279.83 (±35.61)	107.62 (±5.47)	0.16 (±0.17)
zhp-1::AID::3xFLAG; GFP::cosa-1; P_{sun-1}*::TIR1*	250.5 (±30.43)	113.80 (±3.58)	0.12 (±0.30)
zhp-2::AID::3xFLAG; GFP::cosa-1; P_{sun-1}*::TIR1*	270.00 (±18.25)	110.58 (±3.27)	0.11 (±0.17)
zhp-3::AID::3xFLAG; GFP::cosa-1; P_{sun-1}*::TIR1*	263.83 (±20.62)	108.52 (±2.92)	0.06 (±0.14)
GFP::cosa-1; P_{sun-1}*::TIR1; zhp-4::AID::3xFLAG*	260.33 (±16.84)	109.12 (±2.69)	0.34 (±0.35)
zhp-2::AID::3xFLAG; GFP::cosa-1; P_{sun-1}*::TIR1, spo-11::AID::3xFLAG*	277.67 (±21.90)	110.47 (±3.21)	0.11 (±0.17)
plk-2::HA, zhp-2::AID::3xFLAG, zhp-3::V5; dsb-2::AID::3xFLAG, GFP::cosa-1; P_{sun-1}*::TIR1*	270.17 (±21.10)	108.33 (±5.31)	0.29 (±0.35)
plk-2::AID::3xFLAG, zhp-2::HA; GFP::cosa-1; P_{sun-1}*::TIR1*	255.00 (±12.13)	111.28 (±2.10)	0.30 (±0.36)

Note: viability of >100% is a consequence of failing to count some embryos.

Table S2

Alleles generated in this study

Allele	Genotype	Information about mutagenesis
ie43	*zhp-1(ie43)/hT2*; stop codon + frameshift + Xho1 after aa6; sequence inserted is 5'-TAAGCTCGAG-3'	generated using *dpy-10* Co-CRISPR, balanced with *hT2 [bli-4(e937) let-?(q782) qIs48] (I; III)*, #2
ie44	*zhp-1(ie44)/hT2*; stop codon + frameshift + Xho1 after aa6; sequence inserted is 5'-TAAGCTCGAG-3'	generated using *dpy-10* Co-CRISPR, balanced with *hT2 [bli-4(e937) let-?(q782) qIs48] (I; III)*, #4
ie45	*zhp-2(ie45)/hT2*; stop codon + frameshift after aa7; nucleotide c22 was replaced by 5'-TAATAATTAATTAG-3'	generated using *dpy-10* Co-CRISPR, balanced with *hT2 [bli-4(e937) let-?(q782) qIs48] (I; III)*, #18
ie46	*zhp-1(ie46)*; stop codon + frameshift + Xho1 after aa6; sequence inserted is 5'-TAAGCTCGAG-3'; in Hawaii CB4586 background	generated using *dpy-10* Co-CRISPR in Hawaii CB4586. #1
ie51	*htp-3(ie51)* mutant	generated using *dpy-10* Co-CRISPR in *zhp-1(ie62[zhp-1::AID::3xFLAG]) I; meIs8[pie-1p::GFP::cosa-1, unc-119(+)] II; ieSi38[sun-1p::TIR1::mRuby::sun-1 3'UTR, Cbr-unc-119(+)] IV*
ie52	*htp-3(ie52)* mutant	generated using *dpy-10* Co-CRISPR in *zhp-2(ie67[zhp-2::AID::3xFLAG]) I; meIs8[pie-1p::GFP::cosa-1, unc-119(+)] II; ieSi38[sun-1p::TIR1::mRuby::sun-1 3'UTR, Cbr-unc-119(+)] IV*
ie58	*dsb-2(ie58[dsb-2::AID::3xFLAG])*	generated using *dpy-10* Co-CRISPR in *zhp-2(ie67[zhp-2::AID::3xFLAG]) I; meIs8[pie-1p::GFP::cosa-1, unc-119(+)] II; ieSi38[sun-1p::TIR1::mRuby::sun-1 3'UTR, Cbr-unc-119(+)] IV*
ie59	*spo-11(ie59[spo-11::AID::3xFLAG])*	generated using *dpy-10* Co-CRISPR in *zhp-1(ie62[zhp-1::AID::3xFLAG]) I; meIs8[pie-1p::GFP::cosa-1, unc-119(+)] II; ieSi38[sun-1p::TIR1::mRuby::sun-1 3'UTR, Cbr-unc-119(+)] IV*
ie60	*spo-11(ie60[spo-11::AID::3xFLAG])*	generated using *dpy-10* Co-CRISPR in *zhp-2(ie67[zhp-2::AID::3xFLAG]) I; meIs8[pie-1p::GFP::cosa-1, unc-119(+)] II; ieSi38[sun-1p::TIR1::mRuby::sun-1 3'UTR, Cbr-unc-119(+)] IV*
ie61	*zhp-1(ie61[zhp-1::AID::3xFLAG])*	generated using *dpy-10* Co-CRISPR in *ieSi38[sun-1p::TIR1::mRuby::sun-1 3'UTR, Cbr-unc-119(+)] IV*
ie62	*zhp-1(ie62[zhp-1::AID::3xFLAG])*	generated using *dpy-10* Co-CRISPR in *meIs8[pie-1p::GFP::cosa-1, unc-119(+)] II; ieSi38[sun-1p::TIR1::mRuby::sun-1 3'UTR, Cbr-unc-119(+)] IV*
ie63	*zhp-2(ie63[zhp-2::HA])*	generated using *dpy-10* Co-CRISPR in *zhp-1(ie61[zhp-1::AID::3xFLAG]) I; ieSi38[sun-1p::TIR1::mRuby::sun-1 3'UTR, Cbr-unc-119(+)] IV*
ie64	*zhp-3(ie64[zhp-3::V5])*	generated using *dpy-10* Co-CRISPR in *zhp-1(ie61[zhp-1::AID::3xFLAG]) I; ieSi38[sun-1p::TIR1::mRuby::sun-1 3'UTR, Cbr-unc-119(+)] IV*
ie65	*zhp-4(ie65[zhp-4::HA])*	generated using *dpy-10* Co-CRISPR in *zhp-1(ie61[zhp-1::AID::3xFLAG]) I; ieSi38[sun-1p::TIR1::mRuby::sun-1 3'UTR, Cbr-unc-119(+)] IV*
ie66	*zhp-2(ie66[zhp-2::AID::3xFLAG])*	generated using *dpy-10* Co-CRISPR in *ieSi38[sun-1p::TIR1::mRuby::sun-1 3'UTR, Cbr-unc-119(+)] IV*
ie67	*zhp-2(ie67[zhp-2::AID::3xFLAG])*	generated using *dpy-10* Co-CRISPR in *meIs8[pie-1p::GFP::cosa-1, unc-119(+)] II; ieSi38[sun-1p::TIR1::mRuby::sun-1 3'UTR, Cbr-unc-119(+)] IV*
ie68	*zhp-1(ie68[zhp-1::V5])*	generated using *dpy-10* Co-CRISPR in *zhp-2(ie66[zhp-2::AID::3xFLAG]) I; ieSi38[sun-1p::TIR1::mRuby::sun-1 3'UTR, Cbr-unc-119(+)] IV*
ie69	*zhp-3(ie69[zhp-3::V5])*	generated using *dpy-10* Co-CRISPR in *zhp-2(ie66[zhp-2::AID::3xFLAG]) I; ieSi38[sun-1p::TIR1::mRuby::sun-1 3'UTR, Cbr-unc-119(+)] IV*
ie70	*zhp-4(ie70[zhp-4::HA])*	generated using *dpy-10* Co-CRISPR in *zhp-2(ie66[zhp-2::AID::3xFLAG]) I; ieSi38[sun-1p::TIR1::mRuby::sun-1 3'UTR, Cbr-unc-119(+)] IV*
ie72	*zhp-2(ie72[zhp-2::HA])*	generated using Cas9 in *syp-1(me17) V/nT1[unc-?(n754) let-? qIs50] (IV;V)*
ie73	*zhp-2(ie73[zhp-2::HA])*	generated using *dpy-10* Co-CRISPR in *spo-11(me44)/ieT1*
ie74	*zhp-2(ie74[zhp-2::HA])*	generated using CRISPR/Cas9 in *msh-5(me23) IV/nT1[unc-?(n754) let-?] (IV;V)*

ie75	*zhp-2(ie75[zhp-2::HA])*	generated using CRISPR/Cas9 in *cosa-1(we12) III/qC1 III*
ie76	*zhp-3(ie76[zhp-3::AID::3xFLAG])*	generated using *dpy-10* Co-CRISPR in *ieSi38[sun-1p::TIR1::mRuby::sun-1 3'UTR, Cbr-unc-119(+)] IV*
ie77	*zhp-3(ie77[zhp-3::AID::3xFLAG])*	generated using *dpy-10* Co-CRISPR in *meIs8[pie-1p::GFP::cosa-1, unc-119(+)] II; ieSi38[sun-1p::TIR1::mRuby::sun-1 3'UTR, Cbr-unc-119(+)] IV*
ie78	*zhp-1(ie78[zhp-1::V5])*	generated using *dpy-10* Co-CRISPR in *zhp-3(ie76[zhp-3::AID::3xFLAG]) I; ieSi38[sun-1p::TIR1::mRuby::sun-1 3'UTR, Cbr-unc-119(+)] IV*
ie79	*zhp-2(ie79[zhp-2::HA])*	generated using *dpy-10* Co-CRISPR in *zhp-3(ie76[zhp-3::AID::3xFLAG]) I; ieSi38[sun-1p::TIR1::mRuby::sun-1 3'UTR, Cbr-unc-119(+)] IV*
ie80	*zhp-3(ie80[zhp-3::AID::GFP])*	generated using *dpy-10* Co-CRISPR in *ieSi38[sun-1p::TIR1::mRuby::sun-1 3'UTR, Cbr-unc-119(+)] IV*
ie81	*zhp-4(ie81[zhp-4::HA])*	generated using *dpy-10* Co-CRISPR in *zhp-3(ie80[zhp-3::AID::GFP]) I; ieSi38[sun-1p::TIR1::mRuby::sun-1 3'UTR, Cbr-unc-119(+)] IV*
ie82	*zhp-4(ie82[zhp-4::AID::3xFLAG])*	generated using *dpy-10* Co-CRISPR in *ieSi38[sun-1p::TIR1::mRuby::sun-1 3'UTR, Cbr-unc-119(+)] IV*
ie83	*zhp-1(ie83[zhp-1::V5])*	generated using *dpy-10* Co-CRISPR in *ieSi38[sun-1p::TIR1::mRuby::sun-1 3'UTR, Cbr-unc-119(+)] IV; zhp-4(ie82[zhp-4::AID::3xFLAG]) V*
ie84	*zhp-2(ie84[zhp-2::HA])*	generated using *dpy-10* Co-CRISPR in *ieSi38[sun-1p::TIR1::mRuby::sun-1 3'UTR, Cbr-unc-119(+)] IV; zhp-4(ie82[zhp-4::AID::3xFLAG]) V*
ie85	*zhp-3(ie85[zhp-3::V5])*	generated using *dpy-10* Co-CRISPR in *ieSi38[sun-1p::TIR1::mRuby::sun-1 3'UTR, Cbr-unc-119(+)] IV; zhp-4(ie82[zhp-4::AID::3xFLAG]) V*
ie86	*zhp-4(ie86[zhp-4::HA])*	generated using *dpy-10* Co-CRISPR in *zhp-3(jf61)/hT2 [bli-4(e937) let-?(q782) qIs48] (I; III)*
ie87	*zhp-4(ie87[zhp-4::HA])*	generated using CRISPR/Cas9 in *syp-1(me17) V/nT1[unc-?(n754) let-? qIs50] (IV;V)*
ie88	*zhp-4(ie88[zhp-4::HA])*	generated using *dpy-10* Co-CRISPR in *spo-11(me44)/ieT1*
ie89	*zhp-4(ie89[zhp-4::HA])*	generated using CRISPR/Cas9 in *msh-5(me23) IV/nT1[unc-?(n754) let-?] (IV;V)*
ie90	*zhp-4(ie90[zhp-4::HA])*	generated using CRISPR/Cas9 in *cosa-1(we12) III/qC1 III*
ie92	*zhp-3(ie92[zhp-3::V5])*	generated using *dpy-10* Co-CRISPR
ie103	*zhp-3(ie103[zhp-3::V5])*	generated using *dpy-10* Co-CRISPR in *dsb-2(ie58[dsb-2::AID::3xFLAG]), meIs8[pie-1p::GFP::cosa-1, unc-119(+)] II; ieSi38[sun-1p::TIR1::mRuby::sun-1 3'UTR, Cbr-unc-119(+)] IV*
ie104	*zhp-3(ie104[zhp-3::V5])*	generated using *dpy-10* Co-CRISPR in *zhp-2(ie67[zhp-2::AID::3xFLAG]) I; dsb-2(ie58[dsb-2::AID::3xFLAG]), meIs8[pie-1p::GFP::cosa-1, unc-119(+)] II; ieSi38[sun-1p::TIR1::mRuby::sun-1 3'UTR, Cbr-unc-119(+)] IV*
ie105	*plk-2(ie105[plk-2::HA])*	generated using *dpy-10* Co-CRISPR in *zhp-3(ie103[zhp-3::V5]) I; dsb-2(ie58[dsb-2::AID::3xFLAG]), meIs8[pie-1p::GFP::cosa-1, unc-119(+)] II; ieSi38[sun-1p::TIR1::mRuby::sun-1 3'UTR, Cbr-unc-119(+)] IV*
ie106	*plk-2(ie106[plk-2::HA])*	generated using *dpy-10* Co-CRISPR in *zhp-2(ie67[zhp-2::AID::3xFLAG]), zhp-3(ie104[zhp-3::V5]) I; dsb-2(ie58[dsb-2::AID::3xFLAG]), meIs8[pie-1p::GFP::cosa-1, unc-119(+)] II; ieSi38[sun-1p::TIR1::mRuby::sun-1 3'UTR, Cbr-unc-119(+)] IV*
ie107	*zhp-2(ie107[zhp-2::HA])*	generated using *dpy-10* Co-CRISPR in *meIs8[pie-1p::GFP::cosa-1, unc-119(+)] II; ieSi38[sun-1p::TIR1::mRuby::sun-1 3'UTR, Cbr-unc-119(+)] IV*. (*ie107* and *ie108* were made from a single injection)
ie108	*plk-2(ie108[plk-2::AID::3xFLAG])*	generated using *dpy-10* Co-CRISPR in *meIs8[pie-1p::GFP::cosa-1, unc-119(+)] II; ieSi38[sun-1p::TIR1::mRuby::sun-1 3'UTR, Cbr-unc-119(+)] IV*. (*ie107* and *ie108* were made from a single injection)
ie109	*plk-2(ie109[plk-2::HA])*	generated using *dpy-10* Co-CRISPR in *zhp-1(ie62[zhp-1::AID::3xFLAG]) I; meIs8[pie-1p::GFP::cosa-1, unc-119(+)] II; ieSi38[sun-1p::TIR1::mRuby::sun-1 3'UTR, Cbr-unc-119(+)] IV*
ie110	*plk-2(ie110[plk-2::HA])*	generated using *dpy-10* Co-CRISPR in *zhp-2(ie67[zhp-2::AID::3xFLAG]) I; meIs8[pie-1p::GFP::cosa-1, unc-119(+)] II; ieSi38[sun-1p::TIR1::mRuby::sun-1 3'UTR, Cbr-unc-119(+)] IV*

Table S3

crRNAs, repair templates and genotyping primers for transgenes generated in this study

Transgenes	crRNAs and repair templates	Genotyping primers and fragment sizes
zhp-1 null mutant in *ie43* or *ie44*	5'- ttcatcgtttgcaatggatg -3'; 5'- gttgttcggcatgtttcacagaagacgtgggagcaggcggtgataaaaaattgtcttttac ttggcgagcatccacatccattctcgagcttagcaaacgatgaactccatagtgcctac agttctgaaataaatgcaaattgttatttttgaaccatgtttggaacg -3'	F: 5'- gaaaattatcgaaaaactgtcacaaac -3'; R: 5'- gttttccattttcaattgaattgacttc -3'; WT, 563bp; Mutant, 573bp=297bp+276bp (XhoI digestion)
zhp-2 null mutant in *ie45*	5'- tggatccaatgcaatcattg -3'; 5'- ctttcgtacagttttgacagaaaacgtgaccgcatgctgttaggtacagtttcgtttgatttg gtttaatgccacaatgattgcctcgagttagcattggatccaatccatacgtgtttcgagtc ttaaaatacgattaaataaagctcaaagacttctgctagataacaag -3'	Nucleotide c22 was replaced by taataattaattag. F: 5' gactcgaaacacgtatggattg-3'; R: 5'-ggtacagtttcgtttgatttg-3'; WT, 72bp; Mutant, 85bp
zhp-1 null mutant in *ie46*	5'- ttcatcgtttgcaatggatg -3'; 5'- gttgttcggcatgtttcacagaagacgtgggagcaggcggtgataaaaaattgtcttttac ttggcgagcatccacatccattctcgagcttagcaaacgatgaactccatagtgcctac agttctgaaataaatgcaaattgttatttttgaaccatgtttggaacg -3'	F: 5'- gaaaattatcgaaaaactgtcacaaac -3'; R: 5'- gttttccattttcaattgaattgacttc -3'; WT, 563bp; Mutant, 573bp=297bp+276bp (XhoI digestion)
htp-3 null mutant in *ie51* or *ie52*	5'- agtgccgaaatcggatacgg -3' and 5'- tgttcatcgacttcaactgg -3'; 5'- gtcactaaacacgaatcccgtggaaacgtttgtctggacctttgtctatgactcaaccac atctgcaagtgccgaaatctgatgaagtcgatgaacagccagaagaacaaaatgatga tgatgctcagaattctcttcaaattgactctgatgctcagaattctcttcaaattgactctg -3'	N/A
dsb-2::AID::3xFLAG in *ie58*	5'- gaatcgtgttgctcaagctg -3'; 5'- gaagatgtgagaatatatttgtctaaaaacaatggaaagaatgtaattttccaggtcaccg aaccaccaataaacgatatattctttgatcgttttcatcaaccacaactcgaacagcacg attctgttccagaagatggagctggatcacctaaagatccagccaaacctccggccaa ggcacaagttgtgggatggccaccggtgagatcataccggaagaacgtgatggtttcc tgccaaaaatcaagcggtggcccggaggcggcggcgttcgtgaagggagccggatc tgattataaagaccatgatggagactataaggatcacgatattgattacaaagacgatga tgataaatgattatttggaaaaattctaaaaatttaaacttgtatcatttgaatctgtaaattttt tttcaagtatatttaag -3'	F: 5'- ctaagcgttgaagtagccgacaaatg -3'; R: 5'- cgagctaaactggtccgcgaagag -3'; WT, 480bp; inserted, 702bp
spo-11::AID::3xFLAG in *ie59* or *ie60*	5'- tactcgtttataatcgtctc -3'; 5'- gacaggagtatatggctcgattcttgattgctccgagagtcatgtcgatagaaaaagaa attccgattcaaccagaaaccatcatcaacgaatacggatcacctaaagatccagcca aacctccggccaaggcacaagttgtgggatggccaccggtgagatcataccggaag aacgtgatggtttcctgccaaaaatcaagcggtggcccggaggcggcggcgttcgtg aagggagccggttctgattataaagaccatgatggagactataaggatcacgatattga ttacaaagacgatgatgataaaggtagttcgacagatgatgatcgggaagcaaaagac gatgactatatagattcggatgctgaagaaaagttccagaatatgatagataatgatagt g -3'	F: 5'- gtgacacgagaattagactggatg -3'; R: 5'- attgaggaggagcactctg -3'; WT, 532bp; inserted, 730bp
zhp-1::AID::3xFLAG in *ie61* or *ie62*	5'- tcgtctcaatcgaatcgtgg -3'; 5'- cgttgctggttcagatgtagataatgacgaattgctcgattatgtatgctgatatcattgattt ttctgttcctaaagttgctttttcaggatcttctaggattgaggaatcgatctgattcatcatc atccaactgctcgtctcaatctaacagaggaggatctctgtttggagctggatcacctaa agatccagccaaacctccggccaaggcacaagttgtgggatggccaccggtgagatc ataccggaagaacgtgatggtttcctgccaaaaatcaagcggtggcccggaggcggc ggcgttcgtgaagggagccggatctgattataaagaccatgatggagactataaggat cacgatattgattacaaagacgatgatgataaataacataatctgtaatatagatgaccat agttttatttttcagctataaacataaaaatgcttgatttatcttcttcccacatatccagagc aaaacgtgacac -3'	F: 5'- cttcggaatttgtatgtattccctgatcg -3'; R: 5'- cgtgtcgcttgatttatctagtcctag -3'; WT, 562bp; inserted, 784bp
zhp-2::HA in *ie63, ie72, ie73, ie74, ie75, ie79, ie84* or *ie107*	5'- gagttttattgacgaagaat -3'; 5'- gatcataggaatagattgtttggcgcaggacttgagcatccgtcgccaattcttcgtcaa ggagccggatcttacccctacgatgtcccagattatgcttaaaactccctgtatgtcacct ccgtatttttatccttttccacaatttttatttc -3'	F: 5'- gcaattgctgtgattgattaagtg -3'; R: 5'- ggagatattacgggggcaataaac -3'; WT, 211bp; inserted, 250bp
zhp-3::V5 in *ie64,*	5'- gagattaaaacattaatcgg -3'; 5'-	F: 5'- cgaccctctcatcaactaacac -3';

ie69, ie85, ie92, ie103 or *ie104*	gttttcaggatacctcgcacaaaggaaaccgatcaatggtcggagcttcattggacccg ccgatggagccggatctggaaagccaattccaaacccacttcttggactcgactccac ctaatgttttaatctcgtttttttctgaattcgttctttatttgttgatatatacatc -3’	R: 5’- tttcagcactcttcgggtc -3’; WT, 434bp; inserted, 488bp
zhp-4::HA in *ie65, ie70, ie81, ie86, ie87, ie88, ie89* or *ie90*	5’- gagaaaagcacaaggagcat -3’; 5’- ctctgcaatattttacatgataaaatgcgacacatatattaaaaaaaatcgattcaagcat aatctgggacatcgtaggggtatgatccagctccttgactattacgatgctccttgtgcttt tctctttgagcttcatgtttttttcaagtacgggaac -3’	F: 5’- ggaaatttatcgatttttttcggaaattgattg -3’; R: 5’- catgataaaatgcgacacatatattaaa -3’; WT, 236bp; inserted, 275bp
zhp-2::AID::3xFLAG in *ie66* or *ie67*	5’- gagttttattgacgaagaat -3’; 5’- gcaattgctgtgattgattaagtgtaattttttccagatcgattatagtcgccgtgatcatag gaatagattgtttggcgcaggacttgagcatccgtcgccaattcttcgtcaaggagctgg atcacctaaagatccagccaaacctccggccaaggcacaagttgtgggatggccacc ggtgagatcataccggaagaacgtgatggtttcctgccaaaaatcaagcggtggcccg gaggcggcggcgttcgtgaagggagccggatctgattataaagaccatgatggagac tataaggatcacgatattgattacaaagacgatgatgataaataaaactccctgtatgtca cctccgtatttttatccttttccacaatttttatttctattcaaaatcaaaggtttattgcccccc gtaatatctcc -3’	F: 5’- ctccaatgttagttttatctcctgttttc -3’; R: 5’- cgtcgcgttttgtaccataaaacaatc -3’; WT, 476bp; inserted, 698bp
zhp-1::V5 in *ie68, ie78* or *ie83*	5’- tcgtctcaatcgaatcgtgg -3’; 5’- catttttatgtttatagctgaaaaataaaactatggtcatctatattacagattatgttaggtg gagtcgagtccaagaagtgggtttggaattggctttcctgatccagctccaaacagaga tcctcctctgttagattgagacgagcagttggatgatgatgaatcagatcgattcctcaat cctagaagatcc -3’	F: 5’- cgttgctggttcagatgtagataatg -3’; R: 5’- gtgtcacgttttgctctggatatgtg -3’; WT, 275bp; inserted, 329bp
zhp-3::AID::3xFLAG in *ie76* or *ie77*	5’- gagattaaaacattaatcgg -3’; 5’- gtgtactctgacgttttcaggatacctcgcacaaaggaaaccgatcaatggtcggagctt cattggacccgccgatggagctggatcacctaaagatccagccaaacctccggccaa ggcacaagttgtgggatggccaccggtgagatcataccggaagaacgtgatggtttcc tgccaaaaatcaagcggtggcccggaggcggcggcgttcgtgaagggagccggatc tgattataaagaccatgatggagactataaggatcacgatattgattacaaagacgatga tgataaataatgttttaatctcgtttttttctgaattcgttctttatttgttgatatatacatcatgta caattcaactttaatg -3’	F: 5’- cgaccctctcatcaactaacac -3’; R: 5’- tttcagcactcttcgggtc -3’; WT, 434bp; inserted, 656bp
zhp-3::AID::GFP in *ie80*	5’- gagattaaaacattaatcgg-3’; 5’- aactaacacacttacacactttttcgtctctcactctctcattccgggcgctttttgcgcctt tccgctccctctatattccaattctttcgatttttgccacgtgtactctgacgttttcaggatac ctcgcacaaaggaaaccgatcaatggtcggagcttcattggacccgccgatggagga tctggaggcggttctggcggaggttctggtcctaaagatccagccaaacctccggcca aggcacaagttgtgggatggccaccggtgagatcataccggaagaacgtgatggtttc ctgccaaaaatcaagcggtggcccggaggcggcggcgttcgtgaaggtttctaaagg agaagaacttttcacaggagttgttccaatacttgttgaacttgatggagatgtaaatgga cataagttctctgtttctggcgaaggagaaggagatgctacttatggaaaacttactctca agttcatttgcactactggaaaacttcccgttccatggccaactcttgttactactttgactt atggagttcaatgtttcgctcgttatccagaccatatgaaacaacacgatttcttcaaatct gctatgccagaaggatatgttcaagaaagaactattttcttcaaagatgatggaaactac aaaactcgtgcggaagtaaagtttgagggagatactcttgtaaatagaatagaactcaa aggaatagatttcaaagaagatggaaatatacttggacataaacttgaatataactacaa tagtcataaagtttatattactgctgataaacaaaaaaatggaataaagtaaacttcaaa actcgtcataatatagaagatggaagtgttcaacttgctgaccattaccaacaaaatact ccaataggagatggcccagttcttctcccagataatcattatctttctactcaatctgctctt tctaaagacccaaatgaaaaaagagaccatatggttcttttagagttcgttactgcggcg ggaataactcttggaatggatgaactttacaaataatgttttaatctcgtttttttctgaattcg ttctttatttgttgatatatacatcatgtacaattcaactttaatgtttatttcataaaaattgggtt aaaaattccaaatttctttttctctacctagttcacatctgatttaaattttatttgaatatttcg -3’	F: 5’- cgaccctctcatcaactaacac -3’; R: 5’- cacgttcttccggtatgatctc -3’; WT, no product; inserted, 307bp. or F: 5’- cgaccctctcatcaactaacac -3’; R2: 5’- tttcagcactcttcgggtc -3’ WT, 434bp; inserted, 1316bp
zhp-4::AID::3xFLAG in *ie82*	5’- gagaaaagcacaaggagcat -3’; 5’- gttcccgtacttgaaaaaacatgaagctcaaagagaaaagcacaaggagcatcgtaat agtcaaggagctggatcacctaaagatccagccaaacctccggccaaggcacaagtt gtgggatggccaccggtgagatcataccggaagaacgtgatggtttcctgccaaaaat caagcggtggcccggaggcggcggcgttcgtgaagggagccggatctgattataaa gaccatgatggagactataaggatcacgatattgattacaaagacgatgatgataaatg aatcgatttttttaatatatgtgtcgcattttatcatg -3’	F: 5’- ggaaatttatcgatttttttcggaaattgattg -3’; R: 5’- ctaaaactgtactttcaggtcataaatgtatc -3’; WT, 382bp; inserted, 604bp
plk-2::HA in *ie105, ie106, ie109* or *ie110*	5’- tcgattttcttagcgacgcg -3’; 5’- caacgtccgtttggaatctgcagcagatatccagccggcttatccatcatcctcgcgtcg cggagccggatcttacccctacgatgtcccagattatgcttaagaaaatcgatctgcaa caaattgagctcatttccccttaccggttttg -3’	F: 5’- ggagaagttcctccatcgaattc -3’; R: 5’- ggataaaattgattacaaacacggac -3’; WT, 294bp; inserted, 333bp
plk-2::AID::3xFLAG in *ie108*	5’- tcgattttcttagcgacgcg -3’; 5’- gaaagaggagacgaaacacaatgcaccggcggccaatgcagtacgccttccatcga cttccagcaacgtccgtttggaatctgcagcagatatccagccggcttatccatcatcct cgcgtcgcggagctggatcacctaaagatccagccaaacctccggccaaggcacaa gttgtgggatggccaccggtgagatcataccggaagaacgtgatggtttcctgccaaa aatcaagcggtggcccggaggcggcggcgttcgtgaagggagccggatctgattata	F: 5’- ggagaagttcctccatcgaattc -3’; R: 5’- gagcatgatgacacccgaatgtttg -3’; WT, 451bp; inserted, 673bp

	aagaccatgatggagactataaggatcacgatattgattacaaagacgatgatgataaa taagaaaatcgatctgcaacaaattgagctcatttccccttaccggttttgatatttctctga tcaatacacttttatgtccgtgtttgtaatcaattttatcc -3’	

Table S4

Strains used in this study

Strains	Source	Identifier
C. elegans: Hawaiian wild-type isolate	Caenorhabditis Genetics Center	CB4856
C. elegans: syp-1 (me17) V/nT1[unc-?(n754) let-? qIs50] (IV;V)	MacQueen et al., 2002; Caenorhabditis Genetics Center	AV307/CA30
C. elegans: spo-11(me44) IV/ieT1	Chan et al., 2004; Hayashi et al., 2007; this paper	AV157
C. elegans: dsb-2(tm6047) II	This paper; 421 bp deletion null allele mutant; Japanese KO consortium	CA1153
C. elegans: zhp-3(jf61) I/hT2 [bli-4(e937) let-?(q782) qIs48] (I; III)	Jantsch et al., 2004; Bhalla et al., 2008	UV1/CA685
C. elegans: msh-5(me23) IV/nT1 [unc-?(n754) let-?] (IV;V)	Kelly et al., 2000; Caenorhabditis Genetics Center	AV115
C. elegans: meIs8[pie-1p::GFP::cosa-1, unc-119(+)] II	Yokoo et al., 2012; Caenorhabditis Genetics Center	AV630
C. elegans: ieSi38[sun-1p::TIR1::mRuby::sun-1 3' UTR, Cbr-unc-119 (+)] IV	Zhang et al., 2015; Caenorhabditis Genetics Center	CA1199
C. elegans: zhp-1(ie43) I/ hT2 [bli-4(e937) let-?(q782) qIs48] (I; III)	This paper	CA1356
C. elegans: zhp-1(ie44) I/ hT2 [bli-4(e937) let-?(q782) qIs48] (I; III)	This paper	CA1357
C. elegans: zhp-2(ie45) I/ hT2 [bli-4(e937) let-?(q782) qIs48] (I; III)	This paper	CA1358
C. elegans: zhp-1(ie46) I in Hawaii background	This paper	CA1359
C. elegans: meIs8[pie-1p::GFP::cosa-1, unc-119(+)] II; ieSi38[sun-1p::TIR1::mRuby::sun-1 3'UTR, Cbr-unc-119(+)] IV	This paper	CA1364
C. elegans: zhp-1(ie61[zhp-1::AID::3xFLAG]) I; unc-119(ed3) III; ieSi38[sun-1p::TIR1::mRuby::sun-1 3'UTR, Cbr-unc-119(+)] IV	This paper	CA1366
C. elegans: zhp-1(ie62[zhp-1::AID::3xFLAG]) I; meIs8[pie-1p::GFP::cosa-1, unc-119(+)] II; ieSi38[sun-1p::TIR1::mRuby::sun-1 3'UTR, Cbr-unc-119(+)] IV	This paper	CA1367
C. elegans: htp-3(ie51), zhp-1(ie62[zhp-1::AID::3xFLAG]) I; meIs8[pie-1p::GFP::cosa-1, unc-119(+)] II; ieSi38[sun-1p::TIR1::mRuby::sun-1 3'UTR, Cbr-unc-119(+)] IV	This paper	CA1368
C. elegans: zhp-1(ie62[zhp-1::AID::3xFLAG]) I; meIs8[pie-1p::GFP::cosa-1, unc-119(+)] II; ieSi38[sun-1p::TIR1::mRuby::sun-1 3'UTR, Cbr-unc-119(+)], spo-11(ie59[spo-11::AID::3xFLAG]) IV	This paper	CA1369
C. elegans: zhp-1(ie61[zhp-1::AID::3xFLAG]), zhp-2(ie63[zhp-2::HA]) I; unc-119(ed3) III; ieSi38[sun-1p::TIR1::mRuby::sun-1 3'UTR, Cbr-unc-119(+)] IV;	This paper	CA1370
C. elegans: zhp-1(ie61[zhp-1::AID::3xFLAG]), zhp-3(ie64[zhp-3::V5]) I; unc-119(ed3) III; ieSi38[sun-1p::TIR1::mRuby::sun-1 3'UTR, Cbr-unc-119(+)] IV;	This paper	CA1371
C. elegans: zhp-1(ie61[zhp-1::AID::3xFLAG]) I; unc-119(ed3) III; ieSi38[sun-1p::TIR1::mRuby::sun-1 3'UTR, Cbr-unc-119(+)] IV; zhp-4(ie65[zhp-4::HA]) V	This paper	CA1372
C. elegans: zhp-2(ie66[zhp-2::AID::3xFLAG]) I; unc-119(ed3) III; ieSi38[sun-1p::TIR1::mRuby::sun-1 3'UTR, Cbr-unc-119(+)] IV	This paper	CA1374
C. elegans: zhp-2(ie67[zhp-2::AID::3xFLAG]) I; meIs8[pie-1p::GFP::cosa-1, unc-119(+)] II; ieSi38[sun-1p::TIR1::mRuby::sun-1 3'UTR, Cbr-unc-119(+)] IV	This paper	CA1375
C. elegans: htp-3(ie52), zhp-2(ie66[zhp-2::AID::3xFLAG]) I; meIs8[pie-1p::GFP::cosa-1, unc-119(+)] II; ieSi38[sun-1p::TIR1::mRuby::sun-1 3'UTR, Cbr-unc-119(+)] IV	This paper	CA1376
C. elegans: zhp-2(ie66[zhp-2::AID::3xFLAG]) I; meIs8[pie-1p::GFP::cosa-1, unc-119(+)] II; ieSi38[sun-1p::TIR1::mRuby::sun-1 3'UTR, Cbr-unc-119(+)], spo-11(ie60[spo-11::AID::3xFLAG]) IV	This paper	CA1377
C. elegans: zhp-1(ie68[zhp-1::V5]), zhp-2(ie66[zhp-2::AID::3xFLAG]) I; unc-119(ed3) III; ieSi38[sun-1p::TIR1::mRuby::sun-1 3'UTR, Cbr-unc-119(+)] IV	This paper	CA1378
C. elegans: zhp-2(ie66[zhp-2::AID::3xFLAG]), zhp-3(ie69[zhp-3::V5]) I; unc-119(ed3) III; ieSi38[sun-1p::TIR1::mRuby::sun-1 3'UTR, Cbr-unc-119(+)] IV	This paper	CA1379
C. elegans: zhp-2(ie66[zhp-2::AID::3xFLAG]) I; unc-119(ed3) III; ieSi38[sun-1p::TIR1::mRuby::sun-1 3'UTR, Cbr-unc-119(+)] IV; zhp-4(ie70[zhp-4::HA]) V	This paper	CA1380

C. elegans: zhp-2(ie72[zhp-2::HA]) I; syp-1(me17) V/nT1[unc-?(n754) let-? qIs50] (IV;V)	This paper	CA1383
C. elegans: zhp-2(ie73[zhp-2::HA]) I; spo-11(me44) IV/ ieT1	This paper	CA1384
C. elegans: zhp-2(ie74[zhp-2::HA]) I; msh-5(me23) IV/nT1[unc-?(n754) let-?] (IV;V)	This paper	CA1385
C. elegans: zhp-2(ie75[zhp-2::HA]) I; cosa-1(we12) III/qC1	This paper	CA1386
C. elegans: zhp-3(ie76[zhp-3::AID::3xFLAG]) I; unc-119(ed3) III; ieSi38[sun-1p::TIR1::mRuby::sun-1 3'UTR, Cbr-unc-119(+)] IV	This paper	CA1387
C. elegans: zhp-3(ie77[zhp-3::AID::3xFLAG]) I; meIs8[pie-1p::GFP::cosa-1, unc-119(+)] II; ieSi38[sun-1p::TIR1::mRuby::sun-1 3'UTR, Cbr-unc-119(+)] IV	This paper	CA1388
C. elegans: zhp-1(ie78[zhp-1::V5]), zhp-3(ie76[zhp-3::AID::3xFLAG]) I; unc-119(ed3) III; ieSi38[sun-1p::TIR1::mRuby::sun-1 3'UTR, Cbr-unc-119(+)] IV	This paper	CA1389
C. elegans: zhp-2(ie79[zhp-2::HA]), zhp-3(ie76[zhp-3::AID::3xFLAG]) I; unc-119(ed3) III; ieSi38[sun-1p::TIR1::mRuby::sun-1 3'UTR, Cbr-unc-119(+)] IV	This paper	CA1390
C. elegans: zhp-3(ie80[zhp-3::AID::GFP]) I; unc-119(ed3) III; ieSi38[sun-1p::TIR1::mRuby::sun-1 3'UTR, Cbr-unc-119(+)] IV	This paper	CA1391
C. elegans: zhp-3(ie80[zhp-3::AID::GFP]) I; unc-119(ed3) III; ieSi38[sun-1p::TIR1::mRuby::sun-1 3'UTR, Cbr-unc-119(+)] IV; zhp-4(ie81[zhp-4::HA]) V	This paper	CA1392
C. elegans: unc-119(ed3) III; ieSi38[sun-1p::TIR1::mRuby::sun-1 3'UTR, Cbr-unc-119(+)] IV; zhp-4(ie82[zhp-4::AID::3xFLAG]) V	This paper	CA1393
C. elegans: meIs8[pie-1p::GFP::cosa-1, unc-119(+)] II; ieSi38[sun-1p::TIR1::mRuby::sun-1 3'UTR, Cbr-unc-119(+)] IV; zhp-4(ie82[zhp-4::AID::3xFLAG]) V	This paper	CA1394
C. elegans: zhp-1(ie83[zhp-1::V5]) I; unc-119(ed3) III; ieSi38[sun-1p::TIR1::mRuby::sun-1 3'UTR, Cbr-unc-119(+)] IV; zhp-4(ie82[zhp-4::AID::3xFLAG]) V	This paper	CA1395
C. elegans: zhp-2(ie84[zhp-2::HA]) I; unc-119(ed3) III; ieSi38[sun-1p::TIR1::mRuby::sun-1 3'UTR, Cbr-unc-119(+)] IV; zhp-4(ie82[zhp-4::AID::3xFLAG]) V	This paper	CA1396
C. elegans: zhp-3(ie85[zhp-3::V5]) I; unc-119(ed3) III; ieSi38[sun-1p::TIR1::mRuby::sun-1 3'UTR, Cbr-unc-119(+)] IV; zhp-4(ie82[zhp-4::AID::3xFLAG]) V	This paper	CA1397
C. elegans: zhp-3(jf61) I/ hT2 [bli-4(e937) let-?(q782) qIs48] (I; III); zhp-4(ie86[zhp-4::HA]) V	This paper	CA1398
C. elegans: syp-1(me17) V/nT1[unc-?(n754) let-? qIs50] (IV;V); zhp-4(ie87[zhp-4::HA]) V	This paper	CA1399
C. elegans: spo-11(me44) IV/ieT1; zhp-4(ie88[zhp-4::HA]) V	This paper	CA1400
C. elegans: msh-5(me23) IV/nT1[unc-?(n754) let-?] (IV;V); zhp-4(ie89[zhp-4::HA]) V	This paper	CA1401
C. elegans: cosa-1(we12) III/qC1; zhp-4(ie90[zhp-4::HA]) V	This paper	CA1402
C. elegans: zhp-3(ie92[zhp-3::V5]) I	This paper	CA1404
C. elegans: zhp-3(ie92[zhp-3::V5]) I; dsb-2(tm6047) II	This paper	CA1405
C. elegans: zhp-1(ie78[zhp-1::V5]), zhp-3(ie76[zhp-3::AID::3xFLAG]) I; syp-1 (me17) V/nT1[unc-?(n754) let-? qIs50] (IV;V)	This paper	CA1410
C. elegans: dsb-2(ie58[dsb-2::AID::3xFLAG]), meIs8[pie-1p::GFP::cosa-1, unc-119(+)] II; ieSi38[sun-1p::TIR1::mRuby::sun-1 3'UTR, Cbr-unc-119(+)] IV	This paper	CA1421
C. elegans: zhp-2(ie67[zhp-2::AID::3xFLAG]) I; dsb-2(ie58[dsb-2::AID::3xFLAG]), meIs8[pie-1p::GFP::cosa-1, unc-119(+)] II; ieSi38[sun-1p::TIR1::mRuby::sun-1 3'UTR, Cbr-unc-119(+)] IV	This paper	CA1422
C. elegans: meIs8[pie-1p::GFP::cosa-1, unc-119(+)] II; ieSi38[sun-1p::TIR1::mRuby::sun-1 3'UTR, Cbr-unc-119(+)], spo-11(ie59[spo-11::AID::3xFLAG]), IV	This paper	CA1423
C. elegans: zhp-1(ie62[zhp-1::AID::3xFLAG]) I; meIs8[pie-1p::GFP::cosa-1, unc-119(+)] II; ieSi38[sun-1p::TIR1::mRuby::sun-1 3'UTR, Cbr-unc-119(+)] IV; zhp-4(ie82[zhp-4::AID::3xFALG]) V	This paper	CA1424
C. elegans: zhp-3(ie103[zhp-3::V5]) I; dsb-2(ie58[dsb-2::AID::3xFLAG]), meIs8[pie-1p::GFP::cosa-1, unc-119(+)] II; ieSi38[sun-1p::TIR1::mRuby::sun-1 3'UTR, Cbr-unc-119(+)] IV	This paper	CA1425
C. elegans: zhp-2(ie67[zhp-2::AID::3xFLAG]), zhp-3(ie104[zhp-3::V5]) I; dsb-2(ie58[dsb-2::AID::3xFLAG]), meIs8[pie-1p::GFP::cosa-1, unc-119(+)] II; ieSi38[sun-1p::TIR1::mRuby::sun-1 3'UTR, Cbr-unc-119(+)] IV	This paper	CA1426
C. elegans: plk-2(ie105[plk-2::HA]), zhp-3(ie103[zhp-3::V5]) I; dsb-2(ie58[dsb-2::AID::3xFLAG]), meIs8[pie-1p::GFP::cosa-1, unc-119(+)] II; ieSi38[sun-1p::TIR1::mRuby::sun-1 3'UTR, Cbr-unc-119(+)] IV	This paper	CA1427
C. elegans: plk-2(ie106[plk-2::HA]), zhp-2(ie67[zhp-2::AID::3xFLAG]), zhp-3(ie104[zhp-3::V5]) I; dsb-2(ie58[dsb-2::AID::3xFLAG]), meIs8[pie-1p::GFP::cosa-1, unc-119(+)] II; ieSi38[sun-1p::TIR1::mRuby::sun-1 3'UTR, Cbr-unc-119(+)] IV	This paper	CA1428

C. elegans: plk-2(ie108[plk-2::AID::3xFLAG]), zhp-2(ie107[zhp-2::HA]) I; meIs8[pie-1p::GFP::cosa-1, unc-119(+)] II; ieSi38[sun-1p::TIR1::mRuby::sun-1 3'UTR, Cbr-unc-119(+)] IV	This paper	CA1429
C. elegans: plk-2(ie109[plk-2::HA]), zhp-1(ie62[zhp-1::AID::3xFLAG]) I; meIs8[pie-1p::GFP::cosa-1, unc-119(+)] II; ieSi38[sun-1p::TIR1::mRuby::sun-1 3'UTR, Cbr-unc-119(+)] IV	This paper	CA1430
C. elegans: plk-2(ie110[plk-2::HA]), zhp-2(ie67[zhp-1::AID::3xFLAG]) I; meIs8[pie-1p::GFP::cosa-1, unc-119(+)] II; ieSi38[sun-1p::TIR1::mRuby::sun-1 3'UTR, Cbr-unc-119(+)] IV	This paper	CA1431